A Study of the Immune Responses to Therapeutic Inhaled Nanoparticles by Lung Alveolar Macrophages

A thesis submitted to The University of Manchester for the degree of Master of Philosophy in the Faculty of Biology, Medicine and Health

2021

Leonor Jensen Cunha de Bragança

School of Biological Sciences

Division of Infection, Immunity & Respiratory Medicine

Table of Contents

Total Word Count: 19210

List of Tables

List of Figures

List of Abbreviations

AM	Alveolar Macrophage
ASO	Antisense Oligonucleotide
BALF	Bronchoalveolar Lavage Fluid
BSA	Bovine Serum Albumin
CCL	C-C Chemokine Ligand
CCR	C-C Chemokine Receptor
CD	Cluster of Differentiation
CD200R	Cluster of Differentiation 200 Receptor
CF	Cystic Fibrosis
CFTR	Cystic Fibrosis Transmembrane Conductance Regulator
COPD	Chronic Obstructive Pulmonary Disease
CTGF	Connective Tissue Growth Factor
DAPI	4′,6-diamidino-2-phenylindole
DC	Dendritic Cell
DLin-MC3-DMA	Dilinoleylmethyl-4-dimethylaminobutyrate
DMG	Dimyristoyl Glycerol
DMSO	Dimethyl Sulfoxide
DNA	Deoxyribonucleic Acid
DSPC	1,2-distearoyl-sn-glycero-3-phosphocholine
ED50	Median Effective Dose
EDTA	Ethylenediaminetetraacetic Acid
FBS	Foetal Bovine Serum
FcεRI	Receptor for the Fc Region of Immunoglobulin E
FITC	Fluorescein Isothiocyanate
GM-CSF	Granulocyte-Macrophage Colony-Stimulating Factor
GM-CSFR	Granulocyte-Macrophage Colony-Stimulating Factor Receptor
HEPES	4-(2-hydroxyethyl)-1-piperazineethanesulfonic acid
HIF1A	Hypoxia-Inducible Factor 1 Alpha
HLA-DR	Human Leukocyte Antigen – DR Isotype
IFN-γ	Interferon Gamma

Ig	Immunoglobulin
IL	Interleukin
ILC2	Type 2 Innate Lymphoid Cells
IPF	Idiopathic Pulmonary Fibrosis
LDLR	Low-Density Lipoprotein Receptor
LNP	Lipid Nanoparticles
LPS	Lipopolysaccharide
M-CSF	Macrophage Colony-Stimulating Factor
MBP	Major Basic Protein
MC3	(6Z,9Z,28Z,31Z)-heptatriaconta-6,9,28,31-tetraen-19-yl 4-(dimethylamino)butanoate
MCP-1	Monocyte Chemoattractant Protein 1
MFI	Median Fluorescence Intensity
MHCII	Major Histocompatibility Complex Class II
MIP-1α	Macrophage Inflammatory Protein 1 Alpha
MMP	Matrix Metalloproteinase
mRNA	Messenger Ribonucleic Acid
MUC5AC	Mucin 5AC
NF-κB	Nuclear Factor Kappa-Light-Chain-Enhancer of Activated B cells
NLC	Nanostructured Lipid Carrier
NP	Nanoparticle
OF	Oligofectamine
PBS	Phosphate Buffered Saline
PEG	Polyethylene Glycol
PGE2	Prostaglandin E_2
pH	Power of Hydrogen
pK_a	Acid Dissociation Constant at Logarithmic Scale
PMA	Phorbol 12-myristate 13-acetate
PPARγ	Peroxisome Proliferator-Activated Receptor Gamma
PRR	Pattern Recognition Receptor
RBC	Red Blood Cells
RIG-I	Retinoic Acid-Inducible Gene I
ROI	Reactive Oxygen Intermediates

RNA	Ribonucleic Acid
RNI	Reactive Nitrogen Intermediates
RPMI	Roswell Park Memorial Institute
Siglec-F	Sialic Acid-binding Immunoglobulin-like Lectin F
siRNA	Small Interfering Ribonucleic Acid
SIRP-α	Signal Regulatory Protein Alpha
SLN	Solid Lipid Nanoparticle
SOPC	1-stearoyl-2-oleoyl-sn-glycero-3-phosphocholine
SP	Surfactant Protein
SR	Scavenger Receptor
TfR	Transferrin Receptor
TGF-β	Transforming Growth Factor Beta
TLR	Toll-Like Receptor
TNF-α	Tumor Necrosis Factor Alpha
TSLP	Thymic Stromal Lymphopoietin

Abstract

The robustness and versatility of lipid nanoparticles (LNP) have attracted attention in the research field as they can be engineered to transport drugs via the enteral and the parenteral routes, to diseased target organs. Administration by inhalation allows direct access to the lungs therefore lipid nanoparticles serve as good candidates for delivering nanomedicines to treat chronic pulmonary diseases. As the most abundant resident immune cell in the lung, alveolar macrophages (AM) play an important role in patrolling and protecting the lung. Inhaled LNP encapsulating therapeutics would be perceived as non-self by AMs that would internalize the LNP. To be considered as a viable medicine, LNP would have to evade macrophage uptake, however little is known about the molecular features that dictate their uptake. The aim of this study is to understand the properties of LNP that determine their uptake as a means to improve LNP formulation, to suppress internalization by macrophages. The imortalised macrophage cell line ,THP-1, were first used to understand the general response of phagocytes to LNP. We then move onto MH-S cells, a murine alveolar macrophage cell line, that are a better representation of macrophages in the lung. We show that LNP labelled with the hydrophobic, lipophilic fluorescent dye DiD are internalised by both THP-1 and MH-S cells. We further show, using flow cytometry, that LNP internalisation into THP-1 and MH-S cells occurs at 37°C and not at 4°C. Furthermore, internalization of LNP was linear: the longer the incubation time of THP-1 and MH-S with LNP, the more LNP internalized. In this thesis we describe the impact LNP have on macrophage activation. As a gene delivery device, LNP successfully enter cells linearly over time but results showing activation following uptake warrant further investigation on the safety and efficacy of LNP to assess their competency as a therapeutic in humans.

Declaration

No portion of the work referred to in the thesis has been submitted in support of an application for another degree or qualification of this or any other University or other institute of learning.The research was funded by a BBSRC CTP studentship in collaboration with MedImmune.

Copyright Statement

i. The author of this thesis (including any appendices and/or schedules to this thesis) owns certain copyright or related rights in it (the "Copyright") and s/he has given The University of Manchester certain rights to use such Copyright, including for administrative purposes.

ii. Copies of this thesis, either in full or in extracts and whether in hard or electronic copy, may be made only in accordance with the Copyright, Designs and Patents Act 1988 (as amended) and regulations issued under it or, where appropriate, in accordance with licensing agreements which the University has from time to time. This page must form part of any such copies made.

iii. The ownership of certain Copyright, patents, designs, trademarks and other intellectual property (the "Intellectual Property") and any reproductions of copyright works in the thesis, for example graphs and tables ("Reproductions"), which may be described in this thesis, may not be owned by the author and may be owned by third parties. Such Intellectual Property and Reproductions cannot and must not be made available for use without the prior written permission of the owner(s) of the relevant Intellectual Property and/or Reproductions.

iv. Further information on the conditions under which disclosure, publication and commercialization of this thesis, the Copyright and any Intellectual Property and/or Reproductions described in it may take place is available in the University IP Policy (see http://documents.manchester.ac.uk/DocuInfo.aspx?DocID=24420), in any relevant Thesis restriction declarations deposited in the University Library, The University Library's regulations (see http://www.library.manchester.ac.uk/about/regulations/) and in The University's policy on Presentation of Theses.

Acknowledgements

I would first like to extend my gratitude to Professor Jeremy Derrick and to Dr. Tracy Hussell, who guided me and encouraged me in every step of the way to completing my research. You were always available to help and gave me the utmost support during a very difficult time.

I would like express my sincere appreciation to both the Derrick and the Hussell lab for being a great source of laughter, wisdom, motivation and knowledge. Our weekly Zoom meetings helped get me through very challenging moments during the pandemic. Thanks to your patience and your help, a once scared and clueless woman in the lab became an independent woman who cared a little bit less about making mistakes.

Lastly, I would like to thank my family and friends in Portugal and in the UK for their unconditional love and undying support. You never ceased to believe in me and gave me strength when I had to move back to the UK, alone, in the middle of the pandemic in order to complete my research. I am eternally grateful for your support.

1. Introduction

1.1. Background Information

The prevalence and incidence rates of chronic lung diseases have declined annually from 1990 to 2017 but the total number of cases has increased by nearly 40% globally[1]. Asthma and chronic obstructive pulmonary disease (COPD) are the most common chronic lung diseases and are partly responsible for the global morbidity from lung diseases[1,2]. In 2017 alone, 7% of all deaths worldwide were from chronic respiratory diseases[2] (Figure 1.1).

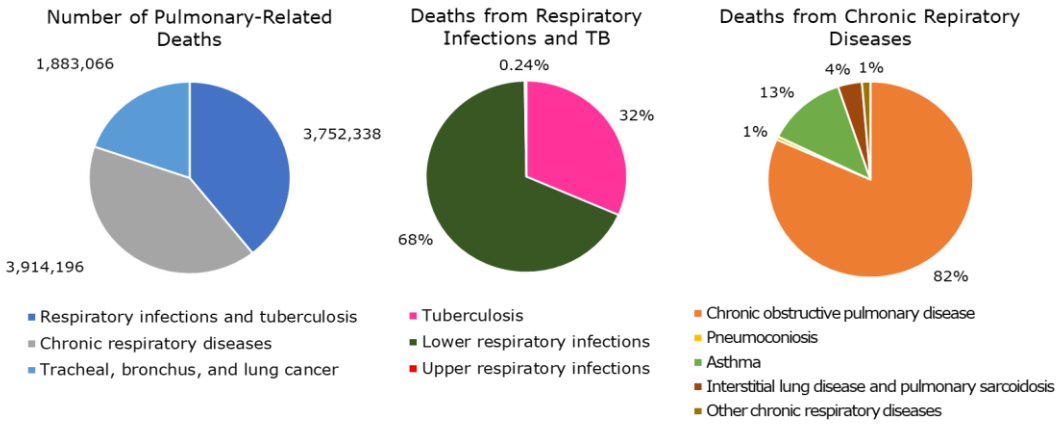

Figure 1.1 Number of global deaths attributed to pulmonary complications and proportions of global deaths attributed to specific pulmonary conditions. In 2017, 7% of global deaths were caused by respiratory infections and TB, 7% of global deaths were caused by chronic respiratory diseases and 3% of global deaths were caused by tracheal, bronchus and lung cancer. In 2017, most deaths from respiratory infections were due to infections in the lower respiratory tract and COPD was the chronic respiratory disease responsible for the most deaths. Adapted from Global Burden of Disease Study 2017 (GBD 2017) Results.

Chronic respiratory diseases are currently treated with traditional small molecule drugs and antibody-based therapeutics. Chronic obstructive pulmonary disease (COPD) is traditionally treated with: bronchodilators such as salbutamol, steroid inhalers such as budesonide and mucolytics such as carbocisteine and acetylcysteine[3]. Asthma is traditionally treated with preventer inhalers such as beclometasone, reliever inhalers such as terbutaline and monoclonal antibody therapies such as benralizumab and omalizumab[4]. However, gene therapy has become an attractive solution for life-threatening, debilitating chronic pulmonary diseases that still have no cure, despite their great global burden[5-7]. Feasibility of

this approach is shown by inhaled delivery of the wild type cystic fibrosis transmembrane conductance regulator CFTR gene with cationic lipid GL-67 as the delivery agent that restores the chloride channel in the lungs of cystic fibrosis (CF) patients by ~25 %, attenuates inflammation in the lower airways and reduces bacterial adherence[8].

Naked nucleic acid delivery for gene therapy is ineffective because genetic material is vulnerable to nuclease degradation and also because the negatively charged phosphate backbone prevents interaction with the negatively charged cell membrane[9-11]. Lipid nanoparticles (LNP) have been widely adopted as vehicles to systematically deliver therapeutics such as genes[12-17] and drugs[18-23] to treat various diseased organs, since their resilient structure protects encapsulated material from enzymatic digestion or immune destruction. Therefore, LNP are an extremely attractive technology to encapsulate gene drugs destined for delivery to diseased pulmonary cells. These solid colloidal nano-sized systems, composed of biocompatible physiological lipids, have low immunogenicity and cytotoxicity, enhanced long-term stability, and their production can be easily scaled-up[11,19,24-30]. Surfactants, like biocompatible glycerides, fatty acids or waxes, are usually included in the formulation as they stabilise and solubilize the loaded drugs[31,32].

For intracellular delivery, cationic lipids are used as the electrostatic affinity between the positive charges on the head group and the negatively-charged cell membranes facilitates the internalization of the LNP[33-37]. High positive charges on the surface of cationic LNP can be cytotoxic and highly immunogenic. If LNP were to be used as inhaled therapeutics for lung pathologies, it is important to investigate if and how the local lung immune system would perceive these non-viral vectors and its response upon exposure to them. Alveolar macrophages (AMs) are the most abundant innate immune cells that reside in the lower airways of the lung and appear dysregulated in lung diseases such as COPD and asthma. LNP are recognized as harmful foreign material by AMs and their interaction could disturb polarization of macrophages, having deleterious repercussions on the immunological function of macrophages and their role in disease[38,39]. Furthermore, AMs could interfere with the delivery of the therapeutic to target cells, preventing the desired therapeutic effects and possibly inducing an immune response against the LNP.

1.2. Alveolar Macrophages

Alveolar macrophages (AMs) are phagocytes that populate the inner surface of the lung underneath the pulmonary surfactant layer coating the alveolar epithelium, where the air-liquid interface has been created [40-43]. As the biggest immune cell population in the lung, they are sentinels that maintain pulmonary homeostasis by engulfing inhaled xenobiotics and pathogens, and by catabolizing lung surfactant into lipids and proteins[44-50]. During embryo development, fetal liver monocytes differentiate into AMs in response to granulocyte-macrophage colony-stimulating factor (GM-CSF) paracrine and transforming growth factor beta (TGF-β) autocrine signalling, resulting in increased expression of the transcription factor peroxisome proliferator-activated receptor gamma (PPARγ) involved in AM development[51]. Therefore, AMs can locally self-renew and replenish their numbers independently of circulating monocytes[5,52-54]. GM-CSF is important for the self-renewal of AMs, the growth of alveolar epithelium, the differentiation of lung-infiltrating monocytes into macrophages, and the maintenance of lung surfactant homeostasis[50,52,55]. Regulating the production and clearance of lung surfactant is important for preventing alveolar collapse and respiratory failure[47].

Normally, AMs do not strictly adopt either a M1 or M2 phenotype but rather integrate characteristics of the two (Table 1.1). AMs with this plasticity efficiently maintain homeostasis by quickly interchanging between phenotypes, depending on the stimuli received from the lung environment[41,56]. AMs can play immunosuppressive as well as pro-inflammatory roles in the lung (Table 1.1).

Table 1.1 Comparison of phenotypes between distinct macrophage populations

	Classically-activated M1 macrophages	*Alternatively-activated M2 macrophages*	*Alveolar macrophages*
Polarization trigger	IFN-γ, LPS	IL-4, IL-13	GM-CSF, PPAR-γ
Production of cytokines	Pro-inflammatory: IL-1β, TNF-α, IL-12	Anti-inflammatory: IL-10, IL-1ra	Anti-inflammatory: IL-10, PGE2, TGF-β Pro-inflammatory: TNF-α, IL-6
Phagocytosis	High	High	Low
Surface markers	MHCII, CD80, CD86 CD64/Fc-γ receptor 1, CCR2	CD206/mannose receptor, CD200R	MHCII, CD11c, CD64/Fc-γ receptor 1, CD141, CD206/mannose receptor

Roles	Arginine→ nitric oxide + citrulline Inhibit proliferation Produce RNI and ROI Tissue injury	Arginine→ornithine + urea Promote proliferation and collagen production Tissue repair and remodelling	Potent microbial antigen-primed, interferon-gamma (IFN-γ)-releasing T cell activators Express genes for phagocytosis, PRRs and transcription factors from pro-inflammatory NF-κB family
References	[26,44,48,55,57,58]		[41,43,44,47,48,59,60]

CD11c, complement receptor 4 subunit; CD141, anticoagulation co-factor

1.2.1. Alveolar Macrophages in Pulmonary Diseases

Pulmonary homeostasis is tightly controlled through intercellular communication and soluble mediators which limit unwanted inflammatory reactions[44,47] (Table 1.2). When this is lost or interfered with, the lungs are at risk of entering into a diseased state. In this state, the local immune system in the lung and the lung environment are dysregulated – they are either over or underactive. Table 1.2 shows how the lung environment tightly regulates and controls activation of AMs, the biggest immune cell population in the lung. Chronic pulmonary diseases compromise the anatomy and change the physiology of the lung. In asthma and COPD, hyperplasia of non-ciliated goblet cells results in mucus hypersecretion and delayed mucociliary clearance due to a reduced number of ciliated cells[61]. It is essential to understand how the normal pulmonary state is dysregulated and to elucidate the pathological changes in the lung during disease to then investigate how this abnormal environment could interfere with the delivery and mode of action of therapeutics. Furthemore, this will help optimize and maximize delivery of gene therapeutics to the diseased cells in the lung.

Table 1.2 Negative regulation of alveolar macrophages

Mediators	*Source of Mediator*	*Negative Regulation of AMs*	*References*
Anti-inflammatory cytokines			
IL-10, TGF-β	Epithelial cells, AMs (autocrine)	Bind IL-10R and TGF-βR to prevent harmful reactions towards harmless antigens	[41,47,48,60]
Surface Markers			
CD200	Type II alveolar epithelial cells	Bind to CD200R to inhibit activation of myeloid cells	[41,48]
CD47		Binds to SIRP-α to	[41,47]

	Healthy cells	inhibit phagocytosis, prevent inflammation by decreasing TNF-α production	
Lung environment			
SPA	Type II alveolar epithelial cells	Binds to SIRP-α to prevent inflammation by inhibiting complement activation and phagocytosis, block binding of TLRs to their ligands	[41,47]
Transcription Factors			
PPAR-γ	Lung stromal cells	Upregulated upon binding of GM-CSF to GM-CSFR, regulates lipid intake and lipid metabolism for lung homeostasis	[41,47,50,62]

1.2.1.1. Chronic Obstructive Pulmonary Disease (COPD)

COPD is a systemic, multimorbid[63] syndrome characterised by chronic lung inflammation and abnormal changes to the lung architecture that impair lung function, resulting in permanent airflow constraints[55,60]. Tobacco smoke from cigarettes, a major cause of COPD[64,65], triggers unwanted inflammatory responses that progressively narrow the airways and destroy the alveoli - chronic obstructive bronchiolitis and emphysema, respectively – causing development of chronic respiratory symptoms[46,66].

Repetitive injury by inhaled irritants results in the release of endogenous danger molecules that bind to Toll-like receptor (TLR)2 and TLR4 on airway epithelial cells. In turn, these cells secrete chemokines that stimulate the infiltration of neutrophils, macrophages and T and B lymphocytes in the lung. These innate immune cells then secrete cytokines that disrupt the tight junctions responsible for the barrier function of the airway epithelial cells and drive abnormal tissue, ultimately scarring lung tissue and destroying lung parenchyma[5,61,64,66]. Activated airway neutrophils, epithelial cells and alveolar macrophages injure the lung by secreting tissue-damaging enzymes[5,55,66] and chemokines that recruit monocytes and neutrophils[26,46,67] (Table 1.3).

Analysis of sputum and bronchoalveolar lavage fluid (BALF) samples from COPD patients showed a substantial increase in alveolar macrophage numbers[55,66,67]. There are several possible explanations to this phenomenon: alveolar macrophages upregulate the expression of monocyte chemoattractant protein 1 (MCP-1), resulting in increased infiltration of monocytes from the blood into the lung[67,68]; mucociliary clearance is defected in COPD patients meaning alveolar macrophages cannot be cleared and remain in the lung for unusually long periods of time[67]; alveolar macrophages in some COPD patients who smoke have shown to upregulate the expression of anti-apoptotic proteins thus enhance cell survival in the lung[69]; since alveolar macrophages have the capacity to self-renew, the persisting inflammatory environment in the lungs of COPD patients could stimulate the proliferation of alveolar macrophages[66].

1.2.1.2. Asthma

Asthma is a respiratory disease, usually manifested in younger individuals, caused by the thickening of the pulmonary wall and obstruction of the airways from mucus hypersecretion[26,70,71]. Atopy is the genetic predisposition to develop hypersensitivity towards environmental allergens and innocuous stimuli[70,72-74]. When atopic individuals are exposed to the allergen for prolonged periods of time, the inflammatory response becomes chronic, resulting in structural changes to the airways[71,74,75] (Table 1.3).

Inhaled allergens bind to pattern recognition receptors (PRRs) on the surface of epithelial cells causing them to release cytokines that promote type 2 immune response activating effector Th2 cells, type 2 innate lymphoid cells (ILC2s), dendritic cells (DCs), basophils, mast cells and eosinophils[71,74-77]. Since DCs are responsible for stimulating the differentiation and clonal expansion of T cells, they are necessary for allergen sensitization and driving Th2 immune responses in asthma and allergy[75]. Activated allergen-specific CD4+ Th2 cells upregulate the production of Th2 cytokines that disrupt the tight junctions holding epithelial cells together, increasing the permeability of the epithelium and jeopardizing the robust barrier[61] (Table 1.3).

Allergen-specific IgE produced by B cells in the lungs binds to FcεRI on pulmonary mast cells and basophils inducing the release of histamines, leukotrienes and Th2 cytokines. These cytokines, like IL-4 and IL-13, drive AMs to alternatively activate and increase the production of chemokines that attract eosinophils towards the lung[26,71,73] (Table 1.3). Eosinophils degranulate and release inflammatory mediators and the toxic cationic major basic protein (MBP)

that causes degranulation of mast cells and basophils, contributing to the pathological progression of the disease[71].

1.2.1.3. Idiopathic Pulmonary Fibrosis (IPF)

IPF is a major type of interstitial lung disease that is progressive, chronic and incurable[73,78]. The accumulation of alternatively activated M2 macrophages and fibroblasts induce inflammation and fibrosis, due to excessive collagen deposition that irreversibly change the lung architecture[79-81] (Table 1.3). Patients eventually die due to disrupted gas exchange which leads to respiratory failure[82].

In IPF, the expression of CD204, a scavenger receptor involved in collagen type I phagocytosis, is upregulated on the surface of alveolar macrophages in response to collagen type I monomer stimulation[79]**.** Binding of collagen type I monomer to CD204 polarizes alveolar macrophages towards the alternatively activated M2 phenotype; furthermore, alveolar macrophages in fibrotic tissue highly express CCR4, the receptor for M2 markers CCL17 and CCL22[78] (Table 1.3)**.**

In IPF, extensive interaction in a positive feedback loop between alveolar macrophages and fibroblasts exacerbates the condition. M2 alveolar macrophages increase the production of the chemokine CCL18 that, in turn, activates production of collagen by fibroblasts, stimulating M2 alveolar macrophages to further produce CCL18[81,83] (Table 1.3). Since CCL18 is correlated with IPF patient mortality, it is used as a marker to predict prognosis[78,79,83]**.**

The cytokine thymic stromal lymphopoietin (TSLP) involved in development of profibrotic type 2 immune responses and its receptor are highly upregulated in IPF[84]. Macrophages secrete TSLP that activate fibroblasts releasing CCL2, resulting in the chemotaxis of monocytes to the lung[82,84]. These monocytes promote fibrogenesis by releasing high levels of pro-inflammatory cytokines such as IFN-α, macrophage inflammatory protein 1-alpha (MIP-1α)/CCL3 and CCL4, which induce the differentiation of fibroblasts into myofibroblasts[81].

Table 1.3 Characteristics and pathophysiology of chronic respiratory diseases

Disease	*Risk Factors*	*Symptoms*	*Secreted mediators*	*Key events*	*Ref.*
COPD	Tobacco smoke Pollutants Occupational exposure	Coughing Sputum production Difficulty breathing	TNF-α, IL-8, MCP-1	Infiltration of neutrophils, macrophages, monocytes	5,55,63,64,66

	α-1-antitrypsin deficiency		IL-1β, IFN-γ Elastase, MMP-2, MMP-9, MMP-12, cathepsin K, L and S	Disrupted tight junctions of airway epithelia Scarring of lung tissue Destruction of lung parenchyma	
Asthma	Atopy Exposure to allergens	Difficulty breathing Wheezing Coughing Sputum production	IL-5, CCL-8, CCL-17, eotaxin-2 TSLP, CCL17, CCL22 IL-25, GM-CSF, M-CSF, TGF-β, IL-1α IL-4 IL-33	Increased infiltration of eosinophils Infiltration of Th2 cells and ILC2 Activation of DCs, basophils, mast cells Disrupted tight junctions of airway epithelia Local production of allergen-specific IgE Bronchial hyper-responsiveness Mucus hypersecretion	[26,70-77]
IPF	Pollutants Irradiation Connective tissue disease Drugs	Shortness of breath Dry cough	CCL18 CCL2 IFN-α, MIP1α, CCL4 Collagen I monomer	Production of collagen by fibroblasts Infiltration of monocytes Differentiation of fibroblasts into myofibroblasts Polarization of macrophages to alternatively activated M2 phenotype	[26,46,79,80,83,85]

1.2.2. Gene Therapy Potential

In the chronic respiratory diseases outlined above, the dysfunctional alveolar macrophages exhibit impaired phagocytosis and efferocytosis[45,46,73,86]. For gene

delivery, this abnormal activity is beneficial as alveolar macrophages can no longer internalize exogenous material as efficiently and thus no longer pose as a barrier. Gene therapeutics for COPD, asthma and IPF are currently at very early stages of development but the outcomes show promise.

1.2.2.1. COPD

As mentioned in Table 1.3, α-1-antitrypsin deficiency is an important genetic risk factor for COPD and is therefore a potential target for gene therapy. There are preliminary studies supporting this approach. For example, delivery of cationic liposomes complexed to a plasmid encoding a recombinant human α-1 antitrypsin gene to New Zealand rabbits results in gene transfection and expression in alveolar epithelial cells for one week after a single administration[87]. Also, transfecting human bronchial epithelial cells with an siRNA encoding p65 and treating with a small molecule inhibitor of the NF-κB pathway dampened proinflammatory cytokines IL-1β and IL-17A that utilize this pathway[88]. Furthermore, since the expression of these proinflammatory cytokines was suppressed, the expression of the MUC5AC gene, usually induced by these cytokines, was also suppressed in the human bronchial epithelial cells[88].

1.2.2.2. Asthma

The pathology of asthma is driven by Th2 immune responses, therefore studies have investigated using gene therapy to skew the Th2 response towards a Th1 response. A study delivered plasmid DNA encoding IFN-γ, a Th1-type immune regulatory cytokine, intravenously to ovalbumin-sensitized mice which counteracted the Th2 immune response: IL-5 production was suppressed reducing airway eosinophilia and IL-13 was suppressed, resulting in reduced bronchial mucus. Furthermore, the delivered IFN-γ gene also reduced dendritic cell and T cell activation. A separate study delivered intravenously a recombinant vaccinia vector encoding IL-12, a Th1-type cytokine, to ovalbumin-sensitized mice resulting in suppression of Th2-type cytokine production and attenuated allergy and airway hyperreactivity due to an increase in endogenous IFN-γ expression[74,89].

1.2.2.3. IPF

As fibrosis is the hallmark of IPF, gene therapeutics under development aim to downregulate the expression of fibrotic proteins. A nanostructured lipid carrier carrying PGE2 and siRNA encoding MMP3, CCL2 and hypoxia-inducible factor 1-alpha (HIF1A) was delivered to a mouse model of IPF via inhalation[90]. As a result,

the expression of the inhibited genes and production of their respective proteins was reduced, leading to attenuation of lung inflammation and fibrosis in the lung[90]. Furthermore expression of the connective tissue growth factor (CTGF), the pro-fibrotic cytokine TGF-β and TGF-β receptor genes were also downregulated such that fibroblast proliferation, activation, migration and collagen production were reduced[90].

1.3. Current Gene Therapy Modalities

Traditional therapies to treat lung diseases are limited to attenuating symptoms, rather than addressing the root cause of the disease. More recently, gene therapy has become a popular area of research as it has great therapeutic potential due to its ability to correct mutations at the post-transcriptional level. Gene therapy works by transfecting diseased cells with: DNA that downregulates the expression of certain genes involved in pathophysiology[18]; DNA that upregulates the expression of certain genes involved in anti-inflammatory pathways in diseased lungs[13,91] (Table 1.4); RNA that inserts a gene that has been deleted or correcting a mutated gene[36,92] (Table 1.4). While both nucleic acids can be used for gene therapy, using RNA over DNA molecules has certain advantages: low immunogenicity, inability to integrate or mutate the genome, absence of nuclear transport and the ability to "pharmacoevolve" where its sequence changes alongside the disease[92-94].

Table 1.4 Gene therapy approaches studied in disease models and the outcomes of their intervention

Gene Therapy Approach	*Disease model*	*Outcome*	*Reference*
mRNA	Congenital surfactant protein B (SP-B) deficiency	Decreased interaction with TLR3, TLR7, TLR8 and RIG-I Increased stability Low immunogenicity Prolonged gene expression	[93]
mRNA	n/a	Increased systemic production of serum protein erythropoietin Increased circulating reticulocytes Increased percentage of	[95]

		circulating RBCs No immunogenicity Does not interfere with potency of regulatory sequences	
mRNA	n/a	Leukotriene inhibitors for lung cancer treatment increase transfection efficacy by 200% Increased endosomal escape	[42]
DNA	Lung cancer	Increased toxicity of drug to cancer cell	[18]
siRNA	Multi-drug resistant lung, breast, colon, and ovarian cancer	Suppress genes of pump drug resistance (drug efflux)	[16,96]
ASOs	Drug-sensitive and multi-drug resistance small-cell lung cancer	Suppress genes of non-pump resistance (anti-apoptosis) Near complete tumour regression	[97,98]
siRNA	Hereditary transthyretin-mediated amyloidosis	Reduced production of misfolded transthyretin protein in the liver Slow progression of hereditary transthyretin-mediated amyloidosis	[99]

Large, negatively-charged DNA and RNA molecules cannot freely diffuse across the cell membrane hence they need a carrier to enter target cells and prevent stimulating an immune response[30,94,100]. Very robust non-viral vectors formulated with materials such as peptides, synthetic and natural polymers have been extensively studied, characterised and reviewed. Compared to viral vectors, non-viral vectors are safer, easier to produce, cost-efficient, easily functionalized to improve transfection and can encapsulate nucleic acid of any size[9,29,101]. This overview will solely focus on non-viral vectors formulated with cationic lipids called lipid nanoparticles (LNP).

1.4. Introduction to Lipid Nanoparticles

1.4.1. Structure and Composition of Lipid Nanoparticles

LNP have been widely adopted as vehicles to deliver therapeutics such as drugs[18-23] and genes[12-17], as their resilient structure protects encapsulated material from enzymatic digestion and immune destruction. Compared to free drugs, delivering drugs encapsulated in LNP exhibits sustained drug release over a longer period of time and exhibits higher antimicrobial activity[102,103].The BioNTech/Pfizer and the Moderna COVID-19 vaccines employ LNP technology as a mRNA carrier, such that these vaccines have 95% efficacy in preventing COVID-19 in individuals who did not have prior infection[104,105]. These spherical, colloidal nano-sized systems composed of biodegradable and biocompatible physiological lipids have low immunogenicity and cytotoxicity and enhanced long-term stability[11,19,24-30]. Surfactants are usually included in the formulation as they stabilise and solubilize the loaded drugs[31,32].

LNP are formulated with: a helper lipid that is usually a neutral phospholipid that interacts with the cell membrane; cholesterol that fits between lipids; polyethylene glycol (PEG)-lipid that controls particle size and prevents clumping during storage; and an ionizable cationic lipid that condenses mRNA[104-106]. The core-shell model best describes the structure of LNP-mRNA: the phospholipid, the PEG and some ionizable cationic lipid and cholesterol are found on the surface layer to protect the LNP while the amorphous, isotropic core is composed of cholesterol and water pores loaded with mRNA, surrounded by inverted ionizable cationic lipids[105,106] (Figure 1.2C). Cholesterol in the LNP formulation contributes to a high encapsulation rate, a low polydispersity index and an LNP structure with a single bilayer, a smooth round shape and a homogeneous core[106]. The ratio of materials affect the efficacy of LNP, and must be changed according to its application and administration route as their physicochemical properties affect their behaviour *in vivo*[104].

For example, a study produced LNP loaded with mRNA encoding luciferase with different PEG contents from 5% to 0.5%. These LNP were administered to BALB/c mice by subretinal injection. The study showed that LNP with a PEG content of 0.5% showed the highest transfection efficiency and highest luciferase expression in the eye[107].

There are two types of LNP used as delivery systems: solid lipid nanoparticles (SLN) and nanostructured lipid carriers (NLC)[29,32]. SLN consist of a solid,

hydrophobic, lipid core capable of transporting hydrophilic and lipophilic compounds coated with a single layer of phospholipids[11,19,32] (Figure 1.2A). NLC consist of a core with a mixture of solid lipids and oils forming an imperfect matrix[29,32,108]. Compared to SLN, NLC have improved drug loading capacity and drug release properties, better drug stability and drug retention, which is beneficial for long-term storage[11,18,32] (Figure 1.2B).

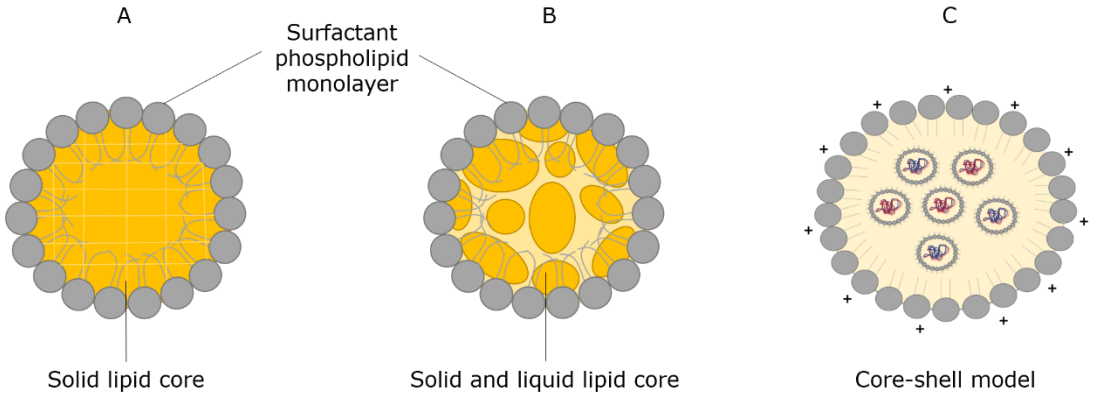

Figure 1.2 Schematic representation of lipid nanoparticle structures. A) solid lipid nanoparticle (SLN) with an organized, almost perfect solid lipid matrix, and B) nanostructured lipid carrier (NLC) composed of an imperfect solid lipid matrix with liquid oil droplets C) core-shell model best describes the structure of mRNA-loaded LNP.

For intracellular delivery, cationic lipids are used, as the electrostatic affinity between the positive charges on the head group and the negatively-charged cell membranes facilitates the internalization of the LNP[33-37]. While beneficial for condensing genetic material[25,29] and for attachment to the cell membrane[9], cationic charges can be dangerous to host cells[94,109,110]. Coating the surface of cationic LNP with the hydrophilic neutral polymer PEG provides stealth properties: the formation of a water shell shielding the positive charges reduces adsorption of biomolecules, impedes opsonisation, evades recognition by immune cells and increases half-life[94,110,111].

Ionizable cationic lipids are increasingly used in the formulation of nanoparticles as they have functional groups with pK_a values less than 7 such that at acidic pH, they become positively charged and can efficiently encapsulate negatively charged polymers into the nanoparticles; however, at physiological pH, they adopt a relatively neutral surface charge which overcomes toxicity inflicted by permanently cationic lipids. Inside endosomes with acidic pH, ionizable cationic lipids become positively charged and are thought to interact with the anionic

lipids of the endosomal membrane to promote release of its cargo into the cytosol[30,33,109,112-122].

1.4.2. Fabrication and Loading of Lipid Nanoparticles

Traditional techniques used to produce nucleic acid-loaded LNP can be laborious, complex, non-reproducible, and frequently produce particles with inadequate size or instability. Improved methods that overcome these limitations have been developed, involving dissolving lipids in ethanol and diluting this organic phase in an aqueous solution containing nucleic acid. Rapid microfluidic mixing of the organic phase with the aqueous phase at fast flow rates creates turbulence, resulting in the self-assembly of LNP encapsulating the genetic material. Faster flow rates and greater PEG-lipid contents produces smaller and more monodisperse LNP[111,119,123].

This superior, reproducible technique achieves nearly 100% encapsulation efficiency and produces LNP with uniform size, without the need for nucleic acid condensing agents[120,121,123]. Using this technique, the production of LNP can be easily scaled-up while maintaining monodispersity[120,122]. However, the use of organic solvents means that a time-consuming dialysis step must be added[120].

1.5. Internalization of Lipid Nanoparticles

Due to their size and physicochemical properties, nanoparticles are internalized by cells through two endocytic pathways called pinocytosis, which encompasses macropinocytosis, clathrin-mediated endocytosis and caveolae-mediated endocytosis, and phagocytosis[37,38,40,44,104] (Figure 1.3). Nanoparticles can be actively internalized through various mechanisms at the same time and when one mechanism fails, another mechanism can take over to internalize the nanoparticle instead[35,44,116].

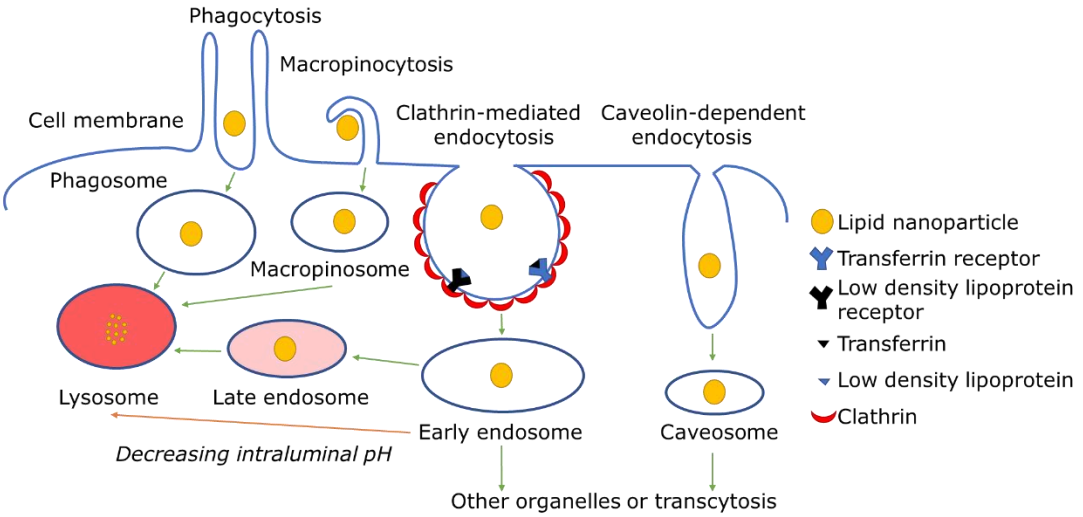

Figure 1.3 Schematic representation of endocytosis and the intracellular fate of the lipid nanoparticle. Cells can internalize exogenous material via the two endocytic pathways phagocytosis and pinocytosis (micropinocytosis, clathrin-mediated endocytosis, caveolin-dependent endocytosis). The intracellular fate of the lipid nanoparticles depends on the route of uptake.

Macropinocytosis involves actin-induced protrusions of the membrane, called macropinosomes, that wrap around and engulf the nanoparticles into the cytosol[35,124]. Clathrin-mediated endocytosis involves recognition of the LNP by scavenger, mannose and TLR receptors and relies on low-density lipoprotein receptor (LDLR) and transferrin receptor (TfR)[44,116,124]. Binding induces a series of processes that include invagination of the cell membrane, formation of clathrin pits enclosing the LNP, shedding of the clathrin from the vesicles, fusion with endosomes and degradation or recycling of the internalized receptor[40,44,124,125]. Caveolae-mediated endocytosis involves invagination of a domain in the cell membrane containing the integral membrane protein caveolin which form vesicles that mediate transcytosis of the nanoparticle[40,44,124]. As a result, the caveolin-coated vesicles do not undergo acidification or contain degradative enzymes, thus escape lysosomal degradation[10]. Therefore, if cationic LNP are being used as non-viral vectors, they should be formulated to be preferentially internalized via the caveolae-mediated endocytosis pathway.

While pinocytosis is performed by all cells, phagocytosis can only be performed by specialized cells called phagocytes, such as macrophages and dendritic cells[38,124] (Figure 1.3). Phagocytosis involves the recognition of opsonized LNP by Fc and complement receptors, and of non-opsonized lipid particles by scavenger receptors (SR)[26,126]. Binding induces the local extension of the cell membrane to

wrap around the particulate matter and to englobe them into phagosomes for their destruction[42,44,60].

When NP are endocytosed, they are expected to traffic through endosomes to lyosomes, or perhaps even exocytosed[127]. Studies have shown that treating low transfecting cell lines with LNP formulations loaded with eGFP mRNA resulted in accumulation in early endosomes and inhibited conversion into late endosomes by interfering with acidifcation of endosomal pH and defective endosomal recycling[127,128]. These arrested endosomes could not undergo normal cargo uptake nor could the LNP-mRNA forumlations escape from them, meaning mRNA was not delivered into the cytosol[128]. Furthermore, the proportion of arrested endosomes increased with time[128]. For efficient transfection, LNP delivery systems must escape the endosomes soon after internalization and localisation into this intracellular compartment[127].

1.6. Role of Physicochemical Properties on Interaction with Cells

Unwanted interaction between nanoparticles and immune cells can result in internalization of nanoparticles which can trigger inflammatory pathways that may develop into harmful responses and increase susceptibility to disease[42,129-131]. The immune system can react to nanoparticles in a similar way to how they react to pathogens[131]. LNP are recognized as harmful foreign material by alveolar macrophages and their interaction could disturb polarization of macrophages, having deleterious repercussions on the immunological function of macrophages and their role in disease[38,39]. Lipid nanoparticle size, surface charge, morphology and stiffness influence how macrophages bind to, internalize and respond to these nanocarriers[49,130,132-134]. To avoid immune responses against LNP, we must first understand how the physicochemical properties of nanoparticles affect their interaction with, and internalization by, host cells.

1.6.1. Size

The size of LNP determines how they are internalized by cells and their fate once they are inside the cells. Micro-sized particles are usually internalized via macropinocytosis, while nano-sized particles are internalized via clathrin-mediated endocytosis and caveolae-mediated endocytosis[44,116,124]. Particles below 6 μm are internalized by phagocytosis, between 100-350 nm are internalized by clathrin-mediated endocytosis and between 20-100 nm are internalized by caveolae-mediated endocytosis[124].

1.6.2. Shape and Stiffness

Spherical nanoparticles are rapidly internalized by macrophages[42,133]. LNP with non-spherical shapes require more cytoskeletal rearrangements, consuming more energy, so are less likely to be uptaken by phagocytes[133]. These shapes with low curvature include fibres, worm-like shapes, rods and cylinders[27,38,42,44]. Rigid and stiffer particles are better recognized and internalized by phagocytes than flexible and softer particles which deform during phagocytosis, rendering it an energy-inefficient process[42,133,135].

1.6.3. Charge

Positively charged LNP overcome natural barriers in gene therapy such as the extracellular environment, the cell membrane, the intracellular environment, and the endosome by taking advantage of their positive charge to associate with negatively-charged cell components. Genetic material is packaged and condensed into LNP for delivery via the electrostatic interaction between the positively charged lipid head group, and the negatively charged phosphate backbone of the nucleic acid[24,29,35,37,100,110,136]. This interaction should be strong enough to protect the genetic material from enzymatic degradation and immune recognition in the extracellular and intracellular environment, but should be weak enough for successful release of the genetic material inside the endosome[9,29]. LNP enter the cell because the cationic lipid component electrostatically interacts with the anionic membrane[29,94] (Figure 1.4). Once inside the cell, the LNP must escape the endosome and enter the cytosol before the fusion of endosomes with lysosomes, to prevent enzymatic destruction of the nucleic acid[116] (Figure 1.4). Pairing between the cationic lipid head group of the nanoparticle and the anionic phospholipid of the endosomal membrane neutralizes the charge on the nanoparticle, resulting in the disassociation of the nucleic acid, endosomal membrane destabilization and release of nucleic acid into the cytosol[33,35,119] (Figure 1.4).

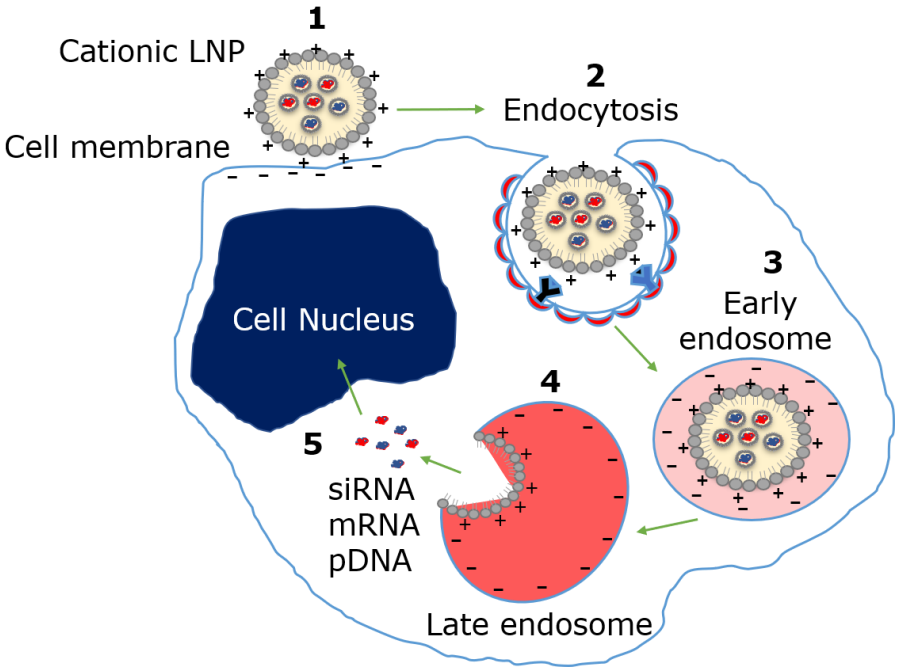

Figure 1.4 Delivery of genetic material by cationic lipid nanoparticles. 1) interaction between positively charged non-viral vector and negatively charged cell membrane, 2) internalization via endocytosis, 3) acidification of endosomes and destabilization of endosomal membrane, 4) escape of genetic material from endosome into the cytosol where siRNA/mRNA remain or 5) transport of DNA into the cell nucleus.

Alnylam Pharmaceuticals has manufactured Patisiran, the first RNA interference therapeutic loaded in a LNP approved by the FDA and EMA, for the treatment of hereditary transthyretin-mediated amyloidosis that causes neuropathy[11,99]. Patisiran is formulated with the ionizable cationic lipid DLin-MC3-DMA (pKa = 6.44), the most potent ionizable cationic lipid; LNP-RNA systems formulated with this lipid have an encapsulation efficiency close to 100%, very low median effective dose (ED50), increased RNA delivery, increased protein production and greater therapeutic effects[30,112,115,121,123,137].

1.6.4. Adverse Effects of Charge in Gene Delivery

A high cationic lipid content improves the transfection efficiency but can also be harmful. If the charge density of the LNP is too high, it stimulates pro-inflammatory Th1 responses after pulmonary administration[24,114,138], associates too strongly to the nucleic acid, which becomes too condensed and fails to dissociate from the nanocarrier[35] and it binds non-specifically to serum proteins that enhance its removal from the circulation[139,140]. The cell membrane can perceive the cationic charges as danger signals, which could ultimately activate pro-apoptotic or pro-inflammatory reactions[141]. The encapsulated nucleic acid may induce a potent innate immune response by acting as agonists of pattern

recognition receptors that sense non-self nucleic acids on the endosomal membrane[9,30,100,142].

Treatment of human alveolar epithelial A549 cells with cationic lipid Oligofectamine (OF) nanoparticles loaded with DNA was deleterious due to upregulated expression of genes involved in apoptosis and oxidative stress, and downregulated expression of genes related to cell growth, maintenance and proliferation. Rather than inducing the intended therapeutic changes in gene expression driven by the encapsulated DNA, off-target changes in gene expression also occurred[143].

These inadvertent toxic reactions can be attenuated by masking the cationic charges on LNP from the immune system with PEG-lipid coats. Inclusion of PEG into the LNP formulation reduces fluctuations in size, ensuring a high transfection efficiency[144]. Hu et al.[144] showed that internalization of PEGylated NP by DCs is much more superior to that of non-PEGylated NP, due to a uniform size distribution at the optimal size range of uptake by DCs. However, the repeated administration of PEGylated LNP induces "accelerated blood clearance": delivery of the first dose produces anti-PEG IgM such that administration of a second dose activates the classical complement pathway, which rapidly degrades the second dose[9,145,146]. If the PEG content is too high, uptake of LNPs decreases meaning cargo delivery is reduced and nucleic acid endosomal escape into the cytosol is hindered, making PEGylation a double-edged sword: it stabilizes NPs whilst also interfering with cellular uptabke by minimizing interaction between positively charged LNP and negatively charged cell membranes[101,114,144,147]. Therefore, acid-labile PEG-lipids should be used instead because at neutral pH the LNP is sterically stabilized but at acidic pH inside the endosomes it loses the PEG coat, allowing escape of the genetic material from the endosome[101].

1.7. Inhaled Delivery of Lipid Nanoparticles to the Lung

Administration of therapeutics by inhalation is an attractive route for non-invasive delivery due to: the lung's large surface area, high membrane permeability, extensive vascularization, poor enzymatic activity which delays metabolism of the drug such that it remains in the lung for prolonged period, absence of first-pass metabolism, minimal systemic and cytotoxic effects and better therapeutic effect at lower fraction of dose[108,114,148].

1.7.1. Inhalable aerosol formulations: properties and production

To exert therapeutic effects in the lung, the LNP must deposit locally, such as in the lower airways[32]. Particles will deposit on different pulmonary structures depending on their aerodynamic diameter, the diameter of a spherical particle with density of 1 g/cm^3 with the same setting velocity as the particle of interest[27,100,108,149]. Large particles (aerodynamic diameter > 5 μm) collide with the lung walls and deposit on bifurcations of the upper airways via impaction due to poor response to changes air stream; particles with aerodynamic diameter between 1-5 μm slowly deposit on bronchioles and alveoli via sedimentation due to gravitational forces where they remain for longer by avoiding mucociliary clearance[32,100,149,150]. As sedimentation is the best method for nanoparticle deposition, inhalation devices create aerosol droplets with aerodynamic diameter between 1.5-3.5 μm to make sure as much drug reaches and remains in the lungs as possible[150,151]. Small, light (aerodynamic diameter < 1 μm) nanoparticles deposit in alveoli by diffusion from a region of high to low concentration, but are easily exhaled due to low inertia[28,32,152].

For delivery, nanoparticles should be nebulised to produce inhalable liquid aerosols, or spray dried into inhalable microaggregates to distribute the LNP through the respiratory tract, to prevent their exhalation after inhalation and to promote deposition in the deep lung[153-155]. As a result, inhalation of cationic LNP loaded with nucleic acids as non-invasive gene therapy results in gene expression restricted to the respiratory tract[154,155].

Processing nanoparticles into inhalable aerosols or powders can change particle size, structure and stability and affect the dose delivered to and received by the patient due to shear stress[152,153]. Furthermore, long-term storage after processing can cause agglomeration of the nanoparticles which, when administered to the lung, may become more attractive to pulmonary clearance mechanisms, shortening half-life[152]. Stability and activity of the nucleic-acid loaded must be preserved during production, storage and delivery as inhaled LNP are vulnerable to elimination by protective mechanisms in the lung: pulmonary surfactant, the mucociliary escalator, secretory immunoglobulins and alveolar macrophages[156].

1.7.2. Drawbacks of Administering LNP by Inhalation

When LNP are inhaled into the lung, they are subject to physical and physiological obstruction due to the complex anatomy of the lung and immune defences that protect the lung from external insult[100,152,157] respectively. The progressive narrowing of the airways and decreasing thickness of the pulmonary walls with increasing airway bifurcations interfere with the deposition of LNP at the desired lung region[44,108]. Anatomical barriers and intrinsic pulmonary clearance mechanisms serve to protect the lung from injury therefore shorten the half-life, decrease the bioavailability and limit the therapeutic effects of inhaled nanomedicines[27,32,42,151,156].

As soon as the particles deposit in the lung, mechanisms for their destruction are initiated[40]. The deeper the particles are deposited, the longer they persist in the lung due to less and slower clearance mechanisms[42,100], thus the higher chance of interaction with the lung environment[158]. However, if the particles persist for too long and if they are present at high concentrations, they can cause injury due to the immune responses against them; these can be acute or chronic effects like fibrosis, and local or systemic effects such as oedema and inflammation[40,158,159]. If nanoparticles are small enough, they can enter the systemic circulation by translocation or diffusion through the thin and highly vascularized alveolar epithelium and the interstitium, which could have toxic systemic effects[27,32,100,108].

1.7.2.1. Upper Airways

When LNP enter the body, they interact with pulmonary fluids containing proteins and lipids that rapidly adsorb to their surface forming a corona that modulates the composition, size and surface charge of the LNP, affecting interactions with cells, their processing, clearance and deposition[138,160-162].

The upper airways, where gas conduction takes place, are kept sterile by the mucociliary escalator composed of a monolayer of ciliated epithelial cells and non-ciliated goblet cells that secrete mucus[27,32,108,148,159]. The impermeable mucus barrier traps the particles preventing their passage to the lower airways, and the cilia beat in order to sweep the mucus so it is coughed out or swallowed[10,27,100,150,163]. Most large insoluble particles are cleared through this mechanism[163]. The residence time of inhaled lipophilic nanoparticles increases the more they interact with pulmonary structures[108]. High mucoadhesion increases residence time in the lung as cationic LNP become immobilised when

they interact with the anionic mucus components; LNP should adhere to the mucus layer only for as long as necessary to be able to penetrate through the mucus layer to the underlying pulmonary epithelium where they exert their therapeutic effects[17,21,159,164]. High mucoadhesion can also increase the chances of nanoparticle clearance via the mucociliary escalator[17,159,164].

1.7.2.2. Lower Airways

The lower airways, where gas exchange takes place, are kept sterile by type II alveolar pneumocytes that produce lung surfactant containing SP-A and SP-D[26,100,108] which opsonise inhaled particles resulting in their internalization by alveolar macrophages[44,162]. They can then destroy the particles within their phagolysosomes or travel to the mucociliary escalator to be removed from the lung[32,150,159,163]. For every alveolus, there are 8-12 AMs, therefore the half-life of inhaled nanomedicines is just a few hours resulting in the need for more frequent administration of the therapeutic, which could result in patient malcompliance and suboptimal therapeutic effects[27,32,40,44]. If LNP agglomerate during storage or upon contact with pulmonary fluids, they can form micron-sized clusters which can increase the chances of being internalized by alveolar macrophages.

1.7.3. Avoiding Pulmonary Clearance Mechanisms

LNP are versatile nanocarriers that can be extensively manipulated to improve gene delivery in terms of biocompatibility and effectiveness to prevent unwanted cytotoxicity and to increase therapeutic effects. These therapeutics can be re-formulated to reduce as much as possible their interaction with innate protective mechanisms in the lung. Furthermore, residence time in the lungs should be maximised to allow the local therapeutic effects to occur when treating chronic lung disease like asthma and COPD[42].

Aerosolized LNP should be designed at an optimal size that allows them to penetrate into and sediment on the deep lung, but avoid recognition and uptake by alveolar macrophages, the dominant clearance mechanism in the deep lung and the most relevant lung defences to this review. The optimal size for phagocytosis is between 1-5 μm[124,165] so nanoparticles should have a size smaller than 1 μm or larger than 6 μm to passively evade interaction with alveolar macrophages and increase residence time in the lung[42].

Since flexible and easily-deformed LNP are less likely to be phagocytosed by alveolar macrophages, the outer layer of the LNP should integrate cholesterol to increase their fluidity and decrease their rigidity[42]. Furthermore, changing the shape of nanoparticles from a sphere to non-spherical shapes like rod, discs or cylinders makes them harder to be recognized and engulfed by alveolar macrophages[146]. Due to their low curvature, they resist uptake by alveolar macrophages because non-spherical shapes are not energetically favorable for membrane wrapping[27,42,44].

Apart from changing the physicochemical properties of LNP, the surface of LNP can be functionalized to avoid interaction with immune host cells. Coating LNP with high density PEG-lipids mask their mucoadhesive properties which allows them to diffuse through the mucosal barrier to the underlying epithelium and prevents their uptake by macrophages which lack surface receptors specific for PEG-lipids[17,42,146,164].

LNP can also be functionalized to actively target specific cell surface receptors without interfering with the pharmacokinetics of the LNP[29,114]. The surface of LNP used to treat cancers can be been modified through the attachment of tumour-specific ligands such as transferrin, folic acid, hyaluronic acid, biotin and anisamide[9,15,18,29]. Studies have shown that functionalized LNP achieved increased intracellular nucleic acid delivery and increased gene expression in cancer cells, reduced non-specific cytotoxicity to healthy lung tissue and minimized accumulation in other organs[9,16,18,29]. Magalhaes et al.[166] treated lung cells with mannosylated lipid NLC under submerged and pseudo air-liquid interface conditions for 24 hours and showed that this did not affect cell membrane integrity, cell morphology nor production and release of IL-1β, TNF-α and IL-8 in media; the NLC formulation was not cytotoxic or pro-inflammatory. Sansare, Warrier and Shinde[102] also showed that mannosylated rifampicin-loaded lipid NLCs had no cytotoxic effects on Raw264.7 cells and were internalized more efficiently than their non-mannosylated counterparts. Following internalization via receptor mediated endocytosis, mannosylated NLCs could be found inside the cell in the cytoplasm around the nuclei[102].

1.8. Research Objectives

As outlined, different non-viral gene therapy modalities are being explored as candidates to treat currently incurable lung pathologies. Amongst these candidates, LNP is an emerging one. The physicochemical properties of LNP

define their interaction with host cells therefore finetuning its formulation can enhance safety and efficacy of their delivery.

Extensive research has been done to develop lipid nanoparticles as vectors for drug and gene delivery but very little research has studied the immune responses to therapeutic inhaled LNP. So far, existing literature on the cytotoxicity and immunogenicity of inhaled lipid nanoparticles is incomplete, but there is evidence that changing physicochemical properties such as size, charge and geometry alters how they are perceived and interact with host cells. The gap in knowledge makes this technology important to explore as LNP have potential to treat life-threatening, debilitating chronic pulmonary diseases that still have no cure. Before investigating their potential as a medicine, it is valuable to analyse how LNP are perceived by the innate immune system in the lung, specifically alveolar macrophages which are the most abundant immune cell in the lung.

The objective of this study is to understand how LNP formulation, cargo and its cellular internalization pathway affect its processing by alveolar macrophages and if alveolar macrophages mount a local immune response against inhaled LNP. The experiments used LNP fabricated with an optimal formulation from the industrial partner, AstraZeneca[119]. The aims of this study were:

- To formulate LNP with SOPC which promotes membrane disruption and improves transfection efficiency [118]
- To use differentiated THP-1 cells as a useful cell line for initial experiments before using MH-S murine alveolar macrophages to understand the internalization process of LNP and if the internalized antigen stimulates activation of these phagocytes.
- To perform internalization kinetics studies where temperature was changed to investigate if uptake of LNP is an active (energy-dependent) or a passive (energy-independent) process.
- To perform internalization kinetics studies over a range of time periods to assess if LNP internalization was a fast or slow, linear or exponential process.
- To measure expression of activation markers following LNP treatment to assess whether the pathway of activation is pro-inflammatory or anti-inflammatory.

2. Materials and Methods

2.1. Materials

The ionizable cationic lipid (6Z,9Z,28Z,31Z)-heptatriaconta-6,9,28,31-tetraen-19-yl 4-(dimethylamino)butanoate (MC3) was synthesised by the Deuteration Facility of the Rutherford Appleton Laboratory. MC3 is stained with the hydrophobic lipophilic DiD red-shifted tracer that is insoluble in water thus only fluoresces once incorporated into lipid membranes. Cholesterol and 1,2-distearoyl-sn-glycero-3-phosphocholine (DSPC) were purchased from Avanti Polar Lipids. Dimyristoyl glycerol-polyethylene gycol (DMG-PEG) was purchased from NOF America Corporation. Roswell Park Memorial Institute (RPMI)-1640 cell culture medium with and without L-glutamine, penicillin-streptomycin solution, L-glutamine, 4-(2-hydroxyethyl)-1-piperazineethanesulfonic acid (HEPES), Dulbecco's phosphate buffered saline (PBS) with and without $MgCl_2$ and $CaCl_2$, phorbol 12-myristate 13-acetate (PMA), dimethyl sulfoxide (DMSO) and trypsin/ethylenediaminetetraacetic acid (EDTA) were purchased from Sigma-Aldrich and Gibco. Heat inactivated foetal bovine serum was purchased from Gibco and Life Technologies. Accutase was purchased from BioLegend. Formaldehyde was purchased from Thermo Fisher Scientific. LysoTracker™ Red DND-99 and CellMask™ Deep Red Plasma membrane Stain were purchased from Invitrogen. LPS-EB Ultrapure (LPS from E. coli 0111:B4, tlrl-3pelps) was obtained from InvivoGen. Fluorescently labelled for measurement of cell surface markers CD11b-AF488 (clone ICRF44), HLA-DR-BV711 (clone L243), CD83-BV421 (clone HB15e), and CD40-APC/Cy7 (clone 5C3) and anti-mouse Siglec-F-FITC (clone S17007L), CD64-BV421 (clone X54-5/7.1), CD11b-BV711 (clone M1/70), CD80-PE/Dazzle 594 (clone 16-10A1), CD86-BV650 (clone GL-1) and CD40-PE/Cy7 (clone 3/23) were purchased from BioLegend and CD86-PerCPeF710 was purchased from eBioscience. Fixable viability dye eFluor 450 and eFluor 455UV were purchased from eBioscience, and LIVE/DEAD™ Fixable Blue Dead Cell Stain Kit for UV excitation and LIVE/DEAD™ Fixable Violet Dead Cell Stain Kit, for 405 nm excitation were purchased from Invitrogen. The source of 4',6-diamidino-2-phenylindole (DAPI) and of CD54-PE are unknown.

2.2. Cell Lines and Cell Culture

THP-1 cells are monocytes derived from a male infant with acute monocytic leukemia (ATCC). MH-S cells are BALB/c alveolar macrophages immortalized by transfection with SV40. MH-S cells express T antigen that disrupts cell cycle control by binding and inhibiting the tumor suppressor proteins Rb and p53, thus

promoting cell cycle progression. MH-S cells are both adherent and non-adherent. THP-1 cells were grown in RPMI 1640 supplemented with 2 mM L-glutamine, 100 U/ml penicillin, 100 µg/ml streptomycin, 10 mM HEPES and 10% heat inactivated foetal bovine serum (FBS). As experiments with MH-S cells were done in a different laboratory to the THP-1 cells, they were maintained according to the protocol of that laboratory. MH-S cells were grown in RPMI-1640 supplemented with 10% FBS, 100 U/ml penicillin and 100 mg/ml streptomycin. Cells were grown in 5.0% CO_2 atmosphere at 37°C. Cell lines were cultured as advised by the ATCC.

2.3. THP-1 Differentiation

Two different differentiation protocols as well as experiments were done in two different laboratories, using THP-1 cells from different sources. Following the first protocol, THP-1 cells were plated at a concentration of 5 x 10^5 THP-1/ml in RPMI-1640 media (Sigma-Aldrich) supplemented with 10% FBS, 100 U/ml penicillin and 100 µg/ml Streptomycin in 6-well plates (Costar) in 5% CO_2 at 37°C. THP-1 were differentiated into macrophage-like cells with 25 nM PMA for 48 hours. For the resting phase, media containing PMA was removed after 48 hours and fresh RPMI 1640 media supplemented with 10% FBS, 100 U/ml penicillin and 100 µg/ml Streptomycin was added to all wells. THP-1 cells were incubated for another 24 hours.

Following the second protocol, THP-1 cells were seeded at a concentration of 1 x 10^6 per well of 6-well plates ml in Roswell Park Memorial Institute (RPMI) 1640 media (Sigma-Aldrich) containing 2 mM L-glutamine supplemented with 100 U/ml Penicillin, 100 µg/ml Streptomycin, 10 mM HEPES and 10% heat inactivated FBS and incubated in 5% CO_2 at 37°C. THP-1 were differentiated into macrophage-like cells with 8 nM PMA for 72 hours. For the resting phase, PMA-containing media was removed, and cells were washed with warm Dulbecco's PBS with calcium and magnesium. Fresh RPMI-1640 containing 2 mM L-glutamine supplemented with 100 U/ml Penicillin, 100 µg/ml Streptomycin, 10 mM HEPES and 10% heat inactivated FBS was added to all wells. THP-1 cells were incubated for another 24 hours in 5.0% CO_2 atmosphere at 37°C.

2.4. Plasmid

The ~3kbp pUC19 and the ~5kbp PMedVac (MedImmune, AstraZeneca) plasmid DNA encode the luciferase reporter gene.

2.5. Pre-Formulation Preparation

Before performing a wash, each dialysis tubing was cut into 40 cm lengths and rinsed with Milli-Q high purity water. A knot was tied on one end of each tubing and filled with water then emptied several times to ensure the inside was well-cleansed. The tubing was filled with water and kept inside a beaker of water. To prepare the sample, PMedVac3 plasmid (MedImmune, AZ) encoding the luciferase gene was added to 20mM pH 4 citric buffer (0.01 mg/ml) and the lipid mixture (MC3/Cholesterol/DSPC/PEG-Lipid = 50/38.5/10/1.5) was dissolved in ethanol.

2.6. LNP Formulation and Fabrication

The syringe pump used to generate the lipid nanoparticles was a Chemyx Fusion 400 (KR Analytical) as each pump can be controlled individually. Before injecting the prepared samples into the inlet streams, the system was rinsed first. Milli-Q® ultrapure water was fed through pump 1 and ethanol was fed through pump 2. After rinsing for a few minutes into the waste tube, the collection channel was rinsed by switching the flow. Ethanol-to-water ratio is 2:3 so the flow rate for ethanol is 4 ml/min and the flow rate for water is 6 ml/min. After rinsing the system, it was dried by running the flow empty with air circulating for around 4 minutes. 12 ml of plasmid sample was placed into a 20 ml syringe and 8 ml of lipid sample into another 20 ml syringe. Both samples were degassed by wrapping parafilm on the tip of the syringe, pulling out the syringe plunger and flicking the syringe a few times to remove the air to ensure reproducibility. The syringes filled with samples were set on their respective pumps. Dead volume was removed by running flow on each channel for a few seconds. Flow was started on both pumps at a flow rate of 4 ml/min for ethanol and 6 ml/min for water. The first 1.5 ml was disposed into the waste tube then the flow was diverted to the collection tube. A clear mixture means that the lipid nanoparticles produced are not big. The last 0.5ml of the mixture were also discarded.

2.7. Dialysis

Dialysis was performed as soon as the LNP sample was prepared, to remove ethanol and avoid changes in quality of the LNP formulation. The prepared lipid nanoparticle sample was poured in a pre-prepared dialysis tubing and a knot was tied in the free end. Dialysis tubing was left in a large beaker filled with 10 mM pH 7.4 PBS buffer. The dialysis PBS buffer was changed 1 h, 3 h, 12 h and 24 h after production. The buffer must be change continually to allow more contaminants to diffuse out of the sample, increasing the purity of the sample.

This process usually takes two days and the samples are collected on the third. The lipid nanoparticles were sterilized by filtration using a 0.2 nm filter. Lipid nanoparticles cannot be autoclaved as they are not stable at high temperatures. Centrifugation was performed to remove the buffer, any residual bacterial components from the plasmid and to concentrate the lipid nanoparticle sample to the required level.

2.8. LNP Uptake Kinetics by THP-1 and MH-S Cells

Cells were seeded into sterile 6-well plates at a concentration of 1 x 10^6 cells/well. THP-1 cells were differentiated as outlined above and MH-S cells were incubated at 37°C in 5% CO_2 overnight/24 h before treatment to settle down and attach to the plate. Cells were treated either with 2 ml of media containing 200 ng/ml LNP or with 2 ml of media containing 25 µg/ml fluorescein isothiocyanate (FITC)-bovine serum albumin (BSA) which is quickly and efficiently taken up by macrophage-like cells. These treatments were compared to untreated cells which were supplied with fresh complete media. The cold plate was left in the fridge at 4°C and the hot plate was incubated at 37°C in 5% CO_2 for 24 h. For THP-1 cells, these steps were repeated for other wells but instead were treated for 30 min, 1 h, 2 h, 4 h and 6 h. Wells were aspirated and washed with Dulbecco's PBS with $MgCl_2$ and $CaCl_2$. For detachment, cells were treated with accutase and incubated at 37°C in 5% CO_2 for 20 minutes. Media was added on top of the accutase to stop its enzymatic activity.

MH-S cells were treated with 2 ml of media containing 200 ng/ml LNP or with 2 ml of media containing 25 µg/ml FITC-BSA at 37°C in 5% CO_2 for 2 h, 6 h, 24 h and 48 h. 2 ml of media from each well was transferred into individual Falcon tubes as there are non-adherent cells in suspension. The cells attached to the wells were washed with Dulbecco's PBS with $MgCl_2$ and $CaCl_2$. The Falcon tubes with the non-adherent cells were centrifuged at 400 g at 4°C for 5 minutes to remove the antigens. After discarding the supernatant, PBS was added to resuspend the pellet and the tubes were centrifuged once more. 2 ml of fresh media was added to each tube to resuspend the pellet. PBS was aspirated from the wells and trypsin was added just enough to cover the wells. The plates were incubated at 37°C in 5% CO_2 for 2 minutes. The detachment process was monitored under the microscope and was aided by tapping the plate on the heel of the hand. Non-adherent cells in the Falcon tubes were transferred back to their respective wells on top of trypsin as the media neutralized the enzymatic activity. For both cell types, cell scrapers were used to further detach the cells. Cells from each well were transferred into tubes and Dulbecco's PBS with $MgCl_2$

and $CaCl_2$ was added up to 14 ml. THP-1 cells were centrifuged at 300 g 4°C for 5 minutes; MH-S cells were centrifuged at 400 g 4°C for 5 minutes. The supernatant was discarded and the pellets were transferred to sterile 96-well plates without being resuspended.

2.9. Staining of THP-1 and MH-S cells for Flow Cytometry

Cells were centrifuged for 5 mins at 4°C at 300 g (THP-1) or 400 g (MH-S). 200 µL of PBS at 4°C was added to all wells. For the Live/Dead control, 100 µL of cells was taken from a well and put into the heat block at 65°C for 5 minutes then put straight into ice for 30 seconds to 1 minute and transferred back to its well. The plates for each cell type were centrifuged again at their respective speeds for 5 minutes at 4°C and the supernatant was discarded. For THP-1 cells, the viability dye eFluor 450 was diluted 1000-fold with ice-cold PBS and 200 µl of the diluted dye was added to all wells. For MH-S cells, the LIVE/DEAD™ Fixable Blue Dead Cell Stain Kit for UV excitation was diluted 1000-fold with ice-cold PBS, and 50 µl of the diluted dye was added to all wells. The unstained control well was supplied with ice-cold PBS instead of the viability dye. For THP-1 cells, the plate was left on ice in the dark for 15 minutes then centrifuged at 300g 4°C for 5 minutes three times. For MH-S cells, the plate was left at room temperature in the dark for 10 minutes then centrifuged at 400g at 4°C for 5 minutes three times. Washing steps with ice-cold PBS were performed in between each centrifugation to make sure all unbound dye was removed. Cells were fixed with 4% paraformaldehyde (PFA) and left either on ice in the dark for 20 minutes or left at room temperature in the dark for 10 minutes. The plates were centrifuged at their respective speeds for 5 minutes at 4°C twice, with a washing step with ice-cold PBS in between each centrifugation. 100 µL of PBS was added to all wells and the cells were transferred from the plates to their own FACS tube containing 300 µl of ice-cold PBS. The tubes were left in the dark on ice until ready for flow cytometry. Cells were acquired using either the BD LSRFortessa flow cytometer or the BD FACSymphony flow cytometer operated by the BD FACSDIVA software (BD Biosciences) where 10,000 events or 50,000 events were recorded for each sample and data was analyzed using the software FlowJo 10.6.2 (TreeStar, Inc., Ashland, OR, USA).

2.10. ImageStream analysis

Cells were stained as described for flow cytometry except that the viability dye LIVE/DEAD™ Fixable Violet Dead Cell Stain Kit, for 405 nm excitation was diluted 500-fold with ice-cold PBS. Cells were run on the the ImageStream^X Mark II

imaging flow cytometer operated by the INSPIRE ISX software (Amnis Corporation, Seattle, WA, USA) where 10,000 events were recorded for each sample. To measure internalization, a mask was created to define the inside of the cell by eroding the mask, in this case by 6 pixels, from the brightfield cell image mask that covers the entirety of the cell, including the cell membrane. For LNP-treated cells, this feature is termed "LNP internal", and for BSA-treated cells it is termed "BSA internal". This feature is invariant to cell size. The intensity of DiD (LNP, ch 11) or FITC (BSA, ch 2) was measured within the eroded mask. The higher the value, the greater the signal coming from LNP inside the cell. Lower values mean little internalization or cell membrane attachment. The percentage of cells that internalized LNP was calculated as the percentage of "LNP internal" cells multiplied by the percentage of cells positive for DiD multiplied by 100. Data was acquired using the image analysis software IDEAS Application v6.2 (Amnis Corporation, Seattle, WA, USA) then exported to FlowJo 10.6.2 (TreeStar, Inc., Ashland, OR, USA) to be analyzed as flow cytometry data. Image processing was performed using NIH ImageJ software (Bethesda, MD).

2.11. Confocal Microscopy

THP-1 cells were seeded onto a µ-Slide 4 well glass bottom microscopy chamber (ibidi Cat#80427) at a concentration of 5 x 10^4 cells/ml, and 700 µl of cell suspension was added to each well. After differentiating the cells, 300 µl fresh media containing 200 ng/ml lipid nanoparticles and 300 µl fresh media containing 25 µg/ml FITC-BSA were added to their respective wells. The microscope chamber was incubated at 37°C in 5% CO_2 for 24 h. These steps were repeated for other wells but instead were incubated for 6 h. The wells were washed with PBS three times leaving 500 µl of PBS after the last wash. Media was removed only from the wells containing BSA-treated cells. CellMask Deep Red plasma membrane stain was diluted 2000-fold from the 5 mg/ml stock with ice-cold PBS and 500 µl of the diluted CellMask was added only to the BSA-treated cells. The microscope chamber was left in the fridge at 4°C for 5 minutes. Media was removed from all wells and only the wells containing BSA-treated cells were washed three times with ice-cold PBS. To fix the cells, 400 µl of 4% formaldehyde was added to all the wells and the microscope chamber was left in the fridge at 4°C for 15 minutes. After fixing, cells were washed three times with ice-cold PBS. DAPI was diluted 1000-fold to 1 µg/ml with ice-cold PBS and 250 µl of diluted DAPI was added to each well. The microscope chamber was left for 1-2 min in the dark. DAPI was removed from all the wells and they were washed three times with cold PBS, leaving 600 µl of PBS in each well after the last wash.

The microscope chamber was left in the fridge at 4°C until ready for confocal microscopy. Samples were visualized on a Leica SP8 Inverted confocal microscope (Leica) and image processing was performed using NIH ImageJ software (Bethesda, MD).

2.12. Measurement of THP-1 Activation Markers

Differentiated THP-1 cells were either stimulated with 200 ng/ml LNP or with 100 ng/ml LPS, as a positive control. The cells were incubated for 24 h at 37°C in 5% CO_2. Cells were harvested as explained in section 2.8, and stained for flow cytometry using the viability dye eFluor 455UV diluted 1000-fold with PBS. The Fc Receptor Binding Inhibitor Polyclonal Antibody (eBioscience) was diluted by 2-fold with ice-cold PBS and the plate was left on ice in the dark for 20 minutes. On top of the Fc block, cells were labelled in 40 µl brilliant staining buffer with combinations of the antihuman antibodies human leukocyte antigen – DR isotype (HLA-DR), CD11b, CD86, CD83, CD40 and CD54. Compensation beads and fluorescence-minus-one (FMO) samples were used to diminish background fluorescence and to correct for spillover. The mean fluorescence intensity for each sample was calculated subtracting the mean fluorescence intensity of the respective isotype control.

2.13. Measurement of MH-S Activation Markers

MH-S cells were seeded at a concentration of 3 x 10^6 cells/ml into two 60 mm TC-treated culture dishes, and at 8 x 10^6 cells/ml in one 100 mm TC-treated culture dish from (Corning). Cells were incubated at 37°C in 5% CO_2 overnight/24 h before treatment to settle down and attach to the plate. Cells in one of the 60 mm culture dishes were treated with 200 ng/ml LNP and cells in the 100 mm were treated with 100 ng/ml LPS and were compared with untreated cells in the remaining 60 mm culture dish. The cells were incubated for 24 h at 37°C in 5% CO_2 and were harvested as previously outlined. Unstained and single stained cells were incubated with 50 µL FcR Blocking reagent, mouse (Miltenyi) diluted by 100-fold with ice-cold PBS. Whole stained, FMO cells and the other flow cytometry controls were stained with 50 µL of a mastermix of the LIVE/DEAD™ Fixable Blue Dead Cell Stain Kit for UV excitation diluted 1000-fold with PBS, as well as the diluted Fc block. The plate was left at 21°C in the dark for 15 minutes. To wash, 100 µL PBA was added to all wells and the plate was centrifuged at 400 g for 5 minutes at 4°C. Antibodies were prepared with PBA at their respective dilutions and cells were labelled with their respective combinations of the anti-mouse antibodies Siglec-F, CD64, CD11b, CD80, CD86

and CD40. The plate was left at room temperature in the dark for 30 minutes. To wash, 100 µL PBA was added to all wells and the plate was centrifuged at 400 g for 5 minutes at 4°C. To fix the cells, 100 µL 4% PFA was added to all wells and the plate was left at room temperature in the dark for 15 minutes. The cells were washed twice with 150 µL PBA then resuspended in 200 µL PBA for flow cytometry. UltraComp eBeads compensation beads (Thermo Fisher Scientific) and FMO samples were used to diminish background fluorescence and to correct for spillover.

2.14. Statistics

Graphical presentations were made and statistical tests were performed as described in the figure legends using Graphpad Prism version 8.0.0 for windows (GraphPad Software, San Diego, California USA). Differences were considered notable when the p-value < 0.05. Data are shown as mean ± SEM and are expressed as median fluorescence intensity (MFI) or percentage of positive cells.

3. Results

3.1. Effect of temperature on the internalization of LNP by THP-1 cells

The first step in the study of internalization kinetics of LNP was to assess whether the uptake of LNP is an active/energy-dependent or a passive/energy-independent mechanism. A simple approach was to investigate the effect of temperature in the internalization process. Cells were incubated at 4°C because at this low temperature, all metabolic processes that require energy are inhibited or slowed down; therefore only passive diffusion through the cell membrane can occur [167]. However, the size of the LNP used is around 170 nm meaning they are too big to passively diffuse through the cell membrane. Therefore, any fluorescence produced from cells at this temperature should be from an extracellular source i.e, LNP bound to the cell surface. Internalization was also measured at 37°C as it is the average internal body temperature in humans; at this higher temperature, energy levels are high enough for active uptake. Untreated cells were incubated in the same conditions: any signal coming from these cells should be autofluorescence. THP-1 cells were incubated with Fluorescein isothiocyanate labelled bovine serum albumin (FITC-BSA) as it is well documented that BSA is readily internalized by macrophages[168-170].

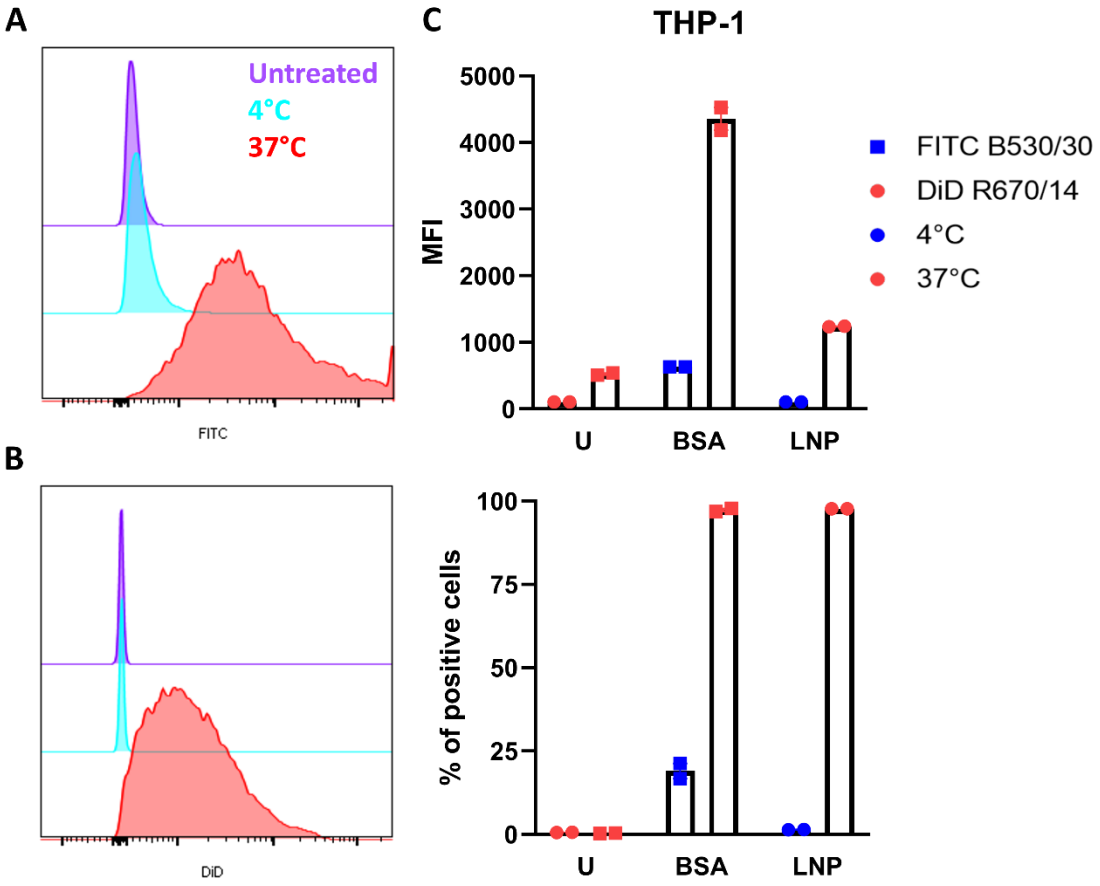

Figure 3.1 Measurement of uptake by THP-1 cells following treatment with BSA and LNP at 4°C and 37°C. THP-1 cells were treated with A) BSA and B) LNP at 4°C (blue) and at 37°C (red) for 24 h while untreated THP-1 cells were supplied with fresh medium and incubated alongside treated cells at 37°C for 24 h. Uptake was measured by flow cytometry. C) Treatment of THP-1 cells with medium (u), BSA (square) and LNP (circle) at 4°C and 37°C for 24 h where the upper panel represents the median fluorescence intensity of the dyes coming from the cells and the lower panel represents the proportion of cells that are positive for the fluorescent dyes. Data is representative of one experiment and symbols represent two technical repeats. A second experiment was done that produced similar results. No statistical tests were performed on this data due to insufficient data points.

After 24 h incubation at 4°C, the THP-1 macrophage-like cells did not internalize BSA or LNP (Figure 3.1A). Like untreated cells, BSA- and LNP-treated cells had little to no fluorescence originating from FITC and DiD labels as seen by the low MFI values (Figure 3.1A-C). FITC is a fluorophore with bright green fluorescence that is conjugated to BSA via the amine group. This fluorophore is commonly used to label proteins. DiD is a lipophilic red-shifted fluorophore that is insoluble in water thus only fluoresces once incorporated into lipid membranes. This fluorophore incorporates within the ionizable cationic lipid structures in the LNP.

While the percentage of cells positive for DiD were comparable to the values of untreated cells, around 20% of BSA-treated cells were positive for FITC fluroescence at 4°C, suggesting internalization was not completely inhibited (Figure 3.1C).

After 24h incubation at 37°C, a clear shift in fluorescence was seen for BSA-treated and LNP treated cells (Figure 3.1A-B). The increase in MFI and percentage of cells positive for FITC and DiD in BSA-treated cells and LNP-treated cells, respectively, at 37°C compared to at 4°C was notable (Figure 3.1C). Compared to 4°C, the MFI of LNP treated cells was around 12-fold higher and the MFI of BSA-treated cells was around 7-fold higher at 37°C (Figure 3.1C). The percentages of cells positive for FITC and DiD were close to 100% at 37°C, significantly higher than the percentages at 4°C (Figure 3.1C). These results are consistent with uptake of BSA and LNP by these cells, or at least with attachment to the cell surface, only at the higher temperature and not at the lower temperature. This suggests that internalization of LNP by these cells was energy-dependent.

3.2. Kinetics of the internalization of LNP by THP-1 cells

The second step in the study of the internalization kinetics of LNP was to assess the pattern of uptake. Internalization could either happen in phases, be a linear process where LNP are internalized consistently over time, or an exponential process where LNP are internalized at increasing rates over time. A simple approach was to treat cells with LNP for different time periods and then analyse the LNP location over time. In a preliminary experiment, differentiated THP-1 cells were treated with LNP and internalization was analysed after 6 h and after 24 h at 37°C using confocal microscopy (Figure 3.2). After 6 h of incubation with LNP, there was some internalization by THP-1 macrophage-like cells: the merged image shows DiD, the label for LNP, over the DAPI, which stains cell nuclei (Figure 3.2). After 24 h of incubation with LNP, the DiD fluorescence intensity was greater and the proportion of DiD over the DAPI in the merged image increased compared to the 6 h time point (Figure 3.2). These results show that the internalization, or binding to the cell membrane, of LNP by THP-1 macrophage-like cells increased over time.

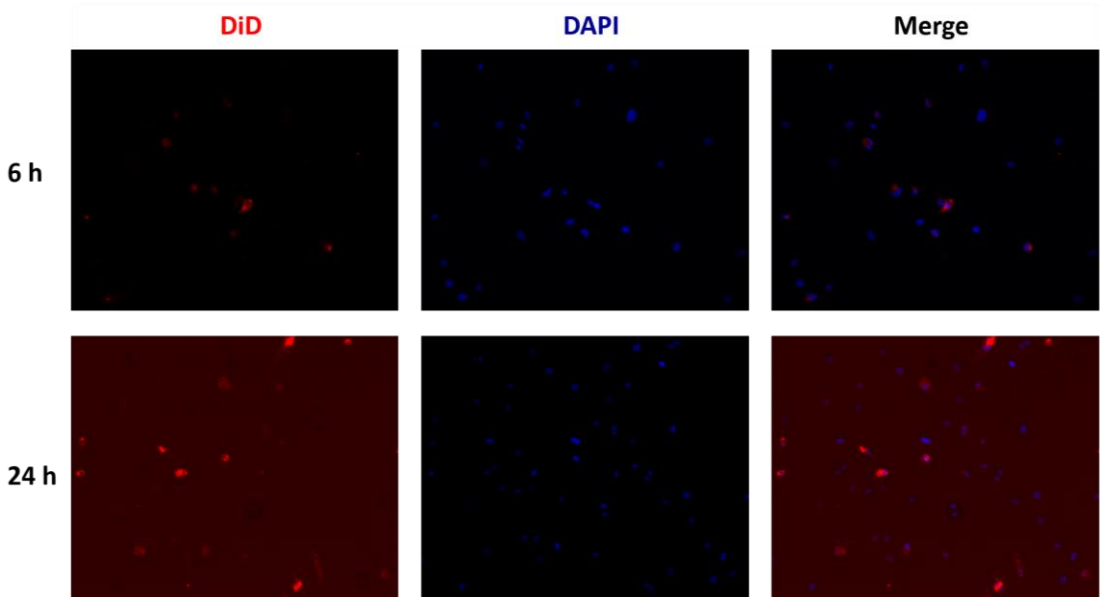

Figure 3.2 Visualization of LNP uptake by THP-1 cells with time. THP-1 cells were treated with LNP for 6 h (top row) and for 24 h (bottom row) at 37°C. Cells were analyzed by confocal microscopy to visualize the location of the LNP following treatment and to assess whether they were internalized. Red fluorescence originates from DiD, the dye labelling the LNP, and blue originates from DAPI which stains fixed THP-1 cells. Results are representative of one experiment.

To further explore the internalization kinetics by the THP-1 macrophage-like cells, the number of incubation time points was increased to be able to see more clearly when internalization initiates and at what point uptake is maximal. Past experiments with macrophages show that the internalization process starts in a matter of minutes and is over within 30 minutes, in some cases even less[171]. Existing literature has shown that cellular internalization increases with increasing incubation time therefore in this study, uptake was measured at different time intervals with an endpoint at 24 h where cells would be expected to have internalized approximately 100% of the LNP[172].

At 4°C, the antigens bound to the surface of the cell and were not actively taken up due to insufficient energy. Since there should not be any internalization of particles at this lower temperature, by subtracting the MFI at 4°C from the MFI at 37°C, the result should give us an indication of the signal of fluorescent particles coming only from inside the cells. Furthermore, subtraction eliminates any background fluorescence and makes the results reproducible and more reliable.

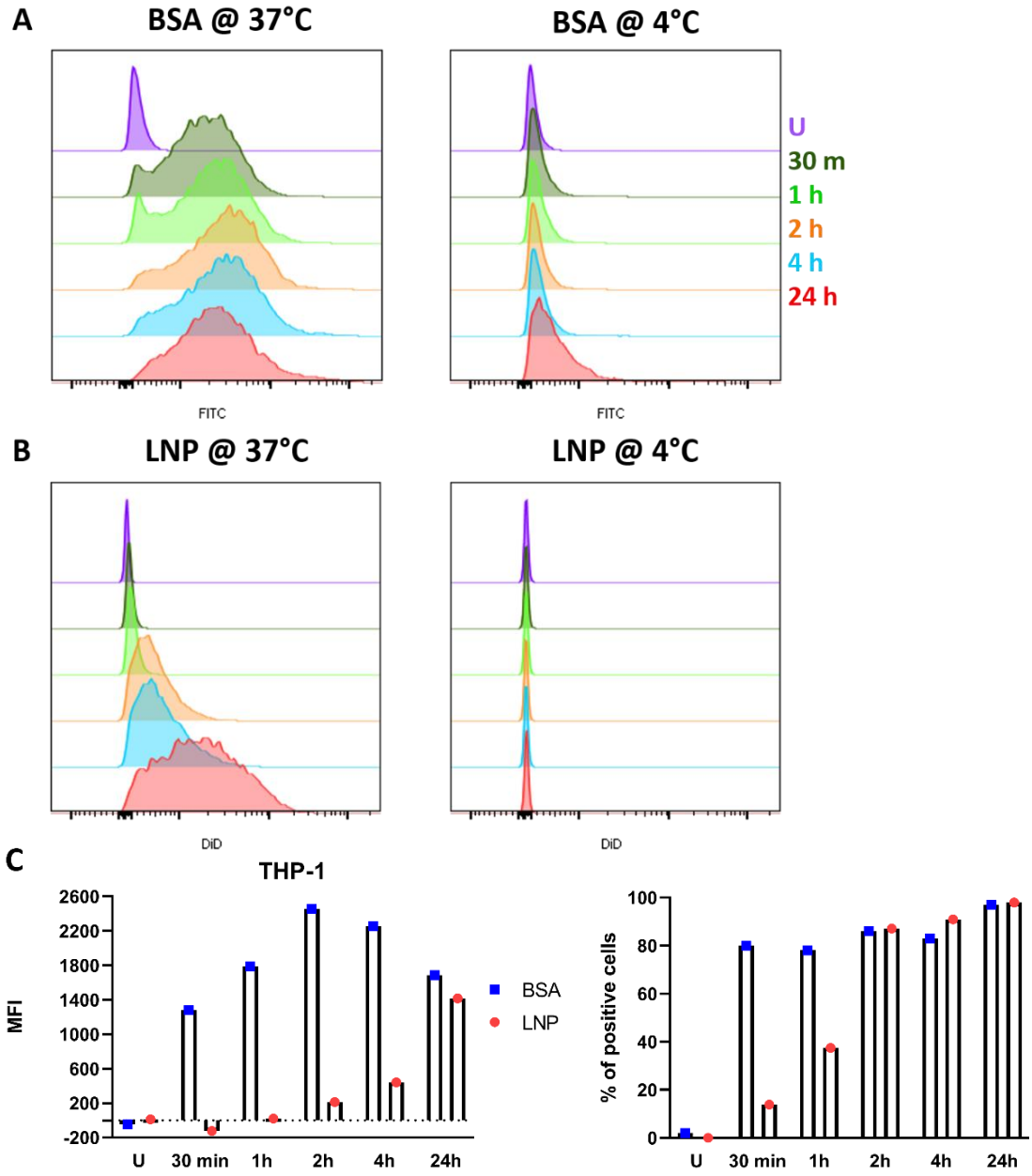

Figure 3.3 Uptake of BSA and LNP by THP-1 cells. THP-1 cells were treated with A) BSA and B) LNP for 30 minutes, 1 h, 2 h, 4 h and 24 h at 4°C and at 37°C while untreated cells were supplied with fresh medium and incubated alongside treated cells at 37°C for 24 h. Uptake was measured by flow cytometry. C) Treatment of THP-1 cells with medium, BSA and LNP over time, for 30 minutes, 1 h, 2 h, 4 h and 24 h, at 37°C where the left panel represents the median fluorescence intensity of the dyes coming from the cells and the right panel represents the proportion of cells that are positive for the fluorescent dyes. By subtracting the MFI at 4°C from the MFI at 37°C, the result should give an indication of the signal of fluorescent particles coming from the inside of the cell. Data is representative of one experiment and symbols represent one data point. No statistical tests were performed on this data due to insufficient data points.

At 4°C, both LNP- and BSA-treated cells did not fluoresce or had extremely low fluorescence in the DiD and the FITC channels, at all time points (Figure 3.3A-B). For all tested time points, the measurements of DiD fluorescence coming from LNP-treated cells were comparable to untreated cells (Figure 3.3B). Although the contribution was minimal, there was an increase in fluorescence for FITC-labelled BSA at 24 h (Figure 3.3A). A possible explanation for this is that at 4°C, energy-dependent processes in the cell are stalled; compared to the other incubation times, 24 hours gave the THP-1 cells enough time for the internalization process to begin such that some BSA was internalized (Figure 3.3A). Nevertheless, as expected, the overall conclusion from these results is that, even with increasing incubation time, cells did not internalize these antigens at 4°C.

At 37°C, internalization of BSA by THP-1 macrophage-like cells commenced and reached maximum uptake quite rapidly, in comparison to the internalization process of LNP (Figure 3.3A-B). By 30 minutes, FITC fluoresence from BSA-treated THP-1 cells was already high (Figure 3.3A) and most likely initiated as soon as the cells were incubated with BSA. In contrast to the untreated cells, whose fluorescence measurements were consistently low, the fluorescence measurements for BSA-treated cells increased over time (Figure 3.3C). The highest percentage of BSA-treated cells positive for FITC was 97%, and was seen after 24 h. However, the MFI reached a peak after 2 h then gradually decreased until the 24-hour time point (Figure 3.3C). This might indicate degradation of BSA after internalization (Figure 3.3C). Results further show that unlike LNP, the relationship between uptake of BSA by THP-1 and time was not linear ($F=0.06837$, $p=0.8107$) (Table 3.1).

The internalization of LNP was much slower than that of BSA. At the 30-minute and at the 1-hour time points, internalization was still negligible and DiD fluorescence coming from LNP-treated cells was comparable to that of untreated cells (Figure 3.3B-C). At 2 h, there was a marked increase in internalization of LNP (Figure 3.3B); between 2 h and 24 h, the MFI for DiD increased drastically (Figure 3.3C). Furthermore, the percentage of LNP-treated cells positive for DiD increased from 37% at 1 h to 87 % at 2 h (Figure 3.3C). The highest MFI and highest percentage of LNP-treated cells positive for DiD, which was 98%, was seen after 24 h (Figure 3.3C). However, the percentage of LNP-treated cells for DiD fluorescence peaked at 2 h and did not appear to increase in the following time points (Figure 3.3C). This possibly indicates that while the number of LNP internalized by the cells continued to increase over time and was maximal at 24 h, the proportion of cells internalizing LNP peaked and stagnated at 2 h (Figure

3.3C). Results further show that internalization of LNP by THP-1 cells over time was linear (F=57.72, p=0.0047) (Table 3.1).

Overall, these results show that the longer the cells were incubated with the antigens, the greater the proportion that internalized the antigens, and the greater the amount of antigen an individual cell internalized.

Table 3.1 Summary table for linear regression analysis of uptake of BSA and LNP by THP-1 cells

	BSA	LNP
Best-fit values		
Slope	-6.994	59.59
Y-intercept	1936	17.49
X-intercept	276.8	-0.2935
1/slope	-0.1430	0.01678
Std. Error		
Slope	26.75	7.843
Y-intercept	292.4	85.72
95% Confidence Intervals		
Slope	-92.12 to 78.14	34.63 to 84.55
Y-intercept	1006 to 2867	-255.3 to 290.3
X-intercept	24.97 to +infinity	-7.007 to 3.613
Goodness of Fit		
R squared	0.02228	0.9506
Sy.x	534.2	156.6
Is slope significantly non-zero?		
F	0.06837	57.72
DFn, DFd	1, 3	1, 3
P value	0.8107	0.0047
Deviation from zero?	Not Significant	Significant

3.3. Effect of temperature on the internalization of LNP by MH-S cells

THP-1 cells are used extensively in research as models of macrophages[49,173-177]. However, THP-1 cells are poor models of alveolar macrophages, which are tissue-resident immune cells, phenotypically distinct to classically and

alternatively activated macrophages. A better model for human alveolar macrophages are MH-S cells, which are murine alveolar macrophages. Therefore, the experiments done with THP-1 cells were repeated with this cell line for comparison. The internalization of LNP by MH-S cells was quantified using the ImageStream^X Mark II imaging flow cytometer by creating a mask defining the inside of the cell. This was done by eroding the brightfield cell image default mask covering the whole cell, including cell membrane. The fluorescence intensities of DiD (LNP) or FITC (BSA) were measured within the eroded mask, which was designated either LNP internal for cells treated with LNP, or BSA internal for cells treated with BSA. Higher values mean greater signal coming from LNP or BSA inside cell and lower values mean cell membrane attachment or little internalization.

The percentage of cells positive for fluorescence was calculated by multiplying the percentage of cells positive for DiD or FITC expression within the internal cell mask by the percentage of cells positive for DiD or FITC expression in total, then multiplying the product by 100. Since a positive fluorescent signal may come from any part of the cell, the result is supposed to represent only the cells that have internalized LNP and to exclude cells that have LNP attached to the cell membrane.

At 4°C, MH-S cells did not internalize LNP as shown by the negligible DiD fluorescence measured from LNP-treated cells, which was comparable to the MFI for DiD in untreated cells at both temperatures (Figure 3.4 B-C). This suggests minimal or no internalization of LNP. While only 20% of LNP-treated cells were positive for DiD at 4°C, there was a notable increase in percentage where nearly 100% of LNP-treated cells were positive for DiD at 37°C (Figure 3.4C). DiD fluorescence measurements for LNP-treated cells at 37°C were 10-fold higher, a notable increase, to that of untreated cells at 37°C and also to LNP-treated cells at 4°C, suggesting that LNP were indeed internalised by the MH-S cells (Figure 3.4B-C). These results are similar to those observed with the THP-1 cells (Figure 3.1B-C): while LNP can still attach to the cell membrane at the low temperature, it can only be internalized by the MH-S cells at the high temperature.

While around 100% of BSA-treated cells were positive for FITC at 37°C and had an MFI for FITC that was 4-fold higher than that of untreated cells at both temperatures, BSA-treated cells exhibited the same behaviour independent of the temperature (Figure 3.4A,C). There was no difference in MFI for FITC for BSA-treated cells at 37°C and at 4°C and around 100% of BSA-treated cells

were positive for FITC at 4°C, suggesting that the cold temperature did not inhibit internalization of BSA and internalization occurred at both temperatures.

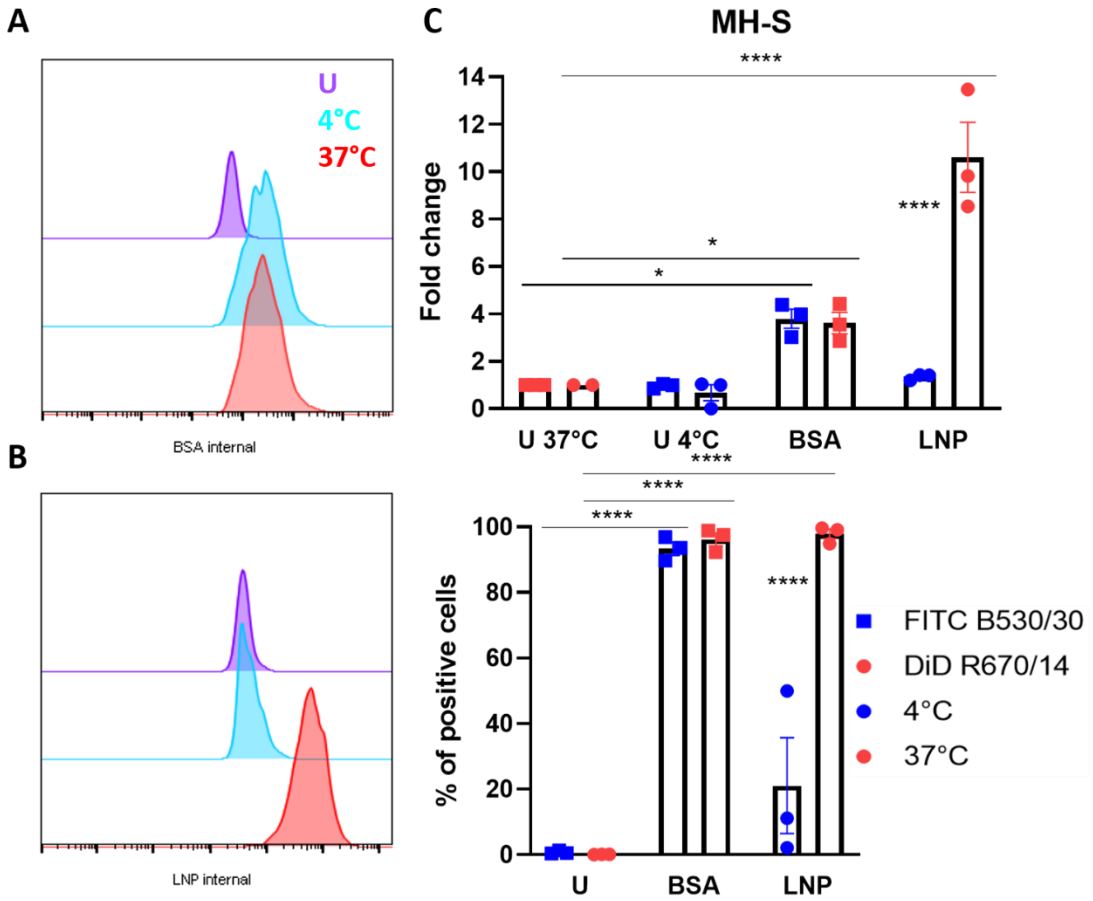

Figure 3.4 Measurement of uptake by MH-S cells following treatment with BSA and LNP at 4°C and at 37°C. MH-S cells were treated with A) BSA and B) LNP at 4°C and at 37°C for 24 h while untreated cells were supplied with fresh medium and incubated alongside treated cells at 37°C for 24 h. Uptake was measured by ImageStream imaging flow cytometry. C) Treatment of MH-S cells with medium, BSA (square) and LNP (circle) at 4°C (blue) and 37°C (red) for 24 h where the left panel represents the median fluorescence intensity of the dyes coming from the cells and the right panel represents the proportion of cells that are positive for the fluorescent dyes. Symbols represent biological repeats where each experiment had two technical replicates. Data was normalised against the control group of untreated cells (U) cultured at the normal cell culture temperature, 37°C, for 24 h. Mixed-effects analysis with Šídák's multiple comparisons test was used to compare between conditions (temperature) and Dunnett's multiple comparisons test was used to compare treatments with the control (untreated), *p<0.05, **p<0.01, ***p<0.001, **** p<0.0001, error bars show mean ± SEM.

Images of the cells were also acquired using the ImageStream to be able to locate the fluorescent particles following a 24-hour treatment at 37°C and at 4°C.

For LNP-treated cells, there was very faint DiD fluorescence coming from the cells at 4°C while for BSA-treated cells, FITC fluorescence seemed to be concentrated on the plasma membrane of the cell suggesting that BSA was attached to the cell membrane at 4°C (Figure 3.5). At 37°C, LNP-treated cells showed diffused fluorescent signal in the cytoplasm, suggesting that LNP were internalized but the bright punctate red dots close to the cell membrane suggest that some LNP remained on the surface and formed clusters (Figure 3.5). At 37°C, BSA-treated cells showed a diffuse fluorescence signal pattern for FITC on the cytoplasm, suggesting that BSA was internalized and localized to the cytoplasm (Figure 3.5).

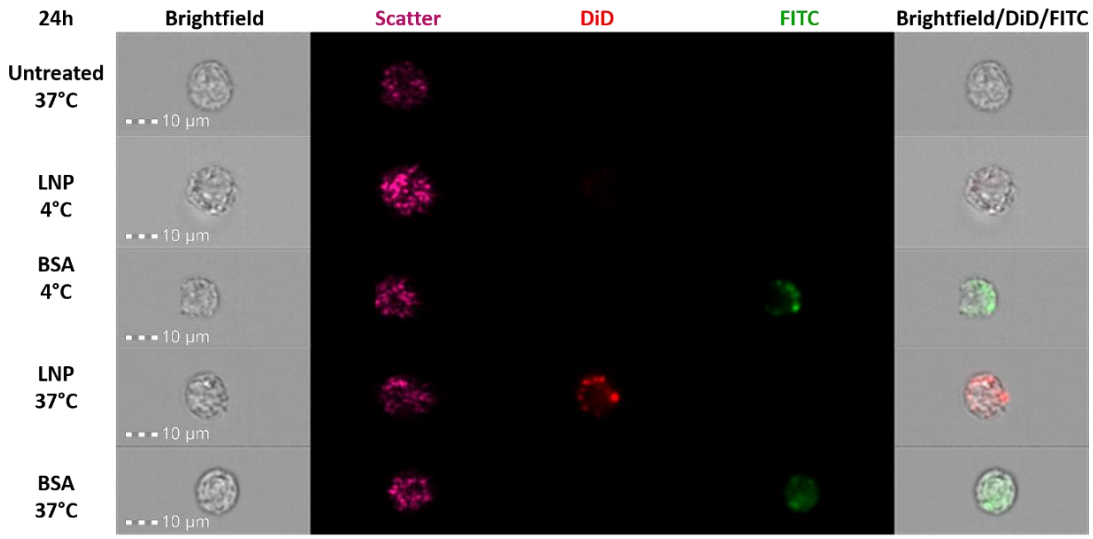

Figure 3.5 Sample cell images of internalized and surface bound LNP following treatment with BSA and LNP at 4°C and at 37°C. MH-S cells were treated with BSA (FITC, green fluorescence) and with LNP (DiD, red fluorescence) at 4°C and at 37°C for 24 h while untreated cells were supplied with fresh medium and incubated alongside treated cells at 37°C for 24 h. Images are representative of MH-S cells that internalized LNP or BSA and cells that bound LNP or BSA but did not internalize them. Columns 3–4 show LNP and BSA, respectively. The last column is a composite image of brightfield, LNP and BSA fluorescence demonstrating internalization. Images of MH-S cells were acquired using ImageStream imaging flow cytometer and are shown as one representative

3.4. Kinetics of the internalization of LNP by MH-S cells

Experiments with two different cell lines demonstrated that internalization was inhibited at 4°C, hence this experiment on internalization kinetics using MH-S cells was only performed at 37°C where uptake was shown to be high. As the percentage of THP-1 cells positive for LNP was high after 24 h, a 48-hour time point was added. Just as cells can take up material from extracellular sources,

they can also release intracellular material to the extracellular environment. Therefore, the 48-hour time point was added to assess whether fluorescence intensity remained high or diminished. A sustained, high fluorescence intensity could mean LNP were still bound to the surface or inside the cells. A decreased fluorescence intensity could mean LNP were released from the cell, were digested inside the cell, or detached from cell surface receptors after reaching saturation.

For LNP-treated cells, the MFI for DiD increased over time: from 2 h to 6 h, the MFI increased 2-fold and from 6 h to 24 h increased by over 2-fold (Figure 3.6B-C). From 24 h to 48 h, the MFI decreased slightly. However, LNP-treated cells showed an increased in MFI for DID of 4-fold from 2 h to 48 h (Figure 3.6C). The fold-change of MFI for DiD between 2 h and the 24 h and 48 h timepoints and between 6 h and the 24 h and 48 h timepoints was notable (Figure 3.6C). By 2 h, the percentage of LNP-treated cells positive for DiD was already at 70%, suggesting that the majority of the LNP were internalized within the very first hours. By 6 h, nearly 100% of LNP-treated cells were positive for DiD and the percentage increased to 100% at 24 h and 48 h (Figure 3.6C). Even though the percentage of cells positive for DiD reached 100% earlier, the MFI continued increasing which suggests that the same cells were still internalizing more LNP (Figure 3.6C). These results further suggest that internalization of LNP was gradual and increased over time (Figure 3.6B). Moreover, they are similar to the observations with THP-1 cells (Figure 3.3B-C): the longer the cells were incubated with the antigen, the greater the proportion of total cells that internalized the antigen, and the greater the amount of antigen an individual cell internalized. Similar to THP-1 cells, internalization of LNP by MH-S cells over time is linear ($F=16.37$, $p=0.0023$) (Table 3.2).

Unlike LNP-treated cells, the MFI for FITC in BSA-treated cells remained constant over time and was not stastitically significant nor significantly higher compared to untreated cells (Figure 3.6A-C). However, the percentage of cells positive for FITC increased over time (Figure 3.6C). In comparison to the previous experiments using THP-1 cells, the fluorescence measurements and proportion of treated cells positive for FITC were inferior to that of DiD (Figure 3.6A-C). These results suggest that the internalization of BSA reached saturation point very early on because internalization of BSA is very quick and occurs within the first minutes/hours. Perhaps BSA was released from the cell or degraded inside the cell earlier; at a later time point, such as 72 h, the MFI and percentage of cells positive for DiD could possibly start to decline in LNP-treated cells. At all time

points, the percentage of BSA-treated cells positive for FITC and percentage of LNP-treated cells positive for DiD were notable and significantly greater than that of untreated cells (Figure 3.6C).

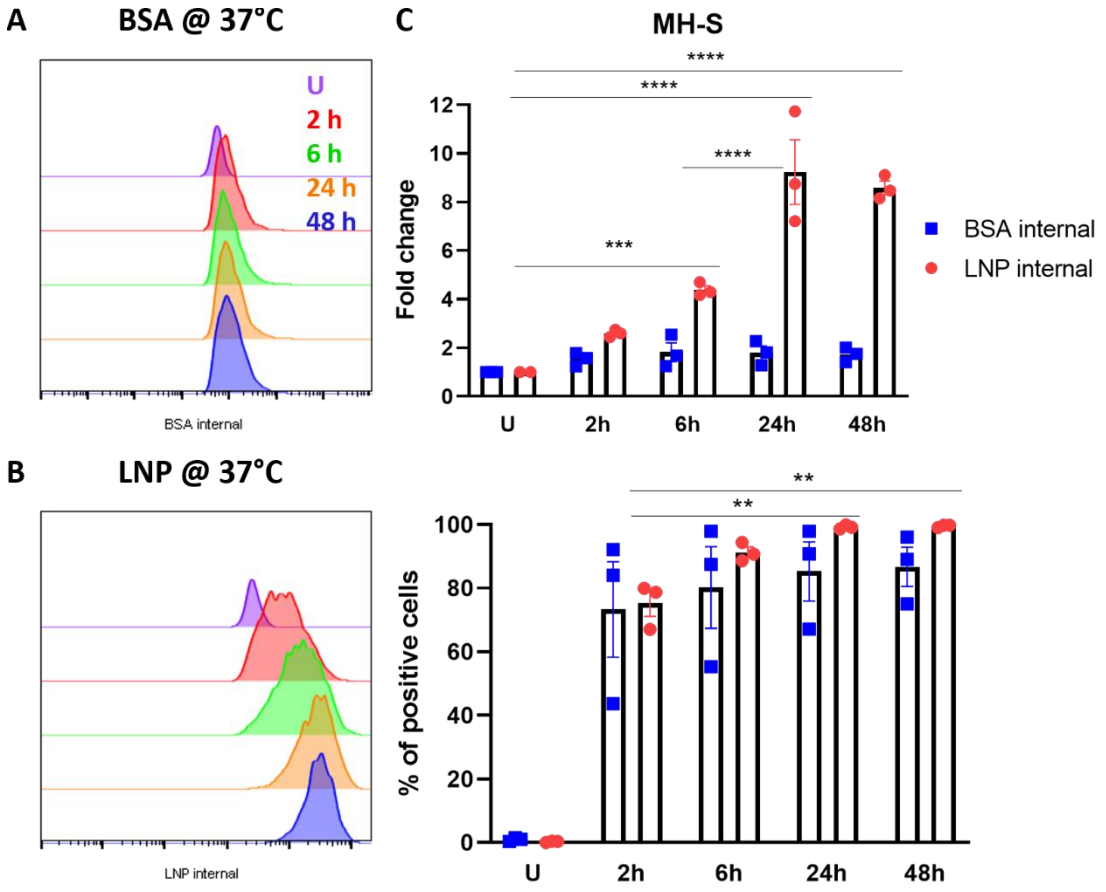

Figure 3.6 Uptake of BSA and LNP by MH-S cells. MH-S cells were treated with A) BSA and B) LNP for 6 h, 24 h, 48 h at 37°C while untreated cells were supplied with fresh medium and incubated alongside treated cells at 37°C for 48 h. Uptake was measured by flow cytometry. C) Treatment of MH-S cells with medium, BSA and LNP over time for 2 h, 6 h, 24 h and 48 h, at 37°C where the top panel represents the median fluorescence intensity of the dyes coming from the cells and the bottom panel represents the proportion of cells that are positive for the fluorescent dyes. Symbols represent biological repeats where each experiment had two technical replicates. Data was normalised against the control group of untreated cells (U) cultured at the normal cell culture temperature, 37°C, for 48 h. Mixed-effects analysis with Dunnett's multiple comparisons test was used to compare treatments with the control (untreated), and Tukey's multiple comparisons test was used to compare conditions (time) within treatments, *p<0.05, **p<0.01, ***p<0.001, **** p<0.0001, error bars show mean ± SEM.

Similar to THP-1 cells, there is no linear relationship between the uptake of BSA by MH-S cells and time (F=0.07347, p=0.7919) (Table 3.2).

Table 3.2 Summary table for linear regression analysis of uptake of BSA and LNP by MH-S cells

	BSA internal	LNP internal
Best-fit values		
Slope	0.001854	0.1281
Y-intercept	1.681	3.640
X-intercept	-907.1	-28.41
1/slope	539.5	7.806
Std. Error		
Slope	0.006838	0.03166
Y-intercept	0.1848	0.8555
95% Confidence Intervals		
Slope	-0.01338 to 0.01709	0.05755 to 0.1986
Y-intercept	1.270 to 2.093	1.733 to 5.546
X-intercept	-infinity to -79.08	-89.60 to -9.386
Goodness of Fit		
R squared	0.007294	0.6207
Sy.x	0.4303	1.993
Is slope significantly non-zero?		
F	0.07347	16.37
DFn, DFd	1, 10	1, 10
P value	0.7919	0.0023
Deviation from zero?	Not Significant	Significant

Images of the cells were also acquired using the ImageStream to see how the location of the LNP or BSA changed inside the cells over time. For LNP-treated cells, little to no DiD fluorescence was seen at 2 h then very dim DiD fluorescence started to appear near the cell membrane at 6 h (Figure 3.7). By 24 h and 48 h, fluorescence was bright and diffused in the cytoplasm while there were also some very bright dots of LNP clusters around the cell membrane (Figure 3.7). The images suggest that LNP bound to the cell membrane were internalized then spread into the cytosol over time (Figure 3.7).

For BSA-treated cells, FITC fluorescence was dim and localised to the borders of the cell at 2 h and 6 h (Figure 3.8). By 24 h, the FITC fluorescence was brighter and seemed to spread through the cell such that by 48 h, FITC fluorescence was diffused through the cytosol (Figure 3.8). Once again, the images suggest that BSA attached to the cell and was internalized quickly, then spread into the cytosol over time (Figure 3.8). The internalization of LNP is a linear process

whilst the internalization of BSA is not linear however Figure 3.7 and Figure 3.8 suggest both particles seem to behave similarly: they first accumulate in the cell membrane during attachment then diffuse throughout the cytosol following internalization.

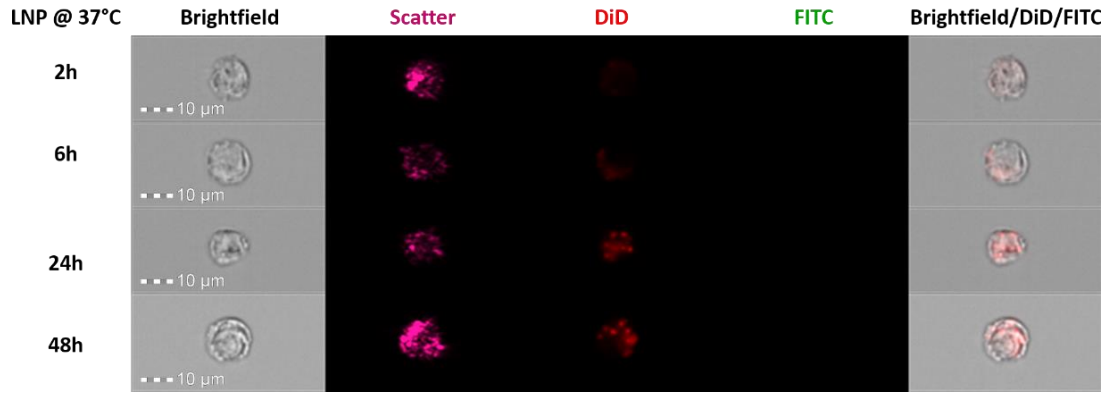

Figure 3.7 Cell images of internalized and surface bound LNP following treatment with LNP over-time. MH-S cells were treated with LNP (DiD, red fluorescence) at 37°C for 2 h, 6 h, 24 h and 48 h. Images are representative of MH-S cells that internalized LNP and cells that bound LNP but did not internalize them. Columns 3–4 show LNP and BSA, respectively. The last column is a composite image of brightfield, LNP and BSA fluorescence demonstrating internalization. As cells were not treated with BSA, no green fluorescence is expected to show on column 4. Images of MH-S cells were acquired using ImageStream and are shown as one representative experiment of three. 10,000 events were collected for each sample. Scale bars, 10 µm.

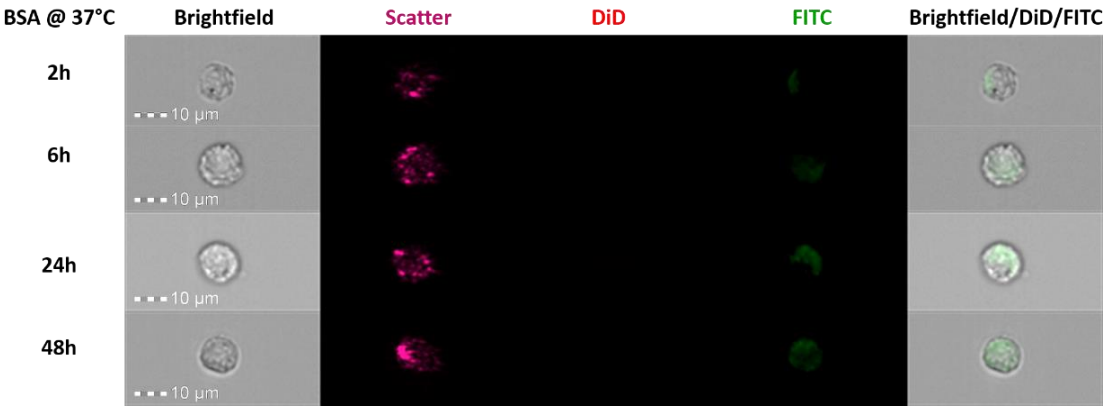

Figure 3.8 Cell images of internalized and surface bound BSA following treatment with BSA over-time. MH-S cells were treated with BSA (FITC, green fluorescence) at 37°C for 2 h, 6 h, 24 h and 48 h. Images are representative of MH-S cells that internalized BSA and cells that bound BSA but did not internalize them. Columns 3–4 show LNP and BSA, respectively. The last column is a composite image of brightfield, LNP and BSA fluorescence demonstrating internalization. As cells were not treated with LNP, no red fluorescence is expected to show on column 3. Images of MH-S cells were acquired using ImageStream and are shown as one representative experiment of three.

3.5. Effect of LNP treatment on activation state of THP-1 cells

Ideally, a drug should not change the macrophage population which otherwise could produce adverse side effects. To investigate whether LNP stimulate the expression of activation markers on the cell surface, differentiated THP-1 macrophage-like cells were treated with LNP and with LPS, a bacterial endotoxin that is also a well-known potent macrophage activator. Cells were incubated for 24 h at 37°C with LNP and LPS, then expression of cluster of differentiation (CD) surface markers of macrophage activation was measured by flow cytometry: CD11b, human leukocyte antigen DR isotype (HLA-DR), CD40, CD54, CD83 and CD86 (Figure 3.9 and Figure 3.10).

There are some important and notable observations to highlight regarading the differences between the MFI for LPS and LNP (Figure 3.9 and Figure 3.10). The MFI for CD11b in LNP-treated THP-1 cells was slightly higher than untreated cells, but slightly lower in LPS-treated cells (Figure 3.9A). Perhaps the basal expression was already high, so any stimulation did not significantly increase expression of CD11b. However, compared to untreated and LPS-treated cells, the percentage of LNP-treated cells positive for CD11b expression was higher (Figure 3.9A).

Only 24% of untreated cells showed positive expression for HLA-DR, which was very low compared to the percentage of cells positive for expression of other cell surface markers (Figure 3.9B). The results following LNP treatment were comparable to those of untreated cells (Figure 3.9B). This means that most cells expressed low levels of HLA-DR. The MFI for HLA-DR and the percentage of cells positive for HLA-DR was slightly higher after LPS treatment compared to untreated and LNP-treated cells (Figure 3.6B). Perhaps the basal expression of HLA-DR in THP-1 cells was already low and any stimulation only slightly increased its expression.

The MFI for CD40 after LPS treatment increased significantly while the MFI for CD40 in LNP-treated cells was comparable to untreated cells (Figure 3.9C). The percentage of cells positive for expression of CD40 was around 100% for all treatments (Figure 3.9C). While untreated and LNP-treated cells were positive for CD40 expression, LPS-treated cells upregulated CD40 expression. A similar trend was seen for the expression of CD54 but with a greater effect (Figure 3.9D). Due to the sensitivity to LPS and its highly immunogenic nature, exposure of cells to this bacterial stimulant resulted in strong upregulation of CD54

expression. Perhaps LNP stimulation wasn't enough to induce a cell-mediated response nor upregulation in activation markers important for immune responses.

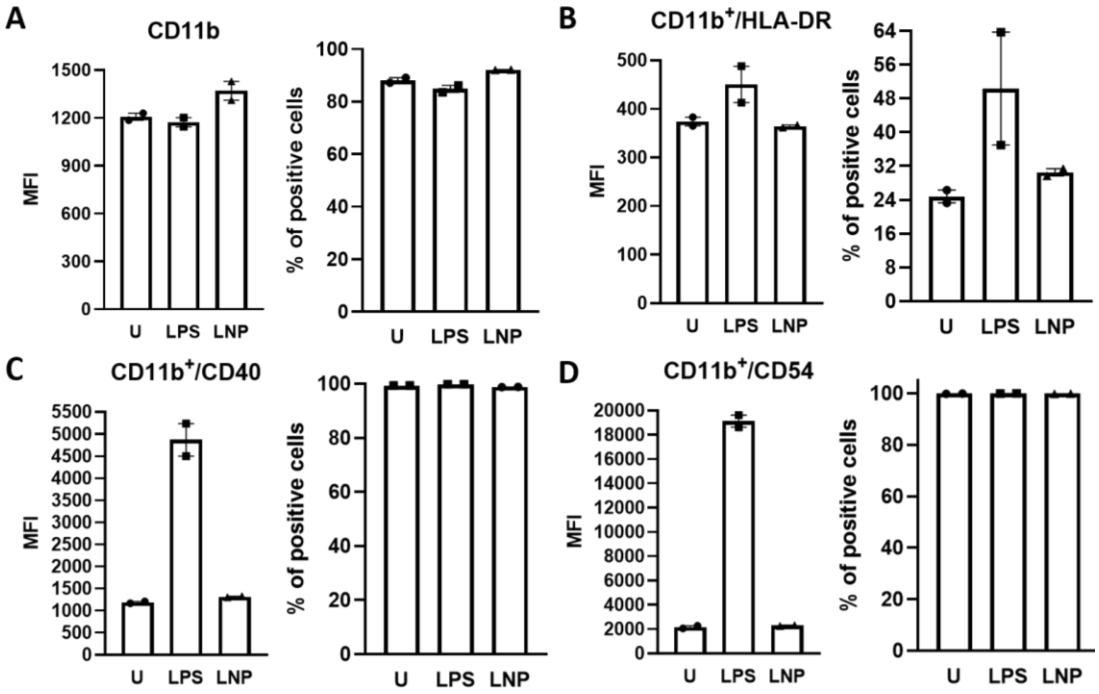

Figure 3.9 Measurement of expression of activation markers in THP-1 cells following treatment with LPS and LNP for 24 h. THP-1 cells were treated with LPS and LNP at 37°C for 24 h and were whole stained to assess activation of THP-1 cells by measuring the expression of the surface markers A) CD11b, B) human leukocyte antigen DR isotype (HLA-DR), C) CD40, D) CD54 by flow cytometry. The left panels represent the median fluorescence intensity of the dyes coming from the cells and the right panels represent the proportion of cells that are positive for the fluorescent dyes. Untreated cells (U) were supplied with fresh medium and incubated alongside treated cells. Data is representative of one experiment and symbols represent two technical repeats. No statistical tests were performed on this data due to insufficient data points.

LPS treatment slightly increased the MFI and percentage of cells positive for expression of CD83, compared to LNP-treated cells and untreated cells (Figure 3.6E). Nevertheless, expression of CD83 after all treatments remained quite low: only around 5% of untreated and LNP-treated cells were positive for expression of CD83 (Figure 3.10A).

While the MFI for CD86 and percentage of cells positive for CD86 in LNP-treated cells were comparable to that of untreated cells, they were lower in LPS-treated cells (Figure 3.10B). This unexpected effect was not seen for other markers;

supposedly LPS activates macrophages thus an upregulation in surface marker expression should be seen.

DiD fluorescence was measured in cells after all treatments to ensure that cells interacted with LNP. As expected, the MFI for DiD in LNP-treated cells was more than three times higher than untreated and LPS-treated cells and nearly 90% of LNP-treated cells were positive for DiD fluorescence (Figure 3.10C). High MFI for DiD in LNP-treated cells and high percentage of cells positive for DiD fluorescence, potentially mean that the cells internalized the LNP over the 24 h period.

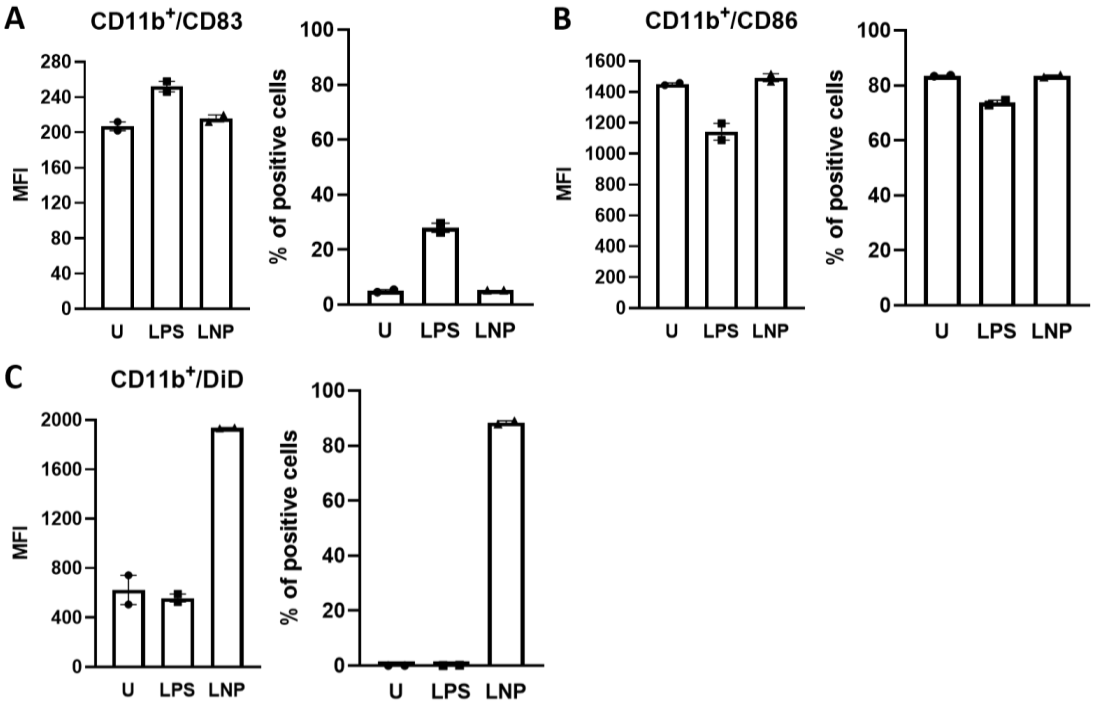

Figure 3.10 Measurement of expression of activation markers in THP-1 cells following treatment with LPS and LNP for 24 h. THP-1 cells were treated with LPS and LNP at 37°C for 24 h and were whole stained to assess activation of THP-1 cells by measuring the expression of the surface markers A) CD83, B) CD86 by flow cytometry. Internalization of LNP was once again assessed by measuring the fluorescence of G) DiD from treated cells. The left panels represent the median fluorescence intensity of the dyes coming from the cells and the right panels represent the proportion of cells that are positive for the fluorescent dyes. Untreated cells (U) were supplied with fresh medium and incubated alongside treated cells. Data is representative of one experiment and symbols represent two technical repeats. No statistical tests were performed on this data

3.6. Effect of LNP treatment on activation state of MH-S cells

Since MH-S cells are the better alveolar macrophage model, expression of activation markers were measured following stimulation with LNP and LPS for 24 h at 37°C. The cluster of differentiation (CD) surface markers measured by flow cytometry for this experiment were tailored to the expression profile of alveolar macrophages: CD80, CD86 and CD40 (Figure 3.12). Signature alveolar macrophage markers, sialic acid-binding immunoglobulin-like lectin F (Siglec-F), CD64, CD11b, were measured to evaluate their expression on the MH-S cell line (Figure 3.11). Most results were not notablebut there are some important observations to highlight.

LPS-treated and LNP-treated cells had comparable MFI values for Siglec-F (Figure 3.11A). Even though percentage of cells positive for Siglec-F in untreated cells was already extremely low, under 2%, treatment with LPS and LNP seemed to decrease expression further (Figure 3.11A). In general, expression of Siglec-F in MH-S cells was low, where around 1% of cells are positive for Siglec-F, or even negative (Figure 3.11A).

CD64 expression seemed to increase with treatment, expecially after stimulation with LNP, as seen by the increased MFI for CD64 in LPS-treated and LNP-treated cells compared to untreated cells (Figure 3.11B). As expected from alveolar macrophages, 100% of cells were positive for CD64 regardless of treatment (Figure 3.11B).

Alveolar macrophages supposedly have low to no expression of CD11b. While LNP treatment seemed to decrease CD11b expression, LPS treatment resulted in a drastic decrease in MFI for CD11b that was notable (Figure 3.11C). LNP treatment slightly increased while LPS treatment slightly decreased the percentage of cells positive for CD11b, compared to untreated cells (Figure 3.11C). In general, CD11b expression in MH-S cells was very low, where around 5% of cells are positive for CD11b (Figure 3.11C).

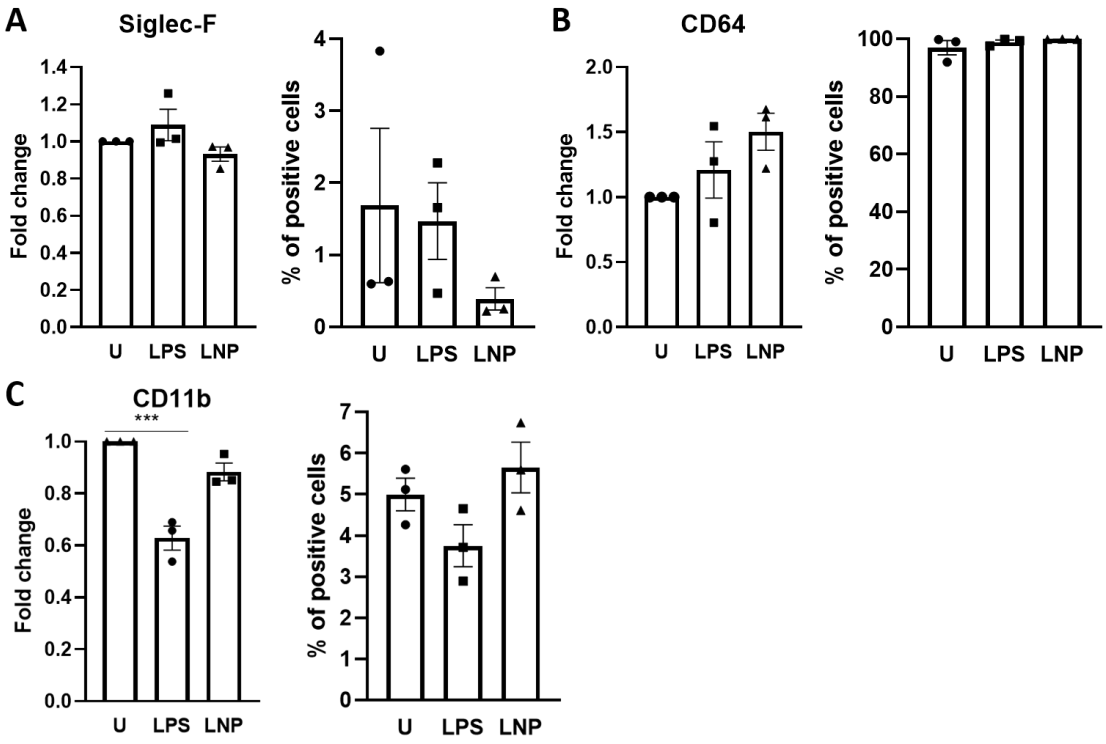

Figure 3.11 Measurement of expression of activation markers in MH-S cells following treatment with LPS and LNP for 24 h. THP-1 cells were treated with LPS and LNP at 37°C for 24 h and were whole stained to assess activation of THP-1 cells by measuring the expression of the surface markers A) Siglec-F, B) CD64, C) CD11b by flow cytometry. The left panels represent the median fluorescence intensity of the dyes coming from the cells and the right panels represent the proportion of cells that are positive for the fluorescent dyes. Untreated cells (U) were supplied with fresh medium and incubated alongside treated cells. Symbols represent biological repeats where each experiment had two technical replicates. Data was normalised against the control group of untreated cells (U) cultured at the normal cell culture temperature, 37°C, for 24 h. One-way ANOVA with Šídák's multiple comparisons test was used to compare treatments with the control (U), *p<0.05, **p<0.01, ***p<0.001, **** p<0.0001, error bars show mean ± SEM.

LNP and LPS treatment increased expression of CD80, CD86 and CD40 in MH-S cells (Figure 3.12A-C). While the increase was greater following LPS treatment, stimulation with LPS or LNP enhanced the MFI for CD80, and the percentage of cells positive for CD80 compared to untreated cells (Figure 3.12A). For CD86, LNP treatment had a greater effect on CD86 expression than LPS treatment. The increase in MFI for CD86 by 1.5-fold in LNP-treated cells compared to untreated cells was notable(Figure 3.12B). Following treatment, the percentage of CD86 in LPS-treated and LNP-treated cells was 100%, while around 80% of untreated cells were positive for CD86 (Figure 3.12B). Like CD80, treatment with LPS had

a greater effect on CD40 expression than LNP treatment, where MFI for CD40 was 3-fold higher than untreated cells following LPS sitmulation and 2-fold higher following LNP stimulation (Figure 3.12C). While around 70% of untreated cells were postive for CD40, nearly 100% of LPS-treated cells and 80% of cells were positive for CD40 where these increases were notable (Figure 3.12C).

While LNP was not as stimulatory as LPS, treatment with LNP still seemed to activate MH-S cells, as the surface marker expression profile of LNP-treated cells was more alike to that of LPS-treated cells than untreated cells (Figure 3.11 and Figure 3.12).

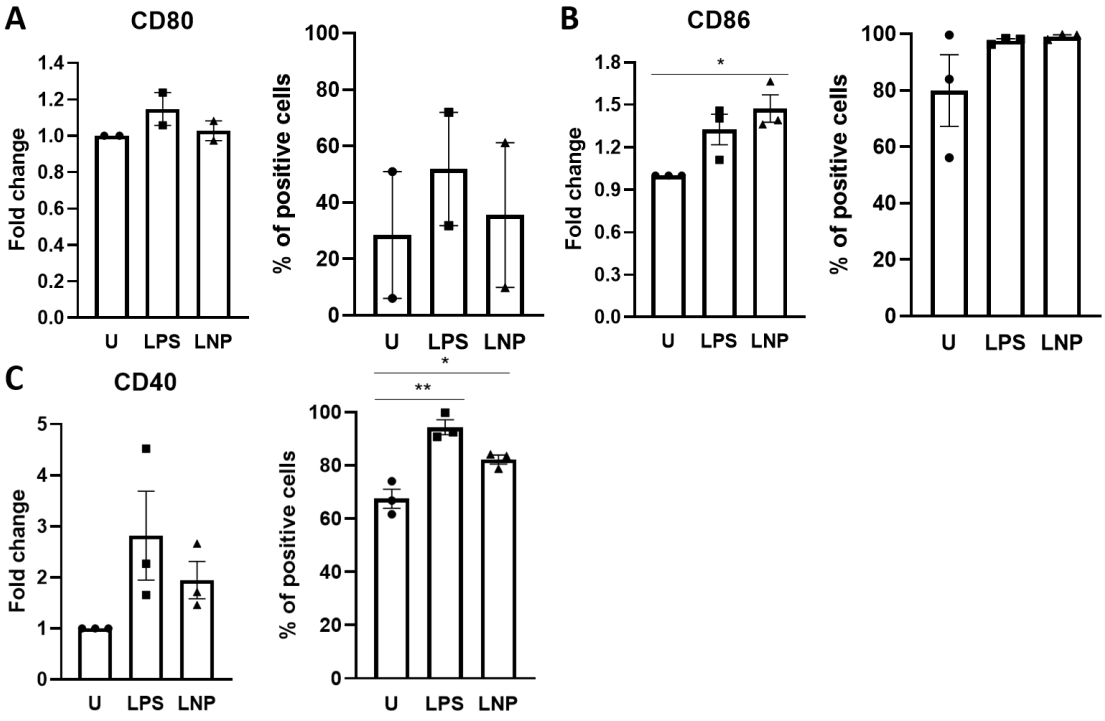

Figure 3.12 Measurement of expression of activation markers in MH-S cells following treatment with LPS and LNP for 24 h. THP-1 cells were treated with LPS and LNP at 37°C for 24 h and were whole stained to assess activation of THP-1 cells by measuring the expression of the surface markers A) CD80, B) CD86, C) CD40 by flow cytometry. The left panels represent the median fluorescence intensity of the dyes coming from the cells and the right panels represent the proportion of cells that are positive for the fluorescent dyes. Untreated cells (U) were supplied with fresh medium and incubated alongside treated cells. Symbols represent biological repeats where each experiment had two technical replicates. Data was normalised against the control group of untreated cells (U) cultured at the normal cell culture temperature, 37°C, for 24 h. One-way ANOVA with Šídák's multiple comparisons test was used to compare treatments with the control (U), *p<0.05, **p<0.01, ***p<0.001, **** p<0.0001, error bars show mean ± SEM.

4. Discussion

An important step in the development of lipid nanoparticles as gene delivery agents to the lung, is to investigate the interactions between lipid nanoparticles and the lung environment. This study focuses specifically on the interaction with alveolar macrophages because inhaled nanomedicines may deposit in the lower airways where alveolar macrophages reside, thus are highly likely to encounter them.

Preliminary experiments were performed *in vitro* using PMA-differentiated THP-1 cells as models of macrophages to understand how phagocytes perceived these particles. Cells were analysed using flow cytometry, due to its ability to isolate and sort cell types from a sample through specific cell markers; flow cytometry also facilitates cell quantification. First, to understand the process of internalization of LNP, THP-1 cells were incubated with LNP at a low temperature and at a high temperature. At temperatures below 10°C, the cell membrane becomes less fluid due to the rigid organisation and the restricted movement of the lipids in the bilayer, so extracellular material can only enter cells by passive diffusion[167,178].

At 4°C, the internalization of both LNP and BSA by THP-1 and MH-S cells was inhibited while at 37°C internalization was successful (Figure 1 and 3). Past studies on different cell lines with dendrimers[178], quantum dots[179] and pullulan nanoparticles[180] have also shown that at low temperatures (4°C), internalization of nanoparticles is inhibited, but at higher temperatures (37°C), internalization of nanoparticles is successful. Kim et al.[181] also showed that energy-dependent uptake of silica-coated magnetic nanoparticles by lung cells was impeded at 4°C but was enhanced at 37°C. Several studies have shown that nanoparticles generally enter cells via endocytosis[35,44,116,179]. As an energy-dependent process, endocytosis is sensitive to, and greatly affected by, changes in temperature[167,178,179]. Results from this study and existing literature suggest that internalization of LNP is an energy-dependent process. Figure 3.4 shows that internalization of BSA at 4°C was not inhibited; while the experiment was done at 4°C, processing and staining of cells for ImageStream is not at 4°C, meaning that during this lengthy process, the temperature control is not consistent such that the temperature increases and there is some internalization.

This experiment showed that uptake was temperature-dependent therefore the effect of time exposed to LNP on internalization was investigated. Confocal microscopy was performed as it helps elucidate whether the LNP were extracellular, attached to the cell surface, or intracellular. If the LNP had been internalized, confocal microscopy allows visualization of the subcellular localisation of the particles. A preliminary experiment with two time points, 6 h and 24 h, showed that the fluorescence intensity of DiD, representing the LNP, was higher in THP-1 cells after 24 h than after 6 h (Figure 3.2). To confirm these observations, a refined experiment with more time points was repeated in THP-1 and MH-S cells and showed that with increasing incubation time, the fluorescence intensity of DiD coming from the cells also increased. Zhang et al.'s[179] work with quantum dots using SPCA-1 human lung tumor cells also showed that cell uptake increases with incubation time. Like the LNP in our study, fluorescence intensity of the quantum dots was initially limited, but greatly increased after 2 h incubation[179]. Likewise, Zhang et al.[178] showed using MCF-7 breast cancer cells that fluorescence intensity of dendrimers increased intracellulary with increasing incubation time.

Like our results with THP-1 and MH-S cells (Figure 3.3 and Figure 3.6) and as shown in ImageStream images of MH-S cells (Figure 3.7 and Figure 3.8), Pandit et al.[182] showed that after 1 h of treating alveolar macrophages with an anionic lipid-drug conjugate nanoparticle incorporating the anti-tubercular drug isoniazid, NPs are initially found inside the cell localized at the cell membrane and by 4 h, the NPs disperse into the cytosol. By 24 h, NPs are found in endosomes where the *Mycobacterium tuberculosis* pathogen invades and settles[182]. Similarly, Berger et al.[175] show using lipid-based Neutraplex nanoparticles encapsulating siRNA that these nanopartiles were already being internalized after 30 minutes of treatment and were found in endosomes and lysosomes. By 1.5 hours, the NPs started to show diffusion of signal in the cytosol by escaping the intracellular compartments and by 24 hours, most NPs were found free and dispersed in the cytosol[175]. Barillet et al.'s[183] work with poly(lactic-co-glycolic acid) (PLGA) NPs showed that they are internalized by DCs within the first hours (about 75% after 3 h and 90% after 6 h) and by 24 h, high numbers of PLGA NPs are found in the cytoplasm of human and murine DCs. Results from this study and existing literature suggest that internalization of LNP is a relatively quick, but time-dependent process.

In Figure 3.6, 100% of MH-S cells were positive for DiD by 6 h, before the last time point at 48 h meaning that either the cell line is sensitive, or that the

concentration of LNP given to the cells is too high and that the system was saturated with LNP. In an *in vivo* setting, the number of LNP per macrophage would have to be limited in order to avoid over-exposing the cells with LNP.

Image analysis of the internalization process of LNP by MH-S cells showed that LNP appears as punctate dots (Figure 3.5 and Figure 3.7). These punctuate dots could either be individual LNP or clusters. The interaction between LNP and the cell membrane can result in clustering, which increases the rate of internalization since less energy is required for the uptake of clusters of NPs than individual particles[184]. Furthermore, existing literature has shown LNP appear similar to pHrodo bioparticles under the microscope – both appear as punctuate dots in bright and dim patches throughout the cell instead of a homogenous layer[185-187]. Cells possibly internalize both types of particles in higher concentrations . Just like LNP, the internalization of pHrodo bioparticles is high at 37°C but inhibited at 4°C[187]. ImageStream cannot accurately exclude the cell membrane like confocal microscopy can for measuring cellular internalization but the appearance of punctate dots in the cell images suggest that LNP were in fact internalized and located in an endocytic compartment from which it did not escape.

Past work has shown that while low temperatures inhibit active uptake processes, they do not affect attachment to the cell surface. Therefore, any fluorescence coming from the cell at lower temperatures is most likely from attachment of the nanoparticles to the cell membrane[178]. Zhang et al.[179] observed that nanoparticle internalization started with the attachment of the nanoparticles to the cell membrane followed by uptake into the cell. Similarly, Zhang et al.[180] showed that during the first few minutes of incubation, the fluorescence of cholesterol-modified pullulan nanoparticles was coming from the cell membrane. However, increasing incubation time resulted in a shift in fluorescence to the inside of the cells. This emphasizes that fluorescence intensity coming from the cell membrane, representing attachment, must be differentiated from fluorescence intensity coming from inside the cell, representing uptake[180]. This discrimination can be done and seen using confocal microscopy.

CD11b part of the integrin family is the α-chain subunit of the complement receptor 3 (CR3) expressed on the surface of macrophages and is involved in phagocytosis and cellular adhesion[188,189]. While undifferentiated THP-1 monocytes do not express CD11b, differentiated THP-1 macrophage-like cells highly upregulate CD11b expression[188,189]. Untreated differentiated THP-1 cells

showed positive expression for CD11b, and expression levels remained unchanged after treatment with LPS and LNP (Figure 3.9A). Forrester et al.[190] compared expression of markers on the surface of THP-1 monocytes and differentiated THP-1 macrophage-like cells, and showed that following LPS stimulation, CD11b expression significantly decreased on THP-1 macrophage-like cells[190]. In contrast, LPS stimulation upregulates the expression of CD11b on the surface of neutrophils and monocytes[191-193].

Siglec-F is expressed mostly on the cell surface of alveolar macrophages; it is a marker of this resident cell population and is frequently used with CD11c or CD64 to isolate alveolar macrophages from lung samples[194]. In this study, MH-S cells did not express Siglec-F, even after stimulation with LPS or LNP, and while no expression of CD11b was expected[195], MH-S cells showed some expression of CD11b with and without stimulation (Figure 3.11A,C). The surface marker profile of the MH-S cell line differs from alveolar macrophages: they do not express Siglec-F and they exhibit heterogeneous expression of CD11b where only a small percentage of MH-S cells express CD11b[194,196].

CD64, mostly known as Fc-gamma receptor 1 (FcγRI), binds monomeric IgG with high affinity, is constitutively found only on macrophages and mediates phagocytosis[197]. In this study, all MH-S cells expressed CD64 and following stimulation with LPS and LNP, expression per cell was upregulated (Figure 3.11B). Similar findings in Misharin et al.'s[198] study showed that during the acute phase of bleomycin-induced lung injury, mouse alveolar macrophages upregulated the expression of CD64. Furthermore, during the fibrotic phase a new subpopulation of alveolar macrophages expressing low levels of Siglec-F exhibited higher CD64 expression than alveolar macrophages expressing high levels of Siglec-F[198]. The higher expression of CD64 could be due to alveolar macrophages migrating into the lung, or proliferating in the lung, to adopt wound-healing properties. Another explanation could be that by upregulating CD64, alveolar macrophages contribute to fibrosis due to their phagocytic abilites.

HLA-DR is a major histocompatibility complex II molecule involved in antigen presentation and T cell activation. Past work has shown conflicting results where some show that differentiated THP-1 cells have low to no expression of HLA-DR[188,190] and others show that, upon differentiation, THP-1 cells upregulate the expression of HLA-DR[199]. This work showed that, regardless of the treatment, the MFI for HLA-DR was consistently the second lowest amongst all cells. The

reason for the inconsistency of HLA-DR is that its expression is not constant, it is always fluctuating.

CD83 and CD86 are costimulatory molecules expressed by antigen-presenting cells involved in T cell activation; as they are more highly expressed by dendritic cells (DCs), they are considered DC activation markers. CD80 and CD86 regulate innate and adaptive immune responses and are necessary for full T-cell activation. While Tsukumo et al.[200] and Miyazawa et al.[201] showed that LPS stimulation strongly upregulated CD86 expression, Riddy et al.[199] showed that differentiated THP-1 cells did not express CD86. In accordance with our results, past work has also shown that the MFI for CD86 and for CD83 in LPS-treated cells were not statistically different to cells treated with medium[202]. Moreover, MFI for CD83 was higher and MFI for CD86 was lower for LPS-treated cells compared to cells treated with medium, as was shown in our experiment[202].

Miyazawa showed that untreated THP-1 cells showed virtually no expression for CD83 but, unlike our work, untreated THP-1 cells had low CD86 and CD40 expression and barely expressed CD54[201]. CD40, part of the tumor necrosis factor (TNR) receptor family, is a costimulatory molecule expressed on macrophages involved in macrophage activation[201]. Binding of CD40 ligand to CD40 upregulates the expression of CD86 and CD54[201], also called intracellular adhesion molecule-1 (ICAM-1) expressed on the surface of macrophages[188]. LPS stimulation has been shown to highly upregulate the expression of CD54 in cells, including THP-1 cells[188,200,203-205]. In accordance with our results, expression of CD40 and CD54 was highest, while expression of CD83 was lowest after LPS stimulation, based on fluorescence measurement[201]. These differences in marker expression after LPS stimulation could be due to the use of different LPS concentrations. While Miyazawa et al.[201] used an LPS concentration of 10 µg/mL, this experiment used a concentration of 100 ng/ml; perhaps that could affect the lack of CD86 upregulation in our study.

While LPS is able to induce and upregulate expression of CD80 on MH-S cells, LNP do not induce CD80 expression, as its MFI values are comparable to that of untreated cells. However, both LNP and LPS stimulation upregulated expression of CD86 and CD64. These results correspond to several existing studies that treated APCs with different nanoparticle formulations. Coolen et al.[206] showed that following internalization of mRNA-loaded polylactic acid nanoparticles, DCs exhibited upregulation of CD80, CD86 and CD40 expressing after 24 h and that the nanoparticles promoted DC maturation. Chavez-Santoscoy et al.[207] showed

that polyanhydride nanoparticles caused alveolar macrophage activation due to an increase in MFI of CD40 and CD86 following a 48 h treatment. Blank et al.[208] intranasally instilled polystyrene nanoparticles into BALB/c mice and saw that following internalization, expression of CD40 and CD86 was increased in all DC populations independent of particle size. Furthermore, they showed that most particles were internalized by alveolar macrophages irrespective of size and that uptake of polystyrene particles also increased costimulatory marker expression in alveolar macrophages, but to a lesser extent than DCs[208]. Hardy et al.[195] intratracheally instilled polystyrene nanoparticles with diameters of 50 nm and 500nm into naïve mice and found that both types of nanoparticles decreased the population of alveolar macrophages. Smaller nanoparticles were internalized to a greater extent than the larger ones and enhanced expression of CD40, CD80 and CD86 in lung DCs and macrophages, especially ones that had internalized a higher number of particles[195]. Furthermore, CD86 upregulation was positively correlated with number of internalized particles[195]. Barillet et al.[183] incubated DCs with PLGA nanoparticles and that following internalization of nanoparticles, DCs showed enhanced expression of the surface maturation marker CD83, and costimulatory molecules CD40, CD80, CD86.

Just like LPS, in all the studies mentioned above, treatment of APCs with these different nanoparticle formulations induced not only increased expression of co-stimulatory molecules but also stimulated production and release of pro-inflammatory cytokines and chemokines[209]. These pro-inflammatory cytokines and chemokines include IFN-α, IFN-β, IL-1ß, IL-6, TNF-a, CXCL10, CCL5, IL-8 which in turn induced an activated state in APCs and enhanced DC recruitment and maturation[183,195,206]. While the nanoparticles themselves might not be cytotoxic, parts of the formulation such as surface ligands or encapsulated nucleic acid might trigger activation[183,206].

LPS had profound effects on surface expression of co-stimulatory molecules in both THP-1 and MH-S cells but the surface marker expression profile of LNP-treated cells was very similar to that of untreated cells in THP-1 cells (Figure 3.9 and Figure 3.10). However, while not as stimulatory as LPS, LNP induced mild activation and initiated some kind of immunogenic response in MH-S cells (Figure 3.11 and Figure 3.12). As a gene delivery vector, LNP should not inadvertently stimulate host cells. Further studies will have to be conducted to investigate their functional impact on alveolar macrophages.

Analysis of how nanoparticles influence phagocytic cells should be taken with caution if cell lines are used, as they do not replicate all features of primary cells in vivo. Alveolar macrophages are regulated by the lung microenvironment and adopt a wound healing phenotype so they possibly might internalize LNP as they would internalize dying cells and extracellular matrix components. However, studies show that alveolar macrophages are poorly phagocytic and do not respond unless there is some structural damage. In this context LNP uptake may be negligable.

Although shelf-life has not been described in this report, we did observe fluctuations in LNP MFI values across experiments with MH-S cells, indicating that LNP are unstable. Using the same batch of LNP over a few months resulted in a deterioration in MFI values for DiD, whilst using new batches of LNP every two weeks maintained high MFI values. It is therefore difficult to reach firm conclusions on the experiments performed as two different cell lines were used sequentially and so alterations may reflect product degradation rather than a difference in sensitivity of each cell type. Future experiments should compare cell lines at the same time.

Another limitation is that BSA is not a good control for LNP. BSA is a protein with a high molecular weight and FITC is a fluorophore also with a high molecular weight. As a result, the reliability of BSA as a control is questioned because the MFI measurements may have been size-related, rather than related to internalization by the cells. Because of this, BSA could have even interfered with the experiments.

To be able to truly compare, good controls should be the same size or at the same concentration as the variable being measured. BSA is not the same size as LNP and the concentration of BSA, which was 25 µg/ml, was much higher than the concentration of LNP, which was 100 ng/ml, used in these experiments. Due to their size differences, the uptake of BSA and LNP by cells are likely to be different: BSA is taken up by phagocytosis and LNPs are taken up by endocytosis. Alternative controls should include empty or unlabelled LNP, LNP loaded with a TLR agonist which we would expect to stimulate macrophages, or LNP loaded with heparin. Heparin is an anionic glycosoaminoglycan produced by cells that exerts anti-coagulant and anti-inflammatory effects, and that polarizes macrophages towards the M2 phentoype. Therefore we would expect LNP loaded with heparin to attenuate inflammation.

The temperature experiments were based on oral temperature, due to the presumption the therapeutic would be inhaled through the mouth. However, the therapeutic can also be inhaled through the nose, where the temperature is around 33°C. The cooler temperature of this route of administration should also have been taken into account in these experiments, to assess which route of administration has conditions that are optimal for delivery of the therapeutic.

Other considerations include the differences in origin of the THP-1 cells and MH-S cells and their analysis using different flow cytometers. The handling procedures and laser intensity of the flow cytometer has a significant impact on the brightness of fluorescence (the mean fluorescent intensity). Therefore, future analysis should use the same flow cytometer with identical acquisition events.

Any *in vitro* method is likely to have limitations as the culturing conditions do not mimic the natural environment of the lung. To better study the fate of the LNP once they enter the lung, alveolar macrophages would be a more relevant option. Extracellular matrix component substrates may also be included in the culture with alveolar macrophages to mimic the lung microenvironment. However, a more recent lung culture system, lung organoids, overcome technical limitations of 2D culture systems[210]. A lung organoid is essentially a 3D human lung tissue made from hydrogels, mimicking the extracellular matrix, and induced pluripotent stem cells or human adult lung stem cells, cultured in enriched medium that differentiate into the various cell types and organize themselves to form the organ[210]. Organoids replicate the anatomy of the lung but lack immune cells[210] therefore to study the fate of LNP once in the lung, alveolar macrophages should be microinjected into the lung organoid lumen along with the LNP.

4.1. Summary of Future Work

The internalization experiments over time with THP-1 and MH-S cells should be repeated and analysed by confocal microscopy to ensure that DiD fluorescence from LNP-treated cells is not due to binding of LNP to the cell membrane. Fluorescence coming from the cell membrane, meaning attachment to the cell surface, must be differentiated from fluorescence coming from inside the cell, meaning internalization. Confocal microscopy, using 3D imaging and Z stacks, allows visualization inside the cell to assess whether the fluorescence intensity shifts from the outside of the cell to the inside of the cell, to quantify LNP and to determine the fate of LNP inside the cell[180].

Once internalized by cells, LNP could affect subsequent phagocytic events. To test this, macrophages should be incubated with LNP for 24 h and then uptake of pHrodo beads assessed.

Alveolar macrophages do not turn over very quickly therefore if LNP do have an effect on alveolar macrophages, they might persist inside the cell for a very long period of time. This could lead to off-target effects. The fate of LNP once inside the cells, whether they are broken down or released into the extracellular environment, should be looked into.

The effect of LNP on the phenotype and the function of MH-S cells should also be investigated by quantitative RT-PCR. This method can analyse changes in gene expression associated with apoptosis and activation. Since cellular damage may alter cell proliferation, the expression levels of Ki67, should also be measured. In addition to quantitative RT-PCR, the supernatant should be analysed following stimulation with LNP to measure secreted products, including released LNP, cytokines and chemokines, by ELISA or Luminex multiplex assay- a higher throughput method. This analysis would help determine whether LNP are taken up by an inflammatory or anti-inflammatory pathway. For any drug delivery device, data on safety and efficacy, such as cell viability experiments, are needed to assess the competency of LNP as a therapeutic in humans. Cell viability should be monitored with assays such as the lactate dehydrogenase assays to further assess the cytotoxicity of the LNP and to determine whether cell viability affects the results of other experiments[175]. Liang et al.[211] showed that treating the macrophage cell line RAW264.7 cells with 250 μg/mL LNP decreased viability over time and in a dose-dependent manner. The apoptotic effect of these LNP was due to their ability to destroy mitochondrial structure in a time- and dose-dependent manner, and their ability to cause depolarization of mitochondrial membrane potential[211].

To investigate the routes of uptake of LNP, MH-S cells should be treated with small molecule inhibitors such as: amiloride and cytochalasin D which inhibit macropinocytosis; protamine that inhibits adsorptive-mediated endocytosis; chlorpromazine and monodansylcadaverine that inhibit clathrin-mediated endocytosis; and filipin and methyl-β-cyclodextrin that inhibits caveolae-mediated endocytosis[178,212-214]. If various small molecule inhibitors block LNP internalization, it could mean various mechanisms are involved in the internalization process- they could act simultaneously or independently of each other.

To assess the effect of LNP size on uptake, LNP with sizes between 20 nm and 1 µm will be produced by changing the amount of PEG lipid in the formulation and manipulating the flow rate during production by rapid microfluidic mixing. After treating MH-S cells with these particles, flow cytometry and confocal microscopy will be performed to determine the ideal size to evade internalization by MH-S cells. By quantifying the proportion of cells that internalized LNP and the fluorescent signal from the cells, we can determine whether LNP were internalized or whether they remained attached to the cell membrane.

While preliminary *in vitro* work is important, *in vivo* studies give a better indication of what happens to LNP once they enter the lung. To understand if LNP are internalized by alveolar macrophages, LNP should be fluorescently labelled and delivered to mice intratracheally to then track their journey.

These future experiments would provide a better understanding of the interactions between LNP and alveolar macrophages as well as the immune responses of alveolar macrophages towards, or as a result of, these LNP. By determining what characteristics of the LNP stimulate cytotoxicity and immunogenicity, these can be re-designed and re-formulated specifically to evade the immune system while successfully delivering the therapeutic to its target cells.

References

1 Xie, M., Liu, X., Cao, X., Guo, M. & Li, X. Trends in prevalence and incidence of chronic respiratory diseases from 1990 to 2017. *Respir Res* **21**, doi:10.1186/s12931-020-1291-8 (2020).

2 Li, X., Cao, X., Guo, M., Xie, M. & Liu, X. Trends and risk factors of mortality and disability adjusted life years for chronic respiratory diseases from 1990 to 2017: systematic analysis for the Global Burden of Disease Study 2017. *BMJ*, m234, doi:10.1136/bmj.m234 (2020).

3 Barnes, P. J. & Stockley, R. A. COPD: current therapeutic interventions and future approaches. *Eur Respir J* **25**, 1084-1106, doi:10.1183/09031936.05.00139104 (2005).

4 Green, R. H., Brightling, C. E., Pavord, I. D. & Wardlaw, A. J. Management of asthma in adults: current therapy and future directions. *Postgrad Med J* **79**, 259-267, doi:10.1136/pmj.79.931.259 (2003).

5 Barnes, P. J. *et al.* Chronic obstructive pulmonary disease. *Nat Rev Dis Primers* **1**, 15076, doi:10.1038/nrdp.2015.76 PMID - 27189863 (2015).

6 Jacobs, C. & Müller, R. H. Production and Characterization of a Budesonide Nanosuspension for Pulmonary Administration. *Pharm Res* **19**, 189-194, doi:10.1023/a:1014276917363 PMID - 11883646 (2002).

7 Rogliani, P. *et al.* Efficacy and safety profile of mucolytic/antioxidant agents in chronic obstructive pulmonary disease: a comparative analysis across erdosteine, carbocysteine, and N-acetylcysteine. *Respir Res* **20**, 104, doi:10.1186/s12931-019-1078-y (2019).

8 Alton, E. *et al.* Cationic lipid-mediated CFTR gene transfer to the lungs and nose of patients with cystic fibrosis: a double-blind placebo-controlled trial. *Lancet* **353**, 947-954, doi:10.1016/s0140-6736(98)06532-5 PMID - 10459902 (1999).
9 Zhao, Y. & Huang, L. Chapter Two Lipid Nanoparticles for Gene Delivery. *Adv Genet* **88**, 13-36, doi:10.1016/b978-0-12-800148-6.00002-x PMID - 25409602 (2014).
10 Bardoliwala, D. *et al.* Nanocarriers in effective pulmonary delivery of siRNA: current approaches and challenges. *Ther Deliv* **10**, 311-332, doi:10.4155/tde-2019-0012 PMID - 31116099 (2019).
11 Jorge, A., Pais, A. & Vitorino, C. Drug Delivery Systems. *Methods Mol Biol* **2059**, 259-283, doi:10.1007/978-1-4939-9798-5_14 PMID - 31435927 (2019).
12 Li, S.-D. & Huang, L. Targeted Delivery of Antisense Oligodeoxynucleotide and Small Interference RNA into Lung Cancer Cells. *Mol Pharmaceut* **3**, 579-588, doi:10.1021/mp060039w PMID - 17009857 (2006).
13 Choi, S. H. *et al.* Novel cationic solid lipid nanoparticles enhanced p53 gene transfer to lung cancer cells. *Eur J Pharm Biopharm* **68**, 545-554, doi:10.1016/j.ejpb.2007.07.011 PMID - 17881199 (2008).
14 Crawford, R. *et al.* Analysis of lipid nanoparticles by Cryo-EM for characterizing siRNA delivery vehicles. *Int J Pharm* **403**, 237-244, doi:10.1016/j.ijpharm.2010.10.025 PMID - 20974237 (2011).
15 Huang, X. *et al.* Targeted Delivery of microRNA-29b by Transferrin-Conjugated Anionic Lipopolyplex Nanoparticles: A Novel Therapeutic Strategy in Acute Myeloid Leukemia. *Clin Cancer Res* **19**, 2355-2367, doi:10.1158/1078-0432.ccr-12-3191 PMID - 23493348 (2013).
16 Taratula, O., Kuzmov, A., Shah, M., Garbuzenko, O. B. & Minko, T. Nanostructured lipid carriers as multifunctional nanomedicine platform for pulmonary co-delivery of anticancer drugs and siRNA. *J Control Release* **171**, 349-357, doi:10.1016/j.jconrel.2013.04.018 PMID - 23648833 (2013).
17 Mastorakos, P. *et al.* Highly compacted biodegradable DNA nanoparticles capable of overcoming the mucus barrier for inhaled lung gene therapy. *Proc Natl Acad Sci U S A* **112**, 8720-8725, doi:10.1073/pnas.1502281112 PMID - 26124127 (2015).
18 Shao, Z. *et al.* Targeted lung cancer therapy: preparation and optimization of transferrin-decorated nanostructured lipid carriers as novel nanomedicine for co-delivery of anticancer drugs and DNA. *Int J Nanomed* **10**, 1223-1233, doi:10.2147/ijn.s77837 PMID - 25709444 (2015).
19 Kharaji, M. H., Doroud, D., Taheri, T. & Rafati, S. Drug Targeting to Macrophages With Solid Lipid Nanoparticles Harboring Paromomycin: an In Vitro Evaluation Against L. major and L. tropica. *Aaps Pharmscitech* **17**, 1110-1119, doi:10.1208/s12249-015-0439-1 PMID - 26552399 (2016).
20 Santos, S. *et al.* Nanostructured lipid carriers loaded with resveratrol modulate human dendritic cells. *Int J Nanomed* **Volume 11**, 3501-3516, doi:10.2147/ijn.s108694 PMID - 27555771 (2016).
21 Makled, S., Nafee, N. & Boraie, N. Nebulized solid lipid nanoparticles for the potential treatment of pulmonary hypertension via targeted delivery of phosphodiesterase-5-inhibitor. *Int J Pharm* **517**, 312-321, doi:10.1016/j.ijpharm.2016.12.026 PMID - 27979766 (2017).
22 Tulbah, A. S. *et al.* Inhaled simvastatin nanoparticles for inflammatory lung disease. *Nanomedicine (Lond)* **12**, 2471-2485, doi:10.2217/nnm-2017-0188 PMID - 28972463 (2017).
23 Vieira, A. C. C. *et al.* Targeted macrophages delivery of rifampicin-loaded lipid nanoparticles to improve tuberculosis treatment. *Nanomedicine*

(Lond) **12**, 2721-2736, doi:10.2217/nnm-2017-0248 PMID - 29119867 (2017).
24 Jensen, D. K. *et al.* Design of an inhalable dry powder formulation of DOTAP-modified PLGA nanoparticles loaded with siRNA. *J Control Release* **157**, 141-148, doi:10.1016/j.jconrel.2011.08.011 PMID - 21864597 (2012).
25 Nayerossadat, N., Maedeh, T. & Ali, P. A. Viral and nonviral delivery systems for gene delivery. *Adv Biomed Res* **1**, 27, doi:10.4103/2277-9175.98152 PMID - 23210086 (2012).
26 Costa, A., Sarmento, B. & Seabra, V. Targeted Drug Delivery Systems for Lung Macrophages. *Curr Drug Targets* **16**, 1565-1581, doi:10.2174/1389450115666141114152713 PMID - 25395103 (2015).
27 El-Sherbiny, I. M., El-Baz, N. M. & Yacoub, M. H. Inhaled nano- and microparticles for drug delivery. *Glob Cardiol Sci Pract* **2015**, 2, doi:10.5339/gcsp.2015.2 PMID - 26779496 (2015).
28 Moreno-Sastre, M., Pastor, M., Salomon, C. J., Esquisabel, A. & Pedraz, J. L. Pulmonary drug delivery: a review on nanocarriers for antibacterial chemotherapy. *J Antimicrob Chemother* **70**, 2945-2955, doi:10.1093/jac/dkv192 PMID - 26203182 (2015).
29 Pozo-Rodríguez, A. d., Solinís, M. Á. & Rodríguez-Gascón, A. Applications of lipid nanoparticles in gene therapy. *Eur J Pharm Biopharm* **109**, 184-193, doi:10.1016/j.ejpb.2016.10.016 PMID - 27789356 (2016).
30 Cullis, P. R. & Hope, M. J. Lipid Nanoparticle Systems for Enabling Gene Therapies. *Mol Ther* **25**, 1467-1475, doi:10.1016/j.ymthe.2017.03.013 PMID - 28412170 (2017).
31 Higa, L. H. *et al.* Ultra-small solid archaeolipid nanoparticles for active targeting to macrophages of the inflamed mucosa. *Nanomedicine (Lond)* **12**, 1165-1175, doi:10.2217/nnm-2016-0437 PMID - 28447893 (2017).
32 Ngan, C. L. & Asmawi, A. A. Lipid-based pulmonary delivery system: a review and future considerations of formulation strategies and limitations. *Drug Deliv Transl Res* **8**, 1527-1544, doi:10.1007/s13346-018-0550-4 PMID - 29881970 (2018).
33 Hafez, I. M., Maurer, N. & Cullis, P. R. On the mechanism whereby cationic lipids promote intracellular delivery of polynucleic acids. *Gene Ther* **8**, 1188-1196, doi:10.1038/sj.gt.3301506 PMID - 11509950 (2001).
34 Gao, K. & Huang, L. Nonviral Methods for siRNA Delivery. *Mol Pharmaceut* **6**, 651-658, doi:10.1021/mp800134q PMID - 19115957 (2008).
35 Rehman, Z. u., Zuhorn, I. S. & Hoekstra, D. How cationic lipids transfer nucleic acids into cells and across cellular membranes: Recent advances. *J Control Release* **166**, 46-56, doi:10.1016/j.jconrel.2012.12.014 PMID - 23266451 (2013).
36 Junquera, E. & Aicart, E. Recent progress in gene therapy to deliver nucleic acids with multivalent cationic vectors. *Adv Colloid Interface Sci* **233**, 161-175, doi:10.1016/j.cis.2015.07.003 PMID - 26265376 (2016).
37 Lin, M.-H., Lin, C.-F., Yang, S.-C., Hung, C.-F. & Fang, J.-Y. The Interplay Between Nanoparticles and Neutrophils. *J Biomed Nanotechnol* **14**, 66-85, doi:10.1166/jbn.2018.2459 PMID - 29463366 (2018).
38 Hirota, K. & Terada, H. in *Molecular Regulation of Endocytosis* (ed Brian Ceresa) Ch. 16, (InTechOpen, 2012).
39 Miao, X., Leng, X. & Zhang, Q. The Current State of Nanoparticle-Induced Macrophage Polarization and Reprogramming Research. *Int J Mol Sci* **18**, 336, doi:10.3390/ijms18020336 PMID - 28178185 (2017).
40 Geiser, M. Update on Macrophage Clearance of Inhaled Micro- and Nanoparticles. *J Aerosol Med Pulm Drug Deliv* **23**, 207-217, doi:10.1089/jamp.2009.0797 PMID - 20109124 (2010).

41 Hussell, T. & Bell, T. J. Alveolar macrophages: plasticity in a tissue-specific context. *Nat Rev Immunol* **14**, 81-93, doi:10.1038/nri3600 PMID - 24445666 (2014).
42 Patel, B., Gupta, N. & Ahsan, F. Particle engineering to enhance or lessen particle uptake by alveolar macrophages and to influence the therapeutic outcome. *Eur J Pharm Biopharm* **89**, 163-174, doi:10.1016/j.ejpb.2014.12.001 PMID - 25497488 (2015).
43 Desch, A. N. *et al.* Flow Cytometric Analysis of Mononuclear Phagocytes in Nondiseased Human Lung and Lung-Draining Lymph Nodes. *Am J Respir Crit Care Med* **193**, 614-626, doi:10.1164/rccm.201507-1376oc PMID - 26551758 (2016).
44 Lee, W.-H., Loo, C.-Y., Traini, D. & Young, P. M. Nano- and micro-based inhaled drug delivery systems for targeting alveolar macrophages. *Expert Opin Drug Deliv* **12**, 1009-1026, doi:10.1517/17425247.2015.1039509 PMID - 25912721 (2015).
45 Mathie, S. A. *et al.* Alveolar macrophages are sentinels of murine pulmonary homeostasis following inhaled antigen challenge. *Allergy* **70**, 80-89, doi:10.1111/all.12536 PMID - 25331546 (2015).
46 Belchamber, K. B. R. & Donnelly, L. E. Macrophages, Origin, Functions and Biointervention. *Results Probl Cell Differ* **62**, 299-313, doi:10.1007/978-3-319-54090-0_12 PMID - 28455714 (2017).
47 Garbi, N. & Lambrecht, B. N. Location, function, and ontogeny of pulmonary macrophages during the steady state. *Pflügers Archiv : European Journal of Physiology* **469**, 561-572, doi:10.1007/s00424-017-1965-3 PMID - 28289977 (2017).
48 Allard, B., Panariti, A. & Martin, J. G. Alveolar Macrophages in the Resolution of Inflammation, Tissue Repair, and Tolerance to Infection. *Front Immunol* **9**, 1777, doi:10.3389/fimmu.2018.01777 PMID - 30108592 (2018).
49 Costa, A., Sarmento, B. & Seabra, V. Mannose-functionalized solid lipid nanoparticles are effective in targeting alveolar macrophages. *Eur J Pharm Sci* **114**, 103-113, doi:10.1016/j.ejps.2017.12.006 PMID - 29229273 (2018).
50 Evren, E., Ringqvist, E. & Willinger, T. Origin and Ontogeny of Lung Macrophages: From Mice to Humans. *Immunology* **160**, 126-138, doi:10.1111/imm.13154 (2019).
51 Yu, X. *et al.* The Cytokine TGF-β Promotes the Development and Homeostasis of Alveolar Macrophages. *Immunity* **47**, 903-912.e904, doi:10.1016/j.immuni.2017.10.007 PMID - 29126797 (2017).
52 Trapnell, B. C. & Whitsett, J. A. GM-CSF Regulates Pulmonary Surfactant Homeostasis and Alveolar Macrophage-Mediated Innate Host Defense. *Physiology* **64**, 775-802, doi:10.1146/annurev.physiol.64.090601.113847 PMID - 11826288 (2002).
53 Guilliams, M. *et al.* Alveolar macrophages develop from fetal monocytes that differentiate into long-lived cells in the first week of life via GM-CSF. *J Exp Medicine* **210**, 1977-1992, doi:10.1084/jem.20131199 PMID - 24043763 (2013).
54 Zasłona, Z. *et al.* Resident Alveolar Macrophages Suppress, whereas Recruited Monocytes Promote, Allergic Lung Inflammation in Murine Models of Asthma. *J Immunol* **193**, 4245-4253, doi:10.4049/jimmunol.1400580 PMID - 25225663 (2014).
55 Yamasaki, K. & Eeden, S. F. v. Lung Macrophage Phenotypes and Functional Responses: Role in the Pathogenesis of COPD. *Int J Mol Sci* **19**, 582, doi:10.3390/ijms19020582 PMID - 29462886 (2018).
56 Mitsi, E. *et al.* Human alveolar macrophages predominately express combined classical M1 and M2 surface markers in steady state. *Respir Res* **19**, 66, doi:10.1186/s12931-018-0777-0 PMID - 29669565 (2018).

57 Lee, J. *et al.* Bronchoalveolar lavage (BAL) cells in idiopathic pulmonary fibrosis express a complex pro-inflammatory, pro-repair, angiogenic activation pattern, likely associated with macrophage iron accumulation. *Plos One* **13**, e0194803, doi:10.1371/journal.pone.0194803 PMID - 29649237 (2018).
58 Atri, C., Guerfali, F. Z. & Laouini, D. Role of Human Macrophage Polarization in Inflammation during Infectious Diseases. *Int J Mol Sci* **19**, 1801, doi:10.3390/ijms19061801 PMID - 29921749 (2018).
59 Kugathasan, K. *et al.* CD11c+ antigen presenting cells from the alveolar space, lung parenchyma and spleen differ in their phenotype and capabilities to activate naïve and antigen-primed T cells. *Bmc Immunol* **9**, 48, doi:10.1186/1471-2172-9-48 PMID - 18700962 (2008).
60 Jubrail, J., Kurian, N. & Niedergang, F. Macrophage phagocytosis cracking the defect code in COPD. *Biomed J* **40**, 305-312, doi:10.1016/j.bj.2017.09.004 PMID - 29433833 (2017).
61 He, Y. *et al.* Rational particle design to overcome pulmonary barriers for obstructive lung diseases therapy. *J Control Release* **314**, 48-61, doi:10.1016/j.jconrel.2019.10.035 (2019).
62 Svedberg, F. R. *et al.* The lung environment controls alveolar macrophage metabolism and responsiveness in type 2 inflammation. *Nat Immunol* **20**, 571-580, doi:10.1038/s41590-019-0352-y PMID - 30936493 (2019).
63 Celli, B. R. & Wedzicha, J. A. Update on Clinical Aspects of Chronic Obstructive Pulmonary Disease. *New Engl J Med* **381**, 1257-1266, doi:10.1056/nejmra1900500 PMID - 31553837 (2019).
64 Agustí, A. & Hogg, J. C. Update on the Pathogenesis of Chronic Obstructive Pulmonary Disease. *New Engl J Med* **381**, 1248-1256, doi:10.1056/nejmra1900475 PMID - 31553836 (2019).
65 Barnes, P. J. *et al.* Chronic obstructive pulmonary disease. *Nat Rev Dis Primers* **1**, 15076, doi:10.1038/nrdp.2015.76 (2015).
66 Vlahos, R. & Bozinovski, S. Role of Alveolar Macrophages in Chronic Obstructive Pulmonary Disease. *Front Immunol* **5**, 435, doi:10.3389/fimmu.2014.00435 PMID - 25309536 (2014).
67 Barnes, P. J. Alveolar Macrophages as Orchestrators of COPD. *Copd J Chronic Obstr Pulm Dis* **1**, 59-70, doi:10.1081/copd-120028701 PMID - 16997739 (2004).
68 Kapellos, T. S., Bassler, K., Aschenbrenner, A. C., Fujii, W. & Schultze, J. L. Dysregulated Functions of Lung Macrophage Populations in COPD. *Journal of Immunology Research* **2018**, 1-19, doi:10.1155/2018/2349045 (2018).
69 Akata, K. & van Eeden, S. F. Lung Macrophage Functional Properties in Chronic Obstructive Pulmonary Disease. *Int J Mol Sci* **21**, doi:10.3390/ijms21030853 (2020).
70 Choi, M., Gu, J., Lee, M. & Rhim, T. A new combination therapy for asthma using dual-function dexamethasone-conjugated polyethylenimine and vitamin D binding protein siRNA. *Gene Ther* **24**, 727-734, doi:10.1038/gt.2017.83 PMID - 28846076 (2017).
71 Lambrecht, B. N., Persson, E. K. & Hammad, H. Myeloid Cells in Asthma. *Microbiol Spectr* **5**, doi:10.1128/microbiolspec.MCHD-0053-2016 (2017).
72 Poon, A. H., Eidelman, D. H., Martin, J. G., Laprise, C. & Hamid, Q. Pathogenesis of severe asthma. *Clin Exp Allergy* **42**, 625-637, doi:10.1111/j.1365-2222.2012.03983.x PMID - 22515387 (2012).
73 Grabiec, A. M. & Hussell, T. The role of airway macrophages in apoptotic cell clearance following acute and chronic lung inflammation. *Semin Immunopathol* **38**, 409-423, doi:10.1007/s00281-016-0555-3 PMID - 26957481 (2016).

74 Lambrecht, B. N., Hammad, H. & Fahy, J. V. The Cytokines of Asthma. *Immunity* **50**, 975-991, doi:10.1016/j.immuni.2019.03.018 PMID - 30995510 (2019).
75 Lambrecht, B. N. & Hammad, H. Dendritic Cell and Epithelial Cell Interactions at the Origin of Murine Asthma. *Ann Am Thorac Soc* **11**, S236-S243, doi:10.1513/annalsats.201405-218aw PMID - 25525726 (2014).
76 Lambrecht, B. N. & Hammad, H. Lung Dendritic Cells in Respiratory Viral Infection and Asthma: From Protection to Immunopathology. *Annu Rev Immunol* **30**, 243-270, doi:10.1146/annurev-immunol-020711-075021 PMID - 22224777 (2012).
77 Lambrecht, B. N. & Hammad, H. The airway epithelium in asthma. *Nat Med* **18**, 684-692, doi:10.1038/nm.2737 PMID - 22561832 (2012).
78 Wuyts, W. A. *et al.* The pathogenesis of pulmonary fibrosis: a moving target. *Eur Respir J* **41**, 1207-1218, doi:10.1183/09031936.00073012 PMID - 23100500 (2012).
79 Stahl, M. *et al.* Lung Collagens Perpetuate Pulmonary Fibrosis via CD204 and M2 Macrophage Activation. *Plos One* **8**, e81382, doi:10.1371/journal.pone.0081382 PMID - 24278429 (2013).
80 Kolahian, S., Fernandez, I. E., Eickelberg, O. & Hartl, D. Immune Mechanisms in Pulmonary Fibrosis. *Am J Resp Cell Mol* **55**, 309-322, doi:10.1165/rcmb.2016-0121tr PMID - 27149613 (2016).
81 Heukels, P., Moor, C. C., Thüsen, J. H. v. d., Wijsenbeek, M. S. & Kool, M. Inflammation and Immunity in IPF Pathogenesis and Treatment. *Resp Med* **147**, 79-91, doi:10.1016/j.rmed.2018.12.015 PMID - 30704705 (2019).
82 Li, G. *et al.* Macrophage-secreted TSLP and MMP9 promote bleomycin-induced pulmonary fibrosis. *Toxicol Appl Pharmacol* **366**, 10-16, doi:10.1016/j.taap.2019.01.011 PMID - 30653976 (2019).
83 Bargagli, E., Prasse, A., Olivieri, C., Muller-Quernheim, J. & Rottoli, P. Macrophage-Derived Biomarkers of Idiopathic Pulmonary Fibrosis. *Pulm Medicine* **2011**, 717130, doi:10.1155/2011/717130 PMID - 21637368 (2011).
84 Datta, A. *et al.* Evidence for a Functional Thymic Stromal Lymphopoietin Signaling Axis in Fibrotic Lung Disease. *J Immunol* **191**, 4867-4879, doi:10.4049/jimmunol.1300588 PMID - 24081992 (2013).
85 Reyfman, P. A. *et al.* Single-Cell Transcriptomic Analysis of Human Lung Provides Insights into the Pathobiology of Pulmonary Fibrosis. *Am J Respir Crit Care Med* **199**, 1517-1536, doi:10.1164/rccm.201712-2410oc PMID - 30554520 (2018).
86 Morimoto, K., Janssen, W. J. & Terada, M. Defective efferocytosis by alveolar macrophages in IPF patients. *Resp Med* **106**, 1800-1803, doi:10.1016/j.rmed.2012.08.020 PMID - 22999220 (2012).
87 Canonico, A. E., Conary, J. T., Meyrick, B. O. & Brigham, K. L. Aerosol and intravenous transfection of human alpha 1-antitrypsin gene to lungs of rabbits. *Am J Resp Cell Mol* **10**, 24-29, doi:10.1165/ajrcmb.10.1.8292378 PMID - 8292378 (1994).
88 Fujisawa, T. *et al.* Regulation of airway MUC5AC expression by IL-1beta and IL-17A; the NF-kappaB paradigm. *J Immunol* **183**, 6236-6243, doi:10.4049/jimmunol.0900614 (2009).
89 Hogan, S. P., Foster, P. S., Tan, X. & Ramsay, A. J. Mucosal IL-12 gene delivery inhibits allergic airways disease and restores local antiviral immunity. *Eur J Immunol* **28**, 413-423, doi:10.1002/(SICI)1521-4141(199802)28:02<413::AID-IMMU413>3.0.CO;2-1 (1998).
90 Garbuzenko, O. B. *et al.* Combinatorial treatment of idiopathic pulmonary fibrosis using nanoparticles with prostaglandin E and siRNA(s).

Nanomedicine **13**, 1983-1992, doi:10.1016/j.nano.2017.04.005 PMID - 28434932 (2017).
91 Zou, Y. *et al.* Effective Treatment of Early Endobronchial Cancer With Regional Administration of Liposome-p53 Complexes. *Jnci J National Cancer Inst* **90**, 1130-1137, doi:10.1093/jnci/90.15.1130 PMID - 9701362 (1998).
92 Dowdy, S. F. Overcoming cellular barriers for RNA therapeutics. *Nat Biotechnol* **35**, 222-229, doi:10.1038/nbt.3802 PMID - 28244992 (2017).
93 Kormann, M. S. D. *et al.* Expression of therapeutic proteins after delivery of chemically modified mRNA in mice. *Nat Biotechnol* **29**, 154-157, doi:10.1038/nbt.1733 PMID - 21217696 (2011).
94 Yin, H. *et al.* Non-viral vectors for gene-based therapy. *Nat Rev Genet* **15**, 541-555, doi:10.1038/nrg3763 PMID - 25022906 (2014).
95 Thess, A. *et al.* Sequence-engineered mRNA Without Chemical Nucleoside Modifications Enables an Effective Protein Therapy in Large Animals. *Mol Ther* **23**, 1456-1464, doi:10.1038/mt.2015.103 PMID - 26050989 (2015).
96 Saad, M., Garbuzenko, O. B. & Minko, T. Co-delivery of siRNA and an anticancer drug for treatment of multidrug-resistant cancer. *Nanomedicine (Lond)* **3**, 761-776, doi:10.2217/17435889.3.6.761 PMID - 19025451 (2008).
97 Pakunlu, R. I. *et al.* Enhancement of the Efficacy of Chemotherapy for Lung Cancer by Simultaneous Suppression of Multidrug Resistance and Antiapoptotic Cellular Defense. *Cancer Res* **64**, 6214-6224, doi:10.1158/0008-5472.can-04-0001 PMID - 15342407 (2004).
98 Garbuzenko, O. B. *et al.* Inhibition of lung tumor growth by complex pulmonary delivery of drugs with oligonucleotides as suppressors of cellular resistance. *Proc Natl Acad Sci U S A* **107**, 10737-10742, doi:10.1073/pnas.1004604107 PMID - 20498076 (2010).
99 Kristen, A. V. *et al.* Patisiran, an RNAi therapeutic for the treatment of hereditary transthyretin-mediated amyloidosis. *Neurodegener Dis Manag* **9**, 5-23, doi:10.2217/nmt-2018-0033 PMID - 30480471 (2019).
100 Thanki, K., Blum, K. G., Thakur, A., Rose, F. & Foged, C. Formulation of RNA interference-based drugs for pulmonary delivery: challenges and opportunities. *Ther Deliv* **9**, 731-749, doi:10.4155/tde-2018-0029 PMID - 30277138 (2018).
101 Chan, C.-L. *et al.* Endosomal escape and transfection efficiency of PEGylated cationic liposome–DNA complexes prepared with an acid-labile PEG-lipid. *Biomaterials* **33**, 4928-4935, doi:10.1016/j.biomaterials.2012.03.038 PMID - 22469293 (2012).
102 Sansare, V., Shinde, U. & Warrier, D. *CELLULAR TRAFFICKING OF NANOCARRIERS IN ALVEOLAR MACROPHAGES FOR EFFECTIVE MANAGEMENT OF PULMONARY TUBERCULOSIS*. (2020).
103 Hosseini, S. M. *et al.* Doxycycline-encapsulated solid lipid nanoparticles as promising tool against Brucella melitensis enclosed in macrophage: a pharmacodynamics study on J774A.1 cell line. *Antimicrob Resist Infect Control* **8**, 62, doi:10.1186/s13756-019-0504-8 (2019).
104 Let's talk about lipid nanoparticles. *Nature Reviews Materials* **6**, 99-99, doi:10.1038/s41578-021-00281-4 (2021).
105 Schoenmaker, L. *et al.* mRNA-lipid nanoparticle COVID-19 vaccines: Structure and stability. *Int J Pharm* **601**, 120586, doi:10.1016/j.ijpharm.2021.120586 (2021).
106 Eygeris, Y., Patel, S., Jozic, A. & Sahay, G. Deconvoluting Lipid Nanoparticle Structure for Messenger RNA Delivery. *Nano Lett* **20**, 4543-4549, doi:10.1021/acs.nanolett.0c01386 (2020).
107 Ryals, R. C. *et al.* The effects of PEGylation on LNP based mRNA delivery to the eye. *Plos One* **15**, e0241006, doi:10.1371/journal.pone.0241006 (2020).

108 Weber, S., Zimmer, A. & Pardeike, J. Solid Lipid Nanoparticles (SLN) and Nanostructured Lipid Carriers (NLC) for pulmonary application: A review of the state of the art. *Eur J Pharm Biopharm* **86**, 7-22, doi:10.1016/j.ejpb.2013.08.013 PMID - 24007657 (2014).
109 Semple, S. C. *et al.* Efficient encapsulation of antisense oligonucleotides in lipid vesicles using ionizable aminolipids: formation of novel small multilamellar vesicle structures. *Biochim Biophys Acta Biomembr* **1510**, 152-166, doi:10.1016/s0005-2736(00)00343-6 PMID - 11342155 (2001).
110 Levine, R. M., Pearce, T. R., Adil, M. & Kokkoli, E. Preparation and Characterization of Liposome-Encapsulated Plasmid DNA for Gene Delivery. *Langmuir* **29**, 9208-9215, doi:10.1021/la400859e PMID - 23837701 (2013).
111 Bao, Y. *et al.* Effect of PEGylation on Biodistribution and Gene Silencing of siRNA/Lipid Nanoparticle Complexes. *Pharm Res* **30**, 342-351, doi:10.1007/s11095-012-0874-6 PMID - 22983644 (2013).
112 Semple, S. C. *et al.* Rational design of cationic lipids for siRNA delivery. *Nat Biotechnol* **28**, 172, doi:10.1038/nbt.1602 PMID - 20081866 (2010).
113 Heyes, J., Palmer, L., Bremner, K. & MacLachlan, I. Cationic lipid saturation influences intracellular delivery of encapsulated nucleic acids. *J Control Release* **107**, 276-287, doi:10.1016/j.jconrel.2005.06.014 PMID - 16054724 (2005).
114 Mansour, H., Haemosu & Wu, X. Nanomedicine in pulmonary delivery. *Int J Nanomed* **Volume 4**, 299-319, doi:10.2147/ijn.s4937 PMID - 20054434 (2009).
115 Jayaraman, M. *et al.* Maximizing the Potency of siRNA Lipid Nanoparticles for Hepatic Gene Silencing In Vivo. *Angew Chem Int Ed* **51**, 8529-8533, doi:10.1002/anie.201203263 PMID - 22782619 (2012).
116 Gilleron, J. *et al.* Image-based analysis of lipid nanoparticle-mediated siRNA delivery, intracellular trafficking and endosomal escape. *Nat Biotechnol* **31**, 638-646, doi:10.1038/nbt.2612 PMID - 23792630 (2013).
117 Leung, A. K. K., Tam, Y. Y. C., Chen, S., Hafez, I. M. & Cullis, P. R. Microfluidic Mixing: A General Method for Encapsulating Macromolecules in Lipid Nanoparticle Systems. *J Phys Chem B* **119**, 8698-8706, doi:10.1021/acs.jpcb.5b02891 PMID - 26087393 (2015).
118 Kulkarni, J. A. *et al.* Design of lipid nanoparticles for in vitro and in vivo delivery of plasmid DNA. *Nanomedicine* **13**, 1377-1387, doi:10.1016/j.nano.2016.12.014 PMID - 28038954 (2017).
119 Yanez Arteta, M. *et al.* Successful reprogramming of cellular protein production through mRNA delivered by functionalized lipid nanoparticles. *Proc Natl Acad Sci U S A* **115**, E3351-E3360, doi:10.1073/pnas.1720542115 (2018).
120 Evers, M. J. W. *et al.* State-of-the-Art Design and Rapid-Mixing Production Techniques of Lipid Nanoparticles for Nucleic Acid Delivery. *Small Methods* **2**, 1700375, doi:10.1002/smtd.201700375 (2018).
121 Kulkarni, J. A., Cullis, P. R. & Meel, R. v. d. Lipid Nanoparticles Enabling Gene Therapies: From Concepts to Clinical Utility. *Nucleic Acid Ther* **28**, 146-157, doi:10.1089/nat.2018.0721 PMID - 29683383 (2018).
122 Buck, J., Grossen, P., Cullis, P. R., Huwyler, J. & Witzigmann, D. Lipid-Based DNA Therapeutics: Hallmarks of Non-Viral Gene Delivery. *Acs Nano* **13**, 3754-3782, doi:10.1021/acsnano.8b07858 PMID - 30908008 (2019).
123 Belliveau, N. M. *et al.* Microfluidic Synthesis of Highly Potent Limit-size Lipid Nanoparticles for In Vivo Delivery of siRNA. *Mol Ther Nucleic Acids* **1**, e37, doi:10.1038/mtna.2012.28 PMID - 23344179 (2012).
124 Gustafson, H. H., Holt-Casper, D., Grainger, D. W. & Ghandehari, H. Nanoparticle uptake: The phagocyte problem. *Nano Today* **10**, 487-510, doi:10.1016/j.nantod.2015.06.006 PMID - 26640510 (2015).

125 Zhang, S., Li, J., Lykotrafitis, G., Bao, G. & Suresh, S. Size-Dependent Endocytosis of Nanoparticles. *Adv Mater* **21**, 419-424, doi:10.1002/adma.200801393 PMID - 19606281 (2009).
126 Donnelly, L. E. & Barnes, P. J. Defective Phagocytosis in Airways Disease. *Chest* **141**, 1055-1062, doi:10.1378/chest.11-2348 PMID - 22474147 (2012).
127 Sayers, E. J. *et al.* Endocytic Profiling of Cancer Cell Models Reveals Critical Factors Influencing LNP-Mediated mRNA Delivery and Protein Expression. *Molecular therapy : the journal of the American Society of Gene Therapy* **27**, 1950-1962, doi:10.1016/j.ymthe.2019.07.018 (2019).
128 Paramasivam, P. *et al.* Endosomal escape of delivered mRNA from endosomal recycling tubules visualized at the nanoscale. *bioRxiv*, 2020.2012.2018.423541, doi:10.1101/2020.12.18.423541 (2020).
129 Kononenko, V., Narat, M. & Drobne, D. Nanoparticle interaction with the immune system. *Arh Hig Rada Toksikol* **66**, 97-108, doi:10.1515/aiht-2015-66-2582 (2015).
130 Liu, Y., Hardie, J., Zhang, X. & Rotello, V. M. Effects of engineered nanoparticles on the innate immune system. *Semin Immunol* **34**, 25-32, doi:10.1016/j.smim.2017.09.011 (2017).
131 Fadeel, B. Hide and Seek: Nanomaterial Interactions With the Immune System. *Front Immunol* **10**, 133, doi:10.3389/fimmu.2019.00133 (2019).
132 Moghimi, S. M. & Szebeni, J. Stealth liposomes and long circulating nanoparticles: critical issues in pharmacokinetics, opsonization and protein-binding properties. *Prog Lipid Res* **42**, 463-478, doi:10.1016/s0163-7827(03)00033-x PMID - 14559067 (2003).
133 Boraschi, D. *et al.* Nanoparticles and innate immunity: new perspectives on host defence. *Semin Immunol* **34**, 33-51, doi:10.1016/j.smim.2017.08.013 PMID - 28869063 (2017).
134 Muhammad, Q. *et al.* Modulation of immune responses with nanoparticles and reduction of their immunotoxicity. *Biomater Sci* **8**, 1490-1501, doi:10.1039/c9bm01643k (2020).
135 Zhao, J. & Stenzel, M. H. Entry of nanoparticles into cells: the importance of nanoparticle properties. *Polym Chem* **9**, 259-272, doi:10.1039/c7py01603d (2017).
136 Dan, N. & Danino, D. Structure and kinetics of lipid–nucleic acid complexes. *Adv Colloid Interface Sci* **205**, 230-239, doi:10.1016/j.cis.2014.01.013 PMID - 24529969 (2014).
137 Maugeri, M. *et al.* Linkage between endosomal escape of LNP-mRNA and loading into EVs for transport to other cells. *Nat Commun* **10**, 4333, doi:10.1038/s41467-019-12275-6 PMID - 31551417 (2019).
138 Getts, D. R., Shea, L. D., Miller, S. D. & King, N. J. C. Harnessing nanoparticles for immune modulation. *Trends Immunol* **36**, 419-427, doi:10.1016/j.it.2015.05.007 PMID - 26088391 (2015).
139 Pozo-Rodríguez, A. d., Solinís, M. A., Gascón, A. R. & Pedraz, J. L. Short- and long-term stability study of lyophilized solid lipid nanoparticles for gene therapy. *Eur J Pharm Biopharm* **71**, 181-189, doi:10.1016/j.ejpb.2008.09.015 PMID - 18940256 (2009).
140 Hwang, T.-L., Aljuffali, I. A., Hung, C.-F., Chen, C.-H. & Fang, J.-Y. The impact of cationic solid lipid nanoparticles on human neutrophil activation and formation of neutrophil extracellular traps (NETs). *Chem Biol Interact* **235**, 106-114, doi:10.1016/j.cbi.2015.04.011 PMID - 25920576 (2015).
141 Lonez, C., Vandenbranden, M. & Ruysschaert, J.-M. Cationic lipids activate intracellular signaling pathways. *Adv Drug Deliv Rev* **64**, 1749-1758, doi:10.1016/j.addr.2012.05.009 PMID - 22634161 (2012).
142 Szebeni, J. & Moghimi, S. M. Liposome triggering of innate immune responses: A perspective on benefits and adverse reactions. *J Liposome*

Res **19**, 85-90, doi:10.1080/08982100902792855 PMID - 19514998 (2009).
143 Omidi, Y. *et al.* Microarray Analysis of the Toxicogenomics and the Genotoxic Potential of a Cationic Lipid-Based Gene Delivery Nanosystem in Human Alveolar Epithelial A549 Cells. *Toxicol Mech Method* **18**, 369-378, doi:10.1080/15376510801891286 PMID - 20020904 (2008).
144 Hu, Y., Hoerle, R., Ehrich, M. & Zhang, C. Engineering the lipid layer of lipid-PLGA hybrid nanoparticles for enhanced in vitro cellular uptake and improved stability. *Acta Biomater* **28**, 149-159, doi:10.1016/j.actbio.2015.09.032 (2015).
145 Ishida, T. *et al.* Injection of PEGylated liposomes in rats elicits PEG-specific IgM, which is responsible for rapid elimination of a second dose of PEGylated liposomes. *J Control Release* **112**, 15-25, doi:10.1016/j.jconrel.2006.01.005 PMID - 16515818 (2006).
146 Andón, F. T. *et al.* Targeting tumor associated macrophages: The new challenge for nanomedicine. *Semin Immunol* **34**, 103-113, doi:10.1016/j.smim.2017.09.004 PMID - 28941641 (2017).
147 Chen, S. *et al.* Influence of particle size on the in vivo potency of lipid nanoparticle formulations of siRNA. *J Control Release* **235**, 236-244, doi:10.1016/j.jconrel.2016.05.059 PMID - 27238441 (2016).
148 Nanjwade, B. K., Adichwal, S. A., Gaikwad, K. R., Parikh, K. A. & Manvi, F. V. Pulmonary Drug Delivery: Novel Pharmaceutical Technologies Breathe New Life into the Lungs. *Pda J Pharm Sci Tech* **65**, 513-534, doi:10.5731/pdajpst.2011.00704 PMID - 22293840 (2011).
149 Sung, J. C., Pulliam, B. L. & Edwards, D. A. Nanoparticles for drug delivery to the lungs. *Trends Biotechnol* **25**, 563-570, doi:10.1016/j.tibtech.2007.09.005 PMID - 17997181 (2007).
150 Paranjpe, M. & Müller-Goymann, C. Nanoparticle-Mediated Pulmonary Drug Delivery: A Review. *Int J Mol Sci* **15**, 5852-5873, doi:10.3390/ijms15045852 PMID - 24717409 (2014).
151 Sosnowski, T. R. Nanosized and Nanostructured Particles in Pulmonary Drug Delivery. *J Nanosci Nanotechnol* **15**, 3476-3487, doi:10.1166/jnn.2015.9863 PMID - 26504967 (2015).
152 Muralidharan, P., Malapit, M., Mallory, E., Hayes, D. & Mansour, H. M. Inhalable nanoparticulate powders for respiratory delivery. *Nanomedicine* **11**, 1189-1199, doi:10.1016/j.nano.2015.01.007 PMID - 25659645 (2015).
153 Zhou, Q. *et al.* Inhaled formulations and pulmonary drug delivery systems for respiratory infections. *Adv Drug Deliv Rev* **85**, 83-99, doi:10.1016/j.addr.2014.10.022 PMID - 25451137 (2015).
154 Stribling, R., Brunette, E., Liggitt, D., Gaensler, K. & Debs, R. Aerosol gene delivery in vivo. *Proc Natl Acad Sci U S A* **89**, 11277-11281, doi:10.1073/pnas.89.23.11277 PMID - 1454808 (1992).
155 Alton, E. W. F. W. *et al.* Non–invasive liposome–mediated gene delivery can correct the ion transport defect in cystic fibrosis mutant mice. *Nat Genet* **5**, ng1093-1135, doi:10.1038/ng1093-135 PMID - 7504552 (1993).
156 Mühlfeld, C. *et al.* Interactions of nanoparticles with pulmonary structures and cellular responses. *Am J Physiol Lung Cell Mol Physiol* **294**, L817-L829, doi:10.1152/ajplung.00442.2007 PMID - 18263666 (2008).
157 Merkel, O. M., Rubinstein, I. & Kissel, T. siRNA Delivery to the lung: What's new? *Adv Drug Deliv Rev* **75**, 112-128, doi:10.1016/j.addr.2014.05.018 PMID - 24907426 (2014).
158 Hayes, A. J. & Bakand, S. Toxicological perspectives of inhaled therapeutics and nanoparticles. *Expert Opin Drug Metab Toxicol* **10**, 933-947, doi:10.1517/17425255.2014.916276 PMID - 24810077 (2014).
159 Ruge, C. A., Kirch, J. & Lehr, C.-M. Pulmonary drug delivery: from generating aerosols to overcoming biological barriers—therapeutic

possibilities and technological challenges. *Lancet Respir Med* **1**, 402-413, doi:10.1016/s2213-2600(13)70072-9 PMID - 24429205 (2013).
160 Ruge, C. A. *et al.* Uptake of nanoparticles by alveolar macrophages is triggered by surfactant protein A. *Nanomedicine* **7**, 690-693, doi:10.1016/j.nano.2011.07.009 PMID - 21839052 (2011).
161 Walkey, C. D., Olsen, J. B., Guo, H., Emili, A. & Chan, W. C. W. Nanoparticle Size and Surface Chemistry Determine Serum Protein Adsorption and Macrophage Uptake. *J Am Chem Soc* **134**, 2139-2147, doi:10.1021/ja2084338 PMID - 22191645 (2012).
162 Konduru, N. V. *et al.* Protein corona: implications for nanoparticle interactions with pulmonary cells. *Part Fibre Toxicol* **14**, 42, doi:10.1186/s12989-017-0223-3 PMID - 29084556 (2017).
163 Mangal, S., Gao, W., Li, T. & Zhou, Q. Pulmonary delivery of nanoparticle chemotherapy for the treatment of lung cancers: challenges and opportunities. *Acta Pharmacol Sin* **38**, 782-797, doi:10.1038/aps.2017.34 PMID - 28504252 (2017).
164 Schneider, C. S. *et al.* Nanoparticles that do not adhere to mucus provide uniform and long-lasting drug delivery to airways following inhalation. *Sci Adv* **3**, e1601556, doi:10.1126/sciadv.1601556 PMID - 28435870 (2017).
165 Doshi, N. & Mitragotri, S. Macrophages Recognize Size and Shape of Their Targets. *Plos One* **5**, e10051, doi:10.1371/journal.pone.0010051 (2010).
166 Magalhaes, J. *et al.* Lipid nanoparticles biocompatibility and cellular uptake in a 3D human lung model. *Nanomedicine (Lond)* **15**, 259-271, doi:10.2217/nnm-2019-0256 (2020).
167 Chanaday, N. L. & Kavalali, E. T. Time course and temperature dependence of synaptic vesicle endocytosis. *FEBS Lett* **592**, 3606-3614, doi:10.1002/1873-3468.13268 (2018).
168 Koppolu, B. & Zaharoff, D. A. The effect of antigen encapsulation in chitosan particles on uptake, activation and presentation by antigen presenting cells. *Biomaterials* **34**, 2359-2369, doi:10.1016/j.biomaterials.2012.11.066 (2013).
169 Stamatiades, E. G. *et al.* Immune Monitoring of Trans-endothelial Transport by Kidney-Resident Macrophages. *Cell* **166**, 991-1003, doi:10.1016/j.cell.2016.06.058 (2016).
170 Yu, M. *et al.* Specifically targeted delivery of protein to phagocytic macrophages. *Int J Nanomed* **10**, 1743-1757, doi:10.2147/IJN.S75950 (2015).
171 Yoshimura, T., Shono, M., Imai, K. & Hong, K. Kinetic Analysis of Endocytosis and Intracellular Fate of Liposomes in Single Macrophages1. *The Journal of Biochemistry* **117**, 34-41, doi:10.1093/oxfordjournals.jbchem.a124717 (1995).
172 Gao, H. *et al.* Ligand modified nanoparticles increases cell uptake, alters endocytosis and elevates glioma distribution and internalization. *Sci Rep* **3**, 2534, doi:10.1038/srep02534 (2013).
173 Estrella, J. L. *et al.* A Novel in vitro Human Macrophage Model to Study the Persistence of Mycobacterium tuberculosis Using Vitamin D3 and Retinoic Acid Activated THP-1 Macrophages. *Front Microbiol* **2**, 67, doi:10.3389/fmicb.2011.00067 PMID - 21747789 (2011).
174 Albuquerque, J., Moura, C. C., Sarmento, B. & Reis, S. Solid Lipid Nanoparticles: A Potential Multifunctional Approach towards Rheumatoid Arthritis Theranostics. *Molecules* **20**, 11103-11118, doi:10.3390/molecules200611103 PMID - 26087258 (2015).
175 Berger, E. *et al.* Cytotoxicity assessment, inflammatory properties, and cellular uptake of Neutraplex lipid-based nanoparticles in THP-1 monocyte-derived macrophages. *Nanobiomedicine* **4**, 1849543517746259, doi:10.1177/1849543517746259 PMID - 29942393 (2017).

176 Banerjee, S., Roy, S., Bhaumik, K. N. & Pillai, J. Mechanisms of the effectiveness of lipid nanoparticle formulations loaded with anti-tubercular drugs combinations toward overcoming drug bioavailability in tuberculosis. *J Drug Target*, 1-42, doi:10.1080/1061186x.2019.1613409 PMID - 31035816 (2019).
177 Steiner, V., Öhlinger, K., Corzo, C., Salar-Behzadi, S. & Fröhlich, E. Cytotoxicity screening of emulsifiers for pulmonary application of lipid nanoparticles. *Eur J Pharm Sci* **136**, 104968, doi:10.1016/j.ejps.2019.104968 PMID - 31233864 (2019).
178 Zhang, J. *et al.* The cellular uptake mechanism, intracellular transportation, and exocytosis of polyamidoamine dendrimers in multidrug-resistant breast cancer cells. *Int J Nanomedicine* **11**, 3677-3690, doi:10.2147/IJN.S106418 (2016).
179 Zhang, A., Guan, Y. & Xu, L. X. Theoretical study on temperature dependence of cellular uptake of QDs nanoparticles. *J Biomech Eng* **133**, 124502, doi:10.1115/1.4005481 (2011).
180 Zhang, Q., Jiang, Li & Liu. Cellular uptake mechanism and intracellular fate of hydrophobically modified pullulan nanoparticles. 1825, doi:10.2147/ijn.s44342 (2013).
181 Kim, J.-S. *et al.* Cellular uptake of magnetic nanoparticle is mediated through energy-dependent endocytosis in A549 cells. *J Vet Sci* **7**, 321-326, doi:10.4142/jvs.2006.7.4.321 (2006).
182 Pandit, S., Roy, S., Pillai, J. & Banerjee, S. Formulation and Intracellular Trafficking of Lipid-Drug Conjugate Nanoparticles Containing a Hydrophilic Antitubercular Drug for Improved Intracellular Delivery to Human Macrophages. *ACS Omega* **5**, 4433-4448, doi:10.1021/acsomega.9b03523 (2020).
183 Barillet, S. *et al.* Immunotoxicity of poly (lactic-co-glycolic acid) nanoparticles: influence of surface properties on dendritic cell activation. *Nanotoxicology* **13**, 606-622, doi:10.1080/17435390.2018.1564078 (2019).
184 Behzadi, S. *et al.* Cellular uptake of nanoparticles: journey inside the cell. *Chem Soc Rev* **46**, 4218-4244, doi:10.1039/c6cs00636a (2017).
185 Opalinski, L. *et al.* High Affinity Promotes Internalization of Engineered Antibodies Targeting FGFR1. *Int J Mol Sci* **19**, doi:10.3390/ijms19051435 (2018).
186 Singh, V., Davidson, A. C., Hume, P. J. & Koronakis, V. Arf6 Can Trigger Wave Regulatory Complex-Dependent Actin Assembly Independent of Arno. *Int J Mol Sci* **21**, doi:10.3390/ijms21072457 (2020).
187 Vemula, P. K. *et al.* Self-assembled hydrogel fibers for sensing the multi-compartment intracellular milieu. *Sci Rep* **4**, 4466, doi:10.1038/srep04466 (2014).
188 Mittar, D., Paramban, R. & McIntyre, C. (ed BD Biosciences) (2011).
189 Small, A., Lansdown, N., Al-Baghdadi, M., Quach, A. & Ferrante, A. Facilitating THP-1 macrophage studies by differentiating and investigating cell functions in polystyrene test tubes. *J Immunol Methods* **461**, 73-77, doi:10.1016/j.jim.2018.06.019 PMID - 30158075 (2018).
190 Forrester, M. A. *et al.* Similarities and differences in surface receptor expression by THP-1 monocytes and differentiated macrophages polarized using seven different conditioning regimens. *Cellular Immunology* **332**, 58-76, doi:10.1016/j.cellimm.2018.07.008 (2018).
191 Gomes, N. E. *et al.* Lipopolysaccharide-induced expression of cell surface receptors and cell activation of neutrophils and monocytes in whole human blood. *Braz J Med Biol Res* **43**, 853-858, doi:10.1590/s0100-879x2010007500078 (2010).
192 Sabroe, I., Jones, E. C., Usher, L. R., Whyte, M. K. & Dower, S. K. Toll-like receptor (TLR)2 and TLR4 in human peripheral blood granulocytes: a

critical role for monocytes in leukocyte lipopolysaccharide responses. *J Immunol* **168**, 4701-4710, doi:10.4049/jimmunol.168.9.4701 (2002).
193 Zhou, X. *et al.* LPS activation of Toll-like receptor 4 signals CD11b/CD18 expression in neutrophils. *Am J Physiol Lung Cell Mol Physiol* **288**, L655-662, doi:10.1152/ajplung.00327.2004 (2005).
194 Brenner, T. A., Rice, T. A., Anderson, E. D., Percopo, C. M. & Rosenberg, H. F. Immortalized MH-S cells lack defining features of primary alveolar macrophages and do not support mouse pneumovirus replication. *Immunol Lett* **172**, 106-112, doi:10.1016/j.imlet.2016.02.012 PMID - 26916143 (2016).
195 Hardy, C. L. *et al.* Differential Uptake of Nanoparticles and Microparticles by Pulmonary APC Subsets Induces Discrete Immunological Imprints. *J Immunol* **191**, 5278-5290, doi:10.4049/jimmunol.1203131 (2013).
196 Sankaran, K. & Herscowitz, H. B. Phenotypic and functional heterogeneity of the murine alveolar macrophage-derived cell line MH-S. *J Leukoc Biol* **57**, 562-568, doi:10.1002/jlb.57.4.562 (1995).
197 Geiser, M. *et al.* The Role of Macrophages in the Clearance of Inhaled Ultrafine Titanium Dioxide Particles. *Am J Resp Cell Mol* **38**, 371-376, doi:10.1165/rcmb.2007-0138oc PMID - 17947511 (2008).
198 Misharin, A. V., Morales-Nebreda, L., Mutlu, G. M., Budinger, G. R. S. & Perlman, H. Flow cytometric analysis of macrophages and dendritic cell subsets in the mouse lung. *Am J Resp Cell Mol* **49**, 503-510, doi:10.1165/rcmb.2013-0086ma PMID - 23672262 (2013).
199 Riddy, D. M. *et al.* Comparative genotypic and phenotypic analysis of human peripheral blood monocytes and surrogate monocyte-like cell lines commonly used in metabolic disease research. *Plos One* **13**, e0197177, doi:10.1371/journal.pone.0197177 (2018).
200 Tsukumo, H., Matsunari, N., Yamashita, K., Kojima, H. & Itagaki, H. Lipopolysaccharide interferes with the use of the human Cell Line Activation Test to determine the allergic potential of proteins. *J Pharmacol Toxicol Methods* **92**, 34-42, doi:10.1016/j.vascn.2018.02.003 (2018).
201 Miyazawa, M., Ito, Y., Yoshida, Y., Sakaguchi, H. & Suzuki, H. Phenotypic alterations and cytokine production in THP-1 cells in response to allergens. **21**, 428-437, doi:10.1016/j.tiv.2006.10.005 (2007).
202 Monguió-Tortajada, M., Franquesa, M., Sarrias, M.-R. & Borràs, F. E. Low doses of LPS exacerbate the inflammatory response and trigger death on TLR3-primed human monocytes. *Cell Death & Disease* **9**, doi:10.1038/s41419-018-0520-2 (2018).
203 Nooteboom, A., Van Der Linden, C. J. & Hendriks, T. Modulation of Adhesion Molecule Expression on Endothelial Cells after Induction by Lipopolysaccharide-Stimulated Whole Blood. *Scandinavian Journal of Immunology* **59**, 440-448, doi:10.1111/j.0300-9475.2004.01413.x (2004).
204 Woodfin, A. *et al.* ICAM-1-expressing neutrophils exhibit enhanced effector functions in murine models of endotoxemia. *Blood* **127**, 898-907, doi:10.1182/blood-2015-08-664995 (2016).
205 Zuckerman, S. H., Gustin, J. & Evans, G. F. Expression of CD54 (Intercellular Adhesion Molecule-1) and the β1 Integrin CD29 Is Modulated by a Cyclic AMP Dependent Pathway in Activated Primary Rat Microglial Cell Cultures. *Inflammation* **22**, 95-106, doi:10.1023/A:1022351908951 (1998).
206 Coolen, A. L. *et al.* Poly(lactic acid) nanoparticles and cell-penetrating peptide potentiate mRNA-based vaccine expression in dendritic cells triggering their activation. *Biomaterials* **195**, 23-37, doi:10.1016/j.biomaterials.2018.12.019 (2019).
207 Chavez-Santoscoy, A. V., Huntimer, L. M., Ramer-Tait, A. E., Wannemuehler, M. & Narasimhan, B. Harvesting murine alveolar

macrophages and evaluating cellular activation induced by polyanhydride nanoparticles. *J Vis Exp*, e3883, doi:10.3791/3883 (2012).
208 Blank, F. *et al.* Interaction of biomedical nanoparticles with the pulmonary immune system. *J Nanobiotechnol* **15**, doi:10.1186/s12951-016-0242-5 (2017).
209 Dong, Y. *et al.* Lipopeptide nanoparticles for potent and selective siRNA delivery in rodents and nonhuman primates. *Proc Natl Acad Sci U S A* **111**, 3955-3960, doi:10.1073/pnas.1322937111 (2014).
210 Paolicelli, G. *et al.* Using Lung Organoids to Investigate Epithelial Barrier Complexity and IL-17 Signaling During Respiratory Infection. *Front Immunol* **10**, doi:10.3389/fimmu.2019.00323 (2019).
211 Liang, W. L. *et al.* Solid lipid nanoparticle induced apoptosis of macrophages via a mitochondrial-dependent pathway in vitro and in vivo. *Int J Nanomedicine* **14**, 3283-3295, doi:10.2147/IJN.S200395 (2019).
212 Guan, S. *et al.* Self-assembled peptide-poloxamine nanoparticles enable in vitro and in vivo genome restoration for cystic fibrosis. *Nat Nanotechnol* **14**, 287-297, doi:10.1038/s41565-018-0358-x (2019).
213 Kou, L., Sun, J., Zhai, Y. & He, Z. The endocytosis and intracellular fate of nanomedicines: Implication for rational design. *Asian J Pharm Sci* **8**, 1-10, doi:10.1016/j.ajps.2013.07.001 (2013).
214 Kuhn, D. A. *et al.* Different endocytotic uptake mechanisms for nanoparticles in epithelial cells and macrophages. *Beilstein J Nanotechnol* **5**, 1625-1636, doi:10.3762/bjnano.5.174 (2014).

Appendix

A. Gating Strategies

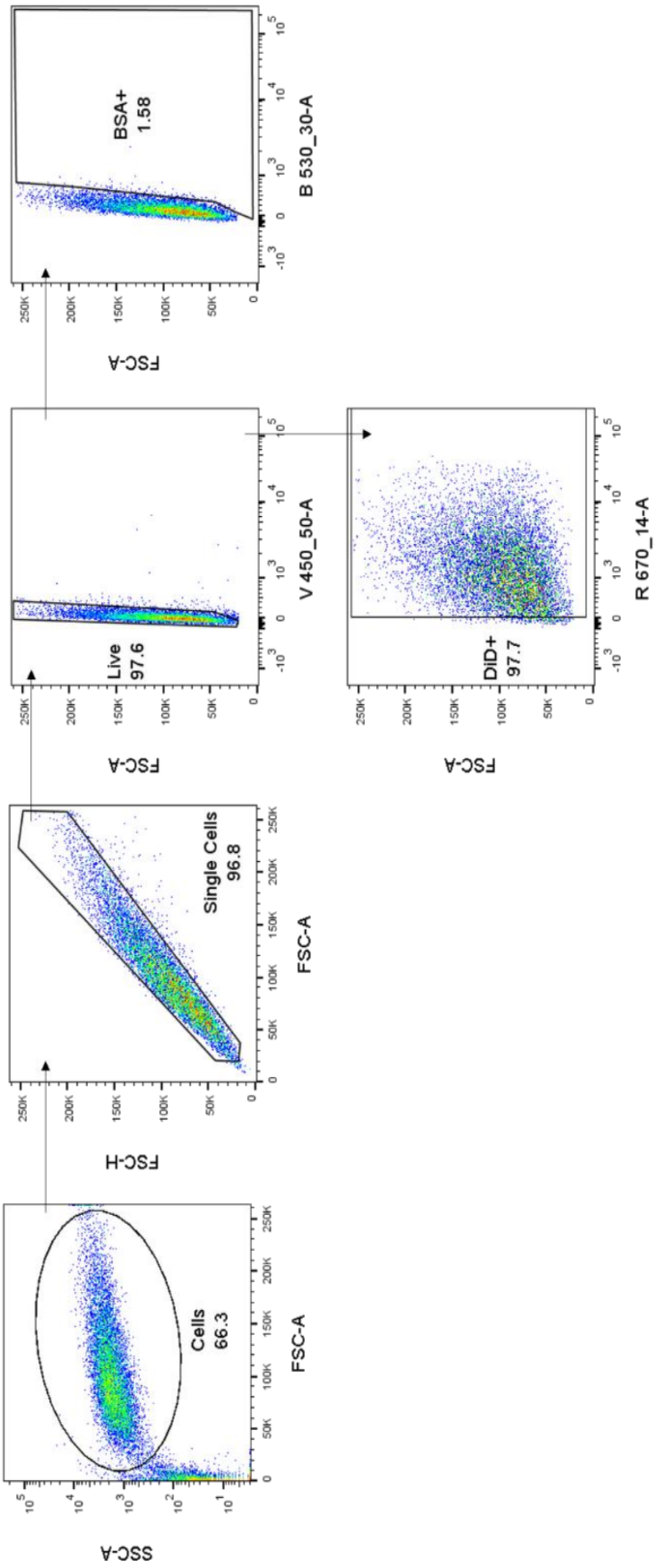

Figure A1 Gating strategy for internalization of LNP by THP-1 cells. Differentiated THP-1 cells were treated with medium, BSA or LNP for 24 h at 37°C. Dot plot of FSC-A versus SSC-A was used to gate for cells and to exclude debris. Then, dot plot of FSC-A versus FSC-H was used to gate for single cells and to exclude doublets. Dot plot of FSC-A versus the viability dye fluorophore was used to gate for live cells. As the cell membrane of live cells is impermeable, live cells cannot absorb the viability dye therefore appear on the left side of the graph. Under the DiD channel, gates were applied to live cells to define cells positive for DiD, the dye labelling the LNP. Under the FITC channel, gates were applied to live cells to define cells positive for FITC, the dye labelling BSA. As the gating strategy was performed on cells treated with LNP, we would not expect to see any cells in the BSA-positive gate. Gates were based off cells treated with medium. Representative images are presented for each gate.

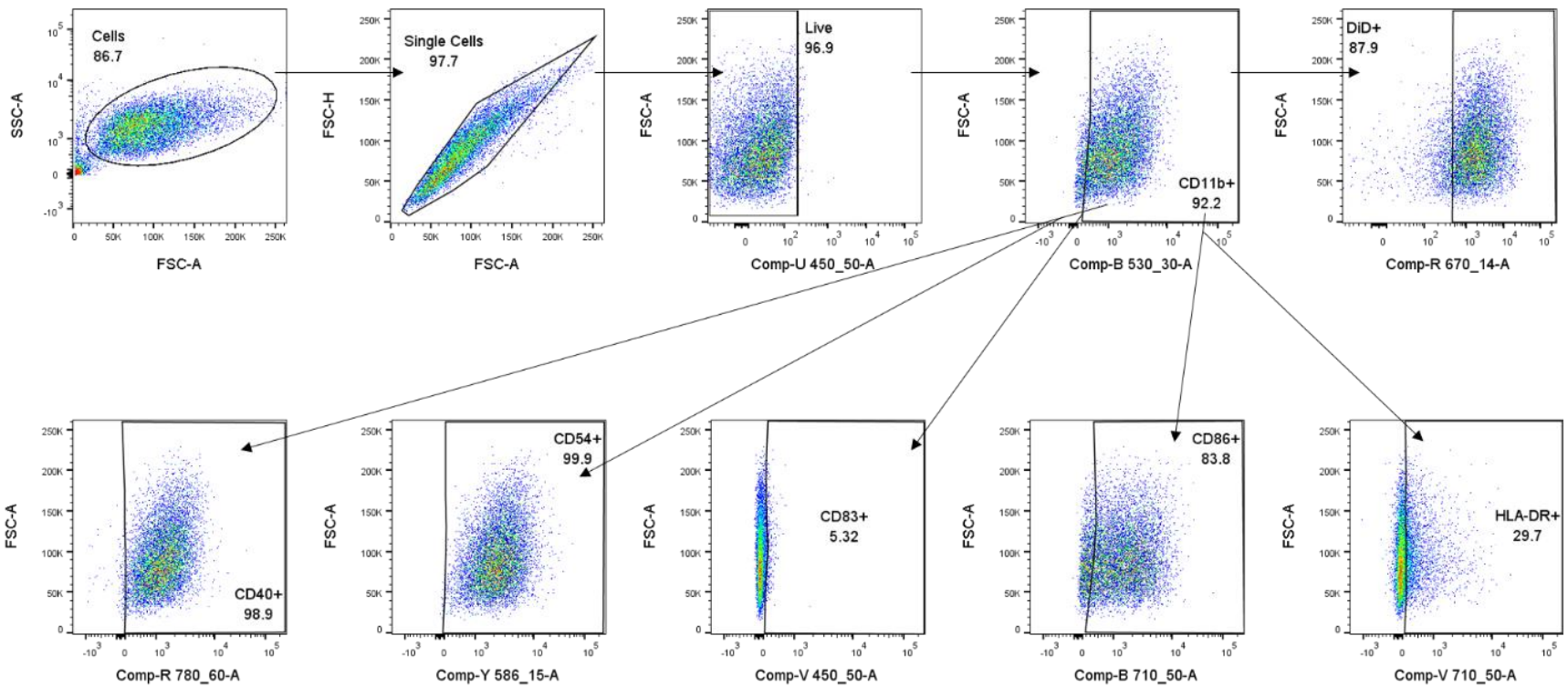

Figure A2 Gating strategy for activation marker expression and internalization of LNP by THP-1 cells. Differentiated THP-1 cells were treated with medium, LPS or LNP for 24 h at 37°C. Dot plot of FSC-A versus SSC-A was used to gate for cells and to exclude debris. Then, dot plot of FSC-A versus FSC-H was used to gate for single cells and to exclude doublets. Dot plot of FSC-A versus the viability dye fluorophore was used to gate for live cells. As the cell membrane of live cells is impermeable, live cells cannot absorb the viability dye therefore appear on the left side of the graph. Under the DiD channel, gates were applied to live cells to define cells positive for DiD, the dye labelling the LNP. Under the different fluorophore channels, gates were applied to live cells to define cells positive for the respectively labelled surface marker. As the gating strategy was performed on whole-stained LNP-treated cells, we expect to see cells in the DiD-positive gate. Gates were based off fluorescent minus one (FMO) samples for each fluorophore

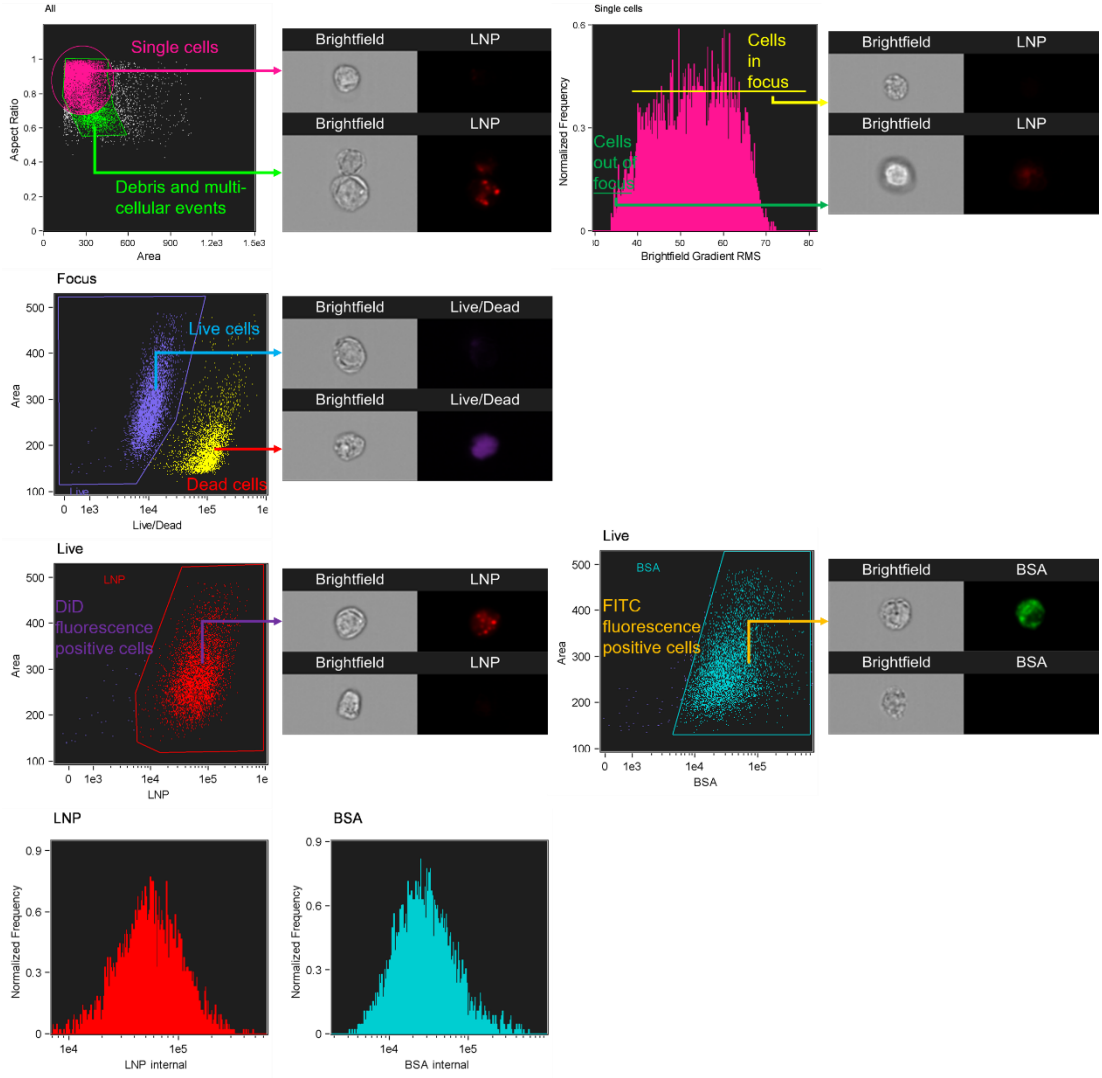

Figure A3 Gating strategy for internalization of LNP by MH-S cells on IDEAS. MH-S cells were treated with LNP or BSA for 24 h at 37°C and analysed by ImageStream. First, a scatter plot of area versus aspect ratio of the brightfield images was used to gate for single cells and to exclude debris and doublets. Second, a histogram for gradient root mean square (RMS), which is a measure of image sharpness, was used to gate for single cells in focus. Higher gradient RMS values mean a more focused image. Third, the intensity of viability dye staining was used to exclude dead cells. On the remeaining living, single cells in focues were gated in terms of intesity of DiD and FITC fluorophore channels to isolate LNP-treated or BSA-treated cells, respectively. To determine internalization of LNP or BSA, the brightfield cell image default mask, which usually covers the whole cell including the cell membrane, was eroded by 6 pixels then the intensity of the fluorophores was measured within the eroded mask. BSA internal and LNP internal gates were drawn to isolate only the cells that had internalized BSA or LNP, respectively. Higher values mean greater signal coming from LNP or BSA inside cell. Lower values mean little internalization or cell membrane attachment. Gating strategy was performed on LNP-treated and BSA-treated cells. Gates were based off cells treated with medium. Representative images are presented for each gate.

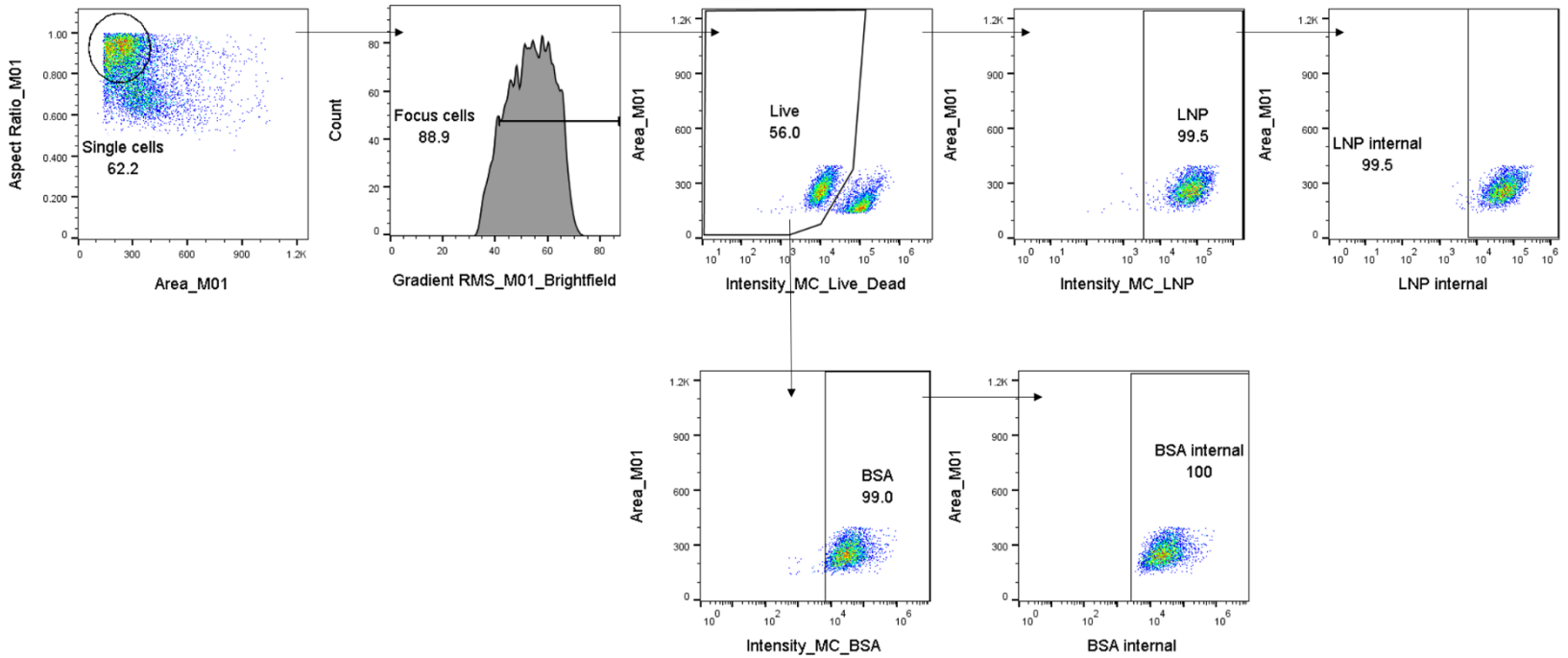

Figure A4 Gating strategy for internalization of LNP by MH-S cells on FlowJo using IDEAS gating. MH-S cells were treated with LNP or BSA for 24 h at 37°C. First, a dot plot of area versus aspect ratio of the birghtfield images was used to gate for single cells. Second, a histogram for gradient root mean square (RMS), which is a measure of image sharpness, was used to gate for single cells in focus. Third, the intensity of viability dye staining was used to exclude dead cells. On the remaining living, single cells in focues were gated in terms of intesity of DiD and FITC fluorophore channels to isolate LNP-treated or BSA-treated cells, respectively. To determine internalization of LNP or BSA, the brightfield cell image default mask, which usually covers the whole cell including the cell membrane, was eroded by 6 pixels then the intensity of the fluorophores within the eroded mask was measured. BSA internal and LNP internal gates were drawn to isolate only the cells that had internalized BSA or LNP, respectively. Higher values mean greater signal coming from LNP or BSA inside cell. Lower values mean little internalization or cell membrane

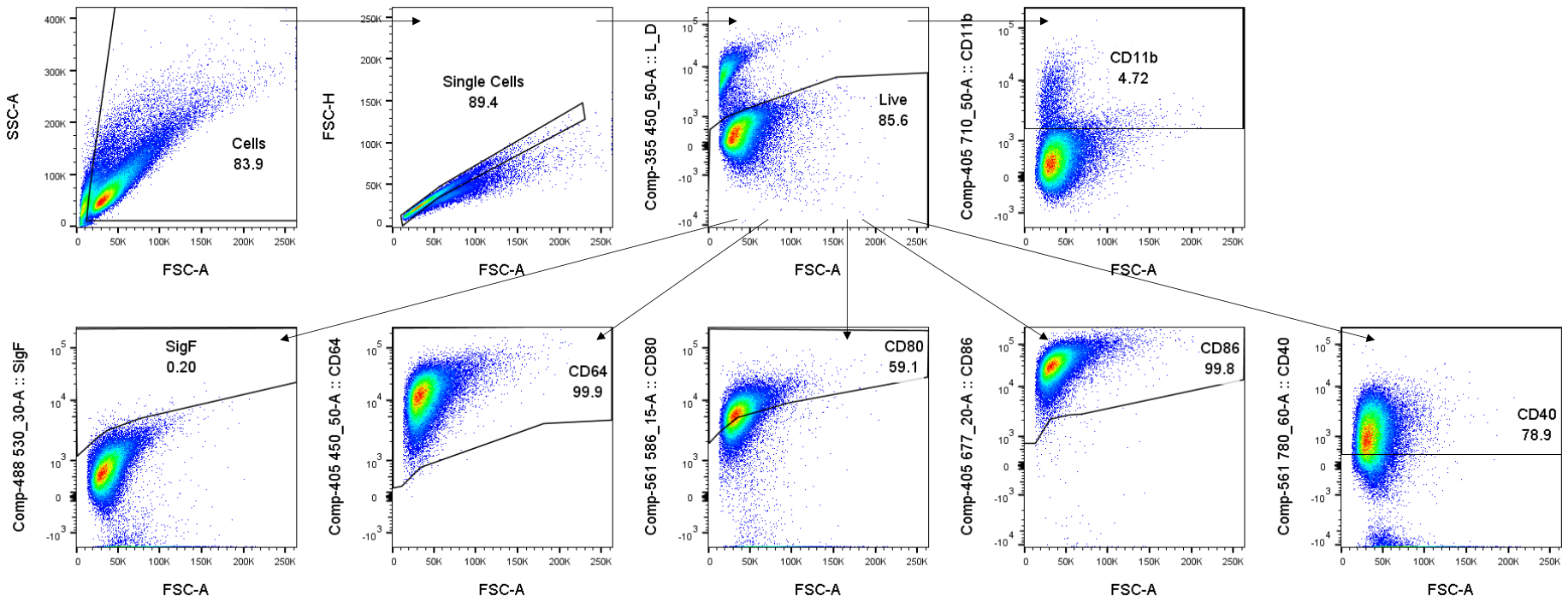

Figure A5 Gating strategy for activation marker expression of LNP by MH-S cells. MH-S cells were treated with medium, LPS or LNP for 24 h at 37°C. Dot plot of FSC-A versus SSC-A was used to gate for cells and to exclude debris. Then, dot plot of FSC-A versus FSC-H was used to gate for single cells and to exclude doublets. Dot plot of FSC-A versus the viability dye fluorophore was used to gate for live cells. As the cell membrane of live cells is impermeable, live cells cannot absorb the viability dye therefore appear at the bottom of the graph. Under the different fluorophore channels, gates were applied to live cells to define cells positive for the respective labelled surface marker. Gating strategy was performed on whole-stained LPS-treated cells. Gates were based off fluorescent minus one (FMO) samples for each fluorophore representing a cell surface marker. Representative images are presented for each gate.

B. Fluorophores, plate layout and antibody calculations

	488 nm Blue	405 nm Violet			640 nm Red	561 nm Yellow/Green		355nm UV	
	530/30	450/50	660/20	710/50	670/14	586/15	780/60	450/50	
	FITC	BV421	BV650	BV711	APC	PE	PE-Cy7	Zombie	
Surface Marker	SiglecF	CD64	CD86	CD11b	LNP	CD80	CD40	L/D	Fc block
Dilution	1 in 200	1 in 100	1 in 200	1 in 200		1 in 200	1 in 200	1 in 1000	1 in 100

	1	2	3	4	5	6	7	8	9	10	11	12
A	U WS + Fc + VD		U WS + Fc + VD		LNP WS + Fc + VD		LNP WS + Fc + VD		LPS WS + Fc + VD		LPS WS + Fc + VD	
B												
C	LPS SigF SS + Fc		LPS CD64 SS + Fc		LPS CD11b SS + Fc		LPS CD80 SS + Fc		LPS CD86 SS + Fc		LPS CD40 SS + Fc	
D	LNP SigF FMO + Fc + VD		LNP CD64 FMO + Fc + VD		LNP CD11b FMO + Fc + VD		LNP CD80 FMO + Fc + VD		LNP CD86 FMO + Fc + VD		LNP CD40 FMO + Fc + VD	
E	LPS SigF FMO + Fc + VD		LPS CD64 FMO + Fc + VD		LPS CD11b FMO + Fc + VD		LPS CD80 FMO + Fc + VD		LPS CD86 FMO + Fc + VD		LPS CD40 FMO + Fc + VD	
F												
G	LNP SS + Fc		Unst. + Fc		L + Fc + VD		L/D + Fc + VD					

	SigF	CD64	CD11b	CD80	CD86	CD40	PBA	
WS	2	4	2	2	2	2	400	
SigF SS	1						200	
CD64 SS		1					100	
CD11b SS			1				200	
CD80 SS				1			200	
CD86 SS					1		200	
CD40 SS						1	200	
SigF FMO		2	1	1	1	1	200	
CD64 FMO	1		1	1	1	1	200	
CD11b FMO	1	2		1	1	1	200	
CD80 FMO	1	2	1		1	1	200	
CD86 FMO	1	2	1	1		1	200	
CD40 FMO	1	2	1	1	1		200	

Fc block	12	VD	1.2	
PBS	1188			
Total	1200			
Fc block	5			
PBS	495			
Total	500			
SUM of WS	300			
SUM of FC only	400			
SUM of Fc and VD	1000			